On the Performance Improvement of Iris Biometric System

Hunny Mehrotra

Department of Computer Science and Engineering
National Institute of Technology Rourkela
Rourkela-769 008, Odisha, India

On the Performance Improvement of Iris Biometric System

Thesis submitted in partial fulfillment
of the requirements for the degree of

Doctor of Philosophy

in

Computer Science and Engineering

by

Hunny Mehrotra
(Roll: 510CS101)

under the guidance of

Prof. Banshidhar Majhi

&

Dr. Pankaj Kumar Sa

Department of Computer Science and Engineering
National Institute of Technology Rourkela
Rourkela-769 008, Odisha, India
March 2014

March 7, 2014

Certificate

This is to certify that the work in the thesis entitled **On the Performance Improvement of Iris Biometric System** by **Hunny Mehrotra**, bearing roll number 510CS101, is a record of an original research work carried out by her under our supervision and guidance in partial fulfillment of the requirements for the award of the degree of **Doctor of Philosophy** in **Computer Science and Engineering**. Neither this thesis nor any part of it has been submitted for any degree or academic award elsewhere.

Pankaj Kumar Sa   **Banshidhar Majhi**
Assistant Professor   Professor

Dedicated To My Family

Acknowledgment

If God brings you to it, he will bring you through it...

Thank you God for showing me the path.

I take this opportunity to thank all those who have contributed in this journey.

Foremost, I would like to express sincere gratitude to my advisor, Prof. Banshidhar Majhi for providing motivation, enthusiasm, and critical atmosphere at the workplace. His profound insights and attention to details have been true inspirations to my research. Prof. Majhi has taught me to handle difficult situations with confidence and courage.

I would like to thank Prof. Pankaj Kumar Sa for his constructive criticism during the entire span of research. His insightful discussions has helped me a lot in improving this work.

It was indeed a privilege to be associated with Prof. Mayank Vatsa and Prof. Richa Singh for research collaboration. They made my stay at IIIT Delhi very comfortable. I have learnt a lot from their knowledge and enthusiasm to achieve excellence. The kind of research discussions we had, has helped me a lot to shape up this dissertation.

My sincere thanks to Prof. S.K. Jena, Prof. S.K. Rath, Prof. A.K. Turuk, Prof. G.K. Panda, and Prof. S. Meher for their continuous encouragement and valuable advice.

I would like to thank my friends and colleagues at NIT Rourkela for the help they have offered during the entire period of my stay.

Finally, I owe the heartfelt thanks to my in-laws and parents for their unconditional love, support, and patience. Special thanks go to my father-in-law who has supported me a lot to finish this piece of work. Thank you mom and dad for always being there when I wanted you the most. Words fall short to express gratitude to my husband, Dr. Badrinath G.S., who has been the constant source of inspiration to me. I am indeed grateful to you for your support and understanding.

Hunny Mehrotra

Abstract

Iris is an established biometric modality with many practical applications. Its performance is influenced by noise, database size, and feature representation. This thesis focusses on mitigating these challenges by efficiently characterising iris texture, developing multi-unit iris recognition, reducing the search space of large iris databases, and investigating if iris pattern change over time.

To suitably characterise texture features of iris, Scale Invariant Feature Transform (SIFT) is combined with Fourier transform to develop a keypoint descriptor-F-SIFT. Proposed F-SIFT is invariant to transformation, illumination, and occlusion along with strong texture description property. For pairing the keypoints from gallery and probe iris images, Phase-Only Correlation (POC) function is used. The use of phase information reduces the wrong matches generated using SIFT. Results demonstrate the effectiveness of F-SIFT over existing keypoint descriptors.

To perform the multi-unit iris fusion, a novel classifier is proposed known as Incremental Granular Relevance Vector Machine (iGRVM) that incorporates incremental and granular learning into RVM. The proposed classifier by design is scalable and unbiased which is particularly suitable for biometrics. The match scores from individual units of iris are passed as an input to the corresponding iGRVM classifier, and the posterior probabilities are combined using weighted sum rule. Experimentally, it is shown that the performance of multi-unit iris recognition improves over single unit iris.

For search space reduction, local feature based indexing approaches are developed using multi-dimensional trees. Such features extracted from annular iris images are used to index the database using k-d tree. To handle the scalability issue of k-d tree, k-d-b tree based indexing approach is proposed. Another indexing approach using R-tree is developed to minimise the indexing errors. For retrieval, hybrid coarse-to-fine search strategy is proposed. It is inferred from the results that unification of hybrid search with R-tree significantly improves the identification performance.

Iris is assumed to be stable over time. Recently, researchers have reported that false rejections increase over the period of time which in turn degrades the performance. An empirical investigation has been made on standard iris aging databases to find whether iris patterns change over time. From the results, it is found that the rejections are primarily due to the presence of other covariates such as blur, noise, occlusion, pupil dilation, and not due to aging.

Keywords: F-SIFT, SIFT, POC, iGRVM, Multi-unit Fusion, k-d tree, k-d-b tree, R-tree, Hybrid retrieval, Iris Aging.

Contents

List of Figures

List of Tables

List of Algorithms

List of Acronyms

Chapter 1

Introduction

Biometrics is an automated method of authenticating an individual based on physiological and behavioral characteristics [1]. The advantage of biometrics over token based (smart cards) and knowledge based (password) approaches is that, it cannot be misplaced or forged. The characteristics are distinct and can distinguish between the *genuine* person and the *imposter*. The physical presence of the subject makes it very difficult to spoof the biometric system. The authentication is performed using various biometric traits like face, fingerprint, iris, ear, etc. The choice of a biological measurement to qualify as a biometric trait is based on the following properties [1, 2]:

- *universality*: every individual should possess the characteristic/trait.

- *uniqueness*: no two persons should have the same characteristic.

- *permanence*: the chosen characteristic should not change over a period of time.

- *collectability*: refers to the ease of acquiring a biometric trait.

- *performance*: refers to the accuracy achieved.

- *acceptability*: indicates the acceptance of a particular biometric trait by the community.

- *circumvention*: shows how easy it is to spoof a biometric trait.

The comparison of various biometric traits based on these characteristics is shown in Table 1.1. Iris is an established biometric modality due to its high universality, uniqueness, stability over time, performance, and ability to counteract spoof attacks (refer Table 1.1). An iris recognition system operates by mathematical analysis of texture patterns that are imaged at certain distance from the eye [3]. Recently, iris biometric has evolved as a mainstream field of biometric applications adverting to its

performance. Such systems are deployed at United Arab Emirates (UAE) linking 27 air, land, and sea-ports of entry [4]. In India, a large-scale project Aadhaar [5] is undertaken to issue unique identification number to everyone across the country using fingerprint, face, and iris. Though in sufficiently matured stage, iris still needs considerable attention by the researchers. The transition of iris from laboratory technology to real time deployment has highlighted some interesting research challenges. For instance, exhaustively searching country-sized iris database, recognition under scenarios when iris data is either noisy or unavailable, and effect of aging on iris [6]. In this thesis, an effort has been made to re-investigate the performance of iris biometric under the aforesaid real-time challenges and identify the measures to mitigate the shortcomings, if any.

Before exploring research issues in iris, it is recommended to consider its anatomical structure in detail. Iris is a thin circular disk in the eye with dark circular opening in the center known as the pupil as shown in Figure 1.1. The texture pattern in iris comprises two tissues: the front pigmented fibrovascular tissue is known as a stroma and, beneath the stroma, pigmented epithelial cells. The stroma is connected to a sphincter muscle, which constricts the pupil in a circular motion, and a set of dilator muscles, which pulls the iris radially to enlarge the pupil [7]. The constriction and dilation of pupil controls the amount of light entering the eye. The flowery pattern surrounding the pupil, commonly referred as *iris*, is unique and used for personnel identification.
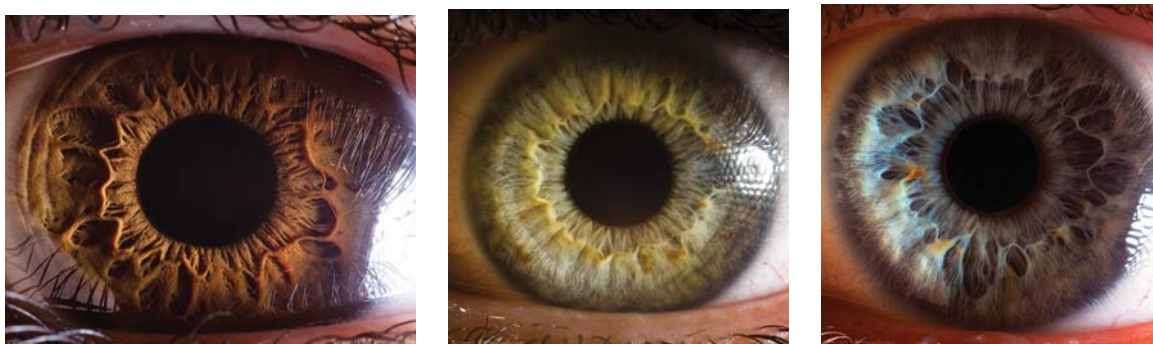
Figure 1.1: Illustration of the front pigmented fibrovascular tissue known as a stroma from high quality eye images [8].

1.1 Automated Iris Biometric System

An iris biometric system is typically a pattern recognition system that acquires the iris image of an individual, extracts features (represented in the form of a template),

Table 1.1: Comparison of different biometric modalities based on their characteristics (H: High, M: Medium, and L: Low) [9].

Modality	Universality	Uniqueness	Permanence	Collectability	Performance	Acceptability	Circumvention
Face	H	L	M	H	L	H	L
Fingerprint	M	H	H	M	H	M	H
Hand Geometry	M	M	M	H	M	M	M
Keystrokes	-	-	L	M	L	M	M
Hand Vein	M	M	M	M	M	M	H
Iris	**H**	**H**	**H**	**M**	**H**	**L**	**H**
Retinal Scan	H	H	M	L	H	L	H
Signature	L	L	L	H	L	H	L
Voice Print	M	L	L	M	L	H	L
F. Thermogram	H	H	L	H	M	H	H
Odor	H	H	H	L	L	M	L
DNA	H	H	H	L	H	L	L
Gait	M	L	L	H	L	H	M
Ear	M	M	H	M	M	H	H

and compares this feature set against the feature set(s) stored in the database. The input biometric template (commonly referred to as *gallery* template) is stored in the database during enrollment. The template which is presented to the biometric system for claiming the identity is known as *probe*. A generic iris biometric system has four major modules:

a. **Image acquisition module** requires an iris biometric scanner to acquire images. The acquisition setup plays a crucial role on the performance of any biometric system. For instance, iris images acquired loosely (without any restriction on the user) may pose serious challenges.

b. **Preprocessing module** extracts the *region of interest* from the input iris image. Preprocessing is performed to localise the inner pupil and the outer iris boundary. The annular ring between pupil and iris boundary are transformed from Cartesian space to polar space using homogeneous rubber sheet model [10]. This transformation generates the normalised iris image which facilitates the feature extraction process.

c. **Feature module** extracts significant details from the normalised iris image using mathematical models. The extracted features should be unique and must achieve

invariance to transformations between the gallery and probe iris images.

d. **Matching module** find the correspondences between the two feature sets using an appropriate matcher. The matcher either validates the identity of an individual by performing one to one comparison or to generates a ranked list of identities for one to many comparisons [1]. Figure 1.2 illustrates different modules of an automated iris biometric system.
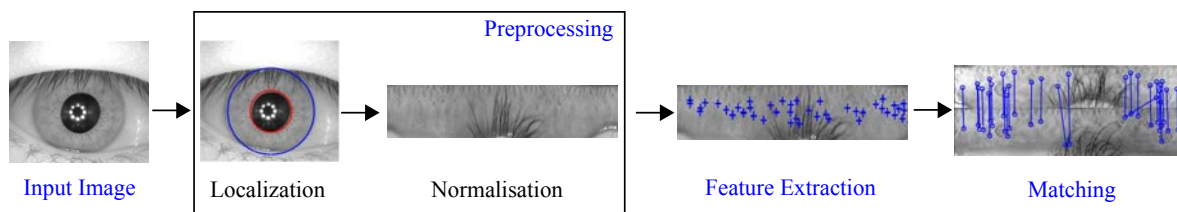
Figure 1.2: Different modules of an automated iris recognition system.

Depending upon the application context, a biometric system operates in verification (also known as recognition) or identification modes as shown in Figure 1.3. In verification mode, the system authenticates the identity claimed by an individual by comparing his template with an already stored template in the database. Identification mode, in contrast, finds the identity of the probe template by searching all gallery templates present in the database.

1.2   Fusion in Biometrics

Biometric system that requires single source of evidence to perform authentication is known as unimodal systems. However, a single biometric trait is not expected to meet all the requirements such as accuracy, cost, availability, etc. [1]. There are some challenges which in general, affects the performance of any biometric system:

- The acquired biometric image may change over time or may be affected by noise. For instance, facial features are subject to age over a period of time. Similarly, fingerprint effected by scar or voice effected by cold may pose vulnerabilities to a biometric system.

- The biometric data may be unavailable for a subset of population. The presence of cuts and bruises on the fingerprint brings down the system performance. Similarly, it is difficult to acquire iris images with some pathological problem in the eye.
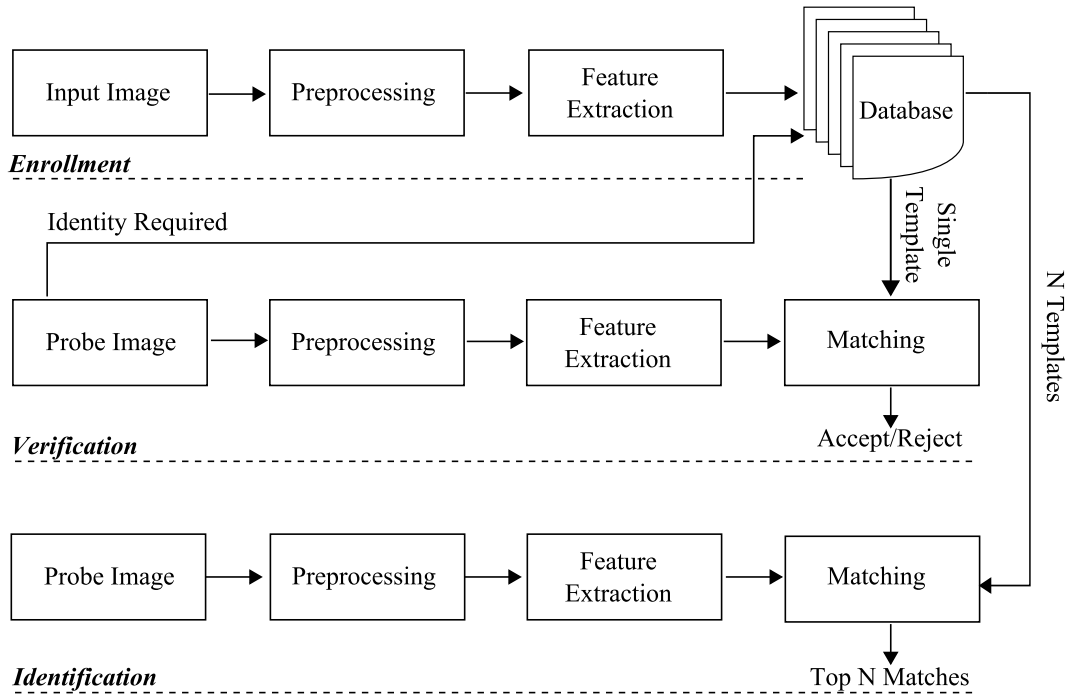
Figure 1.3: Different modes of operation of a generic biometric system.

- Circumvention is easy with a single biometric trait. Some traits such as fingerprint can be spoofed by showing a fake fingerprint structure on a synthetic material.

Multimodal biometric fusion utilises more than one source of evidence for authentication. Fusion is very useful to overcome the limitations inherent to unimodal approaches. Depending upon the *nature of evidence* available, the fusion algorithm can be multi-sensor, multi-algorithm, multi-instance, multi-unit, and multi-modal as shown in Figure 1.4. The *multi-sensor* system utilises more than one sensor to capture single biometric trait of an individual. In *multi-algorithm* system, for a single biometric trait, multiple feature extraction algorithms or multiple matchers are combined. The multiple images of the same biometric trait are acquired from a single biometric sensor in *multi-instance* systems. In *multi-unit* system, multiple units of the same modality are used to perform authentication. For instance, information from left and right iris or fingerprint images can be combined to improve the performance. The multi-unit fusion approaches improve the recognition accuracy without incurring any additional hardware cost. The combination of more than one biometric trait generates a *multi-modal* system [1]. For example, combining iris with the face improves the performance of "on the move" type of recognition systems.

Based on the *level of fusion*, the approaches can be further categorised into sensor level, feature level, match score level, and decision level as shown in Figure 1.5. In
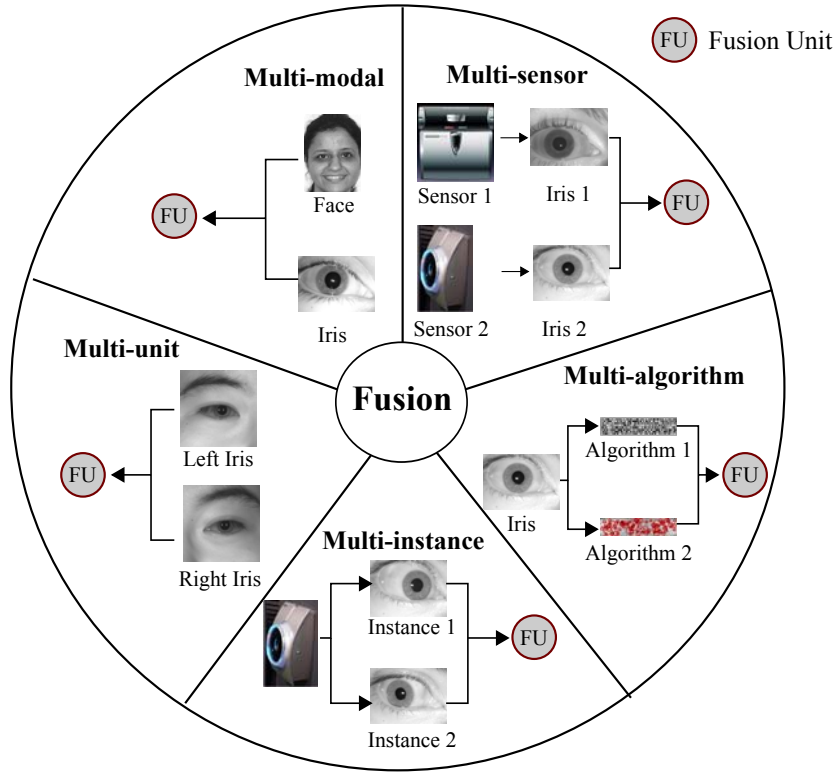
Figure 1.4: Categorisation of fusion approaches depending upon the nature of evidence.

sensor level fusion, the raw biometric data from multiple sensors (multi-sensor) or multiple instances of a biometric from the same sensor (multi-instance) are fused. *Feature level* fusion involves integrating more than one feature set from different biometric algorithms (multi-algorithm) into a single feature set. In *match score* level fusion, the match scores generated from multiple biometric matchers are combined to generate a consolidated score value. In *decision level* fusion, the final recognition decisions are combined to develop a multimodal biometric system.

1.3 Performance Measures

Biometric seldom compares two same templates of a user originating from same biometric trait. There is the difference between two templates due to scanning conditions, change in characteristics with respect to aging, change in acquisition scenarios, etc. Therefore, feature sets originating from the same individual need not always be the same. When two different biometric templates originating from the same individual are different then it is known as **intra-class** variations. However, variations that occur between templates originating from two different individuals are known as **inter-class** variations [11]. The degree of similarity between two feature
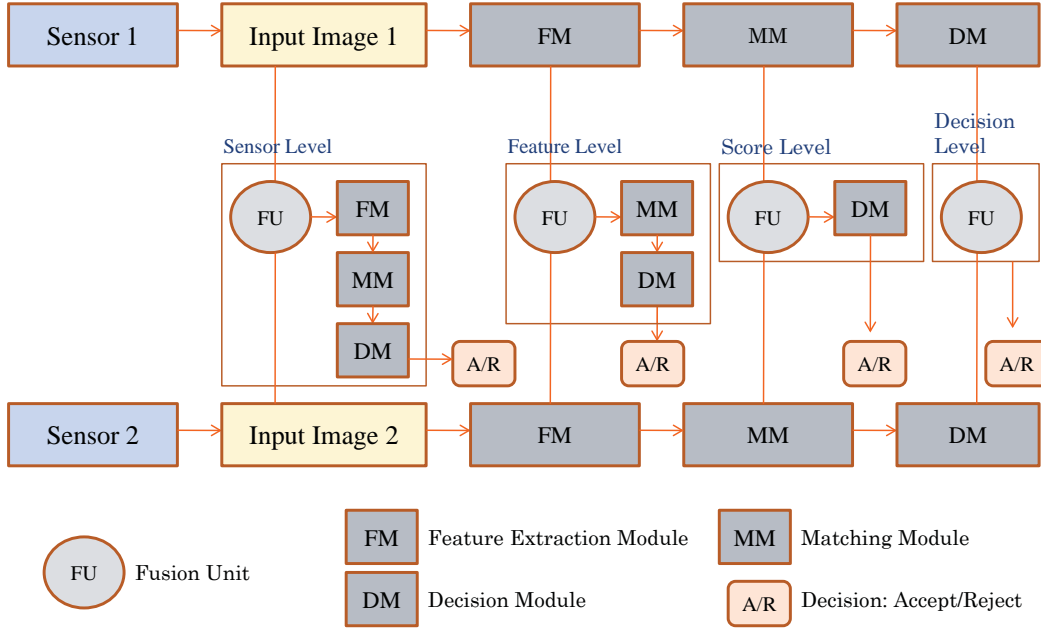
Figure 1.5: Various levels of fusion in multimodal biometric.

sets is indicated by the matching score. A *genuine* score is the result of matching two samples of the same individual. If comparison involves matching two biometric samples originating from different individuals then it is termed as an *imposter* score.

1.3.1   Recognition Performance

The error rate equations for system operating in recognition mode are discussed as follows:

- **False Acceptance Rate** (FAR) or False Match Rate (FMR) is defined as percentage of imposters incorrectly matched to the non-matching template.

- **False Rejection Rate** (FRR) or False Non Match Rate ($FNMR$) is the percentage of genuine people incorrectly rejected by the system.

- **Equal Error Rate** (EER) is the point where FAR equals FRR. In general, lower the equal error rate value, higher the accuracy of the biometric system.

- **Genuine Acceptance Rate** (GAR) is the percentage of genuine scores being correctly accepted and is defined as $GAR = 1 - FRR$. A hypothetical score distribution curve is shown in Figure 1.6. This curve graphically demonstrates the performance measures used in recognition mode.

- **Receiver Operating Characteristic** (ROC) curve is a comprehensive way to analyse the performance of a biometric system. It depicts the dependence of FAR with GAR for change in the value of threshold. The curve can be plotted using linear, logarithmic or semi-logarithmic scale.
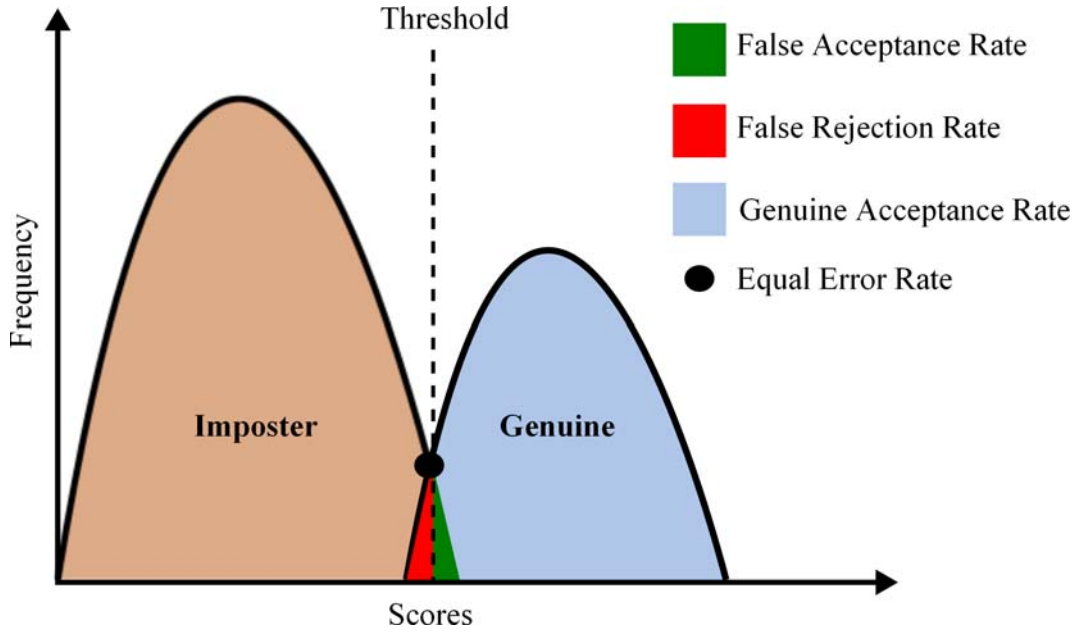
Figure 1.6: A hypothetical curve demonstrating the performance measures used during recognition mode.

1.3.2 Identification Performance

During identification, the gallery space is partitioned into bins for search time reduction. The error rate equations of systems operating in identification mode [11] are:

- **Penetration Rate** (PR). The portion of total database to be scanned on an average against each probe search is called penetration rate, which can be defined as

$$PR = \frac{E}{N} \tag{1.1}$$

where E is the expected number of comparisons required for single probe search and N is the total number of images enrolled in the database. On encountering a match, the search does not stop but continues through the entire partition [11].

- **Bin Miss Rate** (BM). This error rate occurs when the search attempt is made in the bin which is not the correct bin. BM occurs due to inconsistencies in the binning process.

- To mark the tradeoff between performance and speed, an error measure γ [12] is empirically defined as

$$\gamma = \sqrt{(1 - PR) \times (1 - BM)} \tag{1.2}$$

γ can be considered as a supportive but not conclusive measure of identification.

- **Cumulative Match Characteristic (CMC) Curve**. The rank-k identification indicates the number of correct identities that occur in top k matches. Let R_k denote the number of elements of probe set in top k, then the probability of identification is given by $pi = \frac{R_k}{N}$. Cumulative Match Characteristic curve represents the probability of identification pi at various ranks k.

- **Correct Recognition Rate (CRR)** measures the rank-1 accuracy, defined as

$$CRR = \frac{R_1}{N} \tag{1.3}$$

where R_1 is the number of correct identities at rank-1.

1.4 Research Challenges

Though iris is an established biometric modality, there still exist some open research challenges that need to be addressed. Some of these challenges are discussed as follows:

1. The error rates of iris increase, especially the false rejections, when images are acquired on the move. Such acquisition systems are particularly suitable for video surveillance and criminal identification. In such applications, the variation in capturing distance and illumination determines the size of the pupil which in turn controls the area enclosing iris. In order to perform recognition under such variations, traditional approaches transform iris from Cartesian to polar space. This transformation introduces the effect of aliasing in iris images [13].

2. Traditional iris recognition approaches are severely affected by the quality of the input data. Further, some medical conditions such as accidental damage may tamper the patterns and degrade the performance of unimodal systems.

3. Deployment of iris for many real time applications have led to the creation of many large scale databases [5, 14]. On such large biometric databases, probe identification with limited computation resources is very challenging. Performing an exhaustive search on the country sized databases (N individuals enrolled) demands unacceptably long response time to find the identity of an individual.

4. Maltoni et al. [9] have further stated that during identification, the probability of falsely non-matching the template is same as recognition whereas the probability of false match increases linearly with the database size. If FMR signifies the false matches for the verification system, then the false matches during identification are given by

$$FMR_N = 1 - (1 - FMR)^N \tag{1.4}$$

where N is the number of templates enrolled in the database. In Equation (1.4), the expression $(1 - FMR)$ defines the probability that the probe does not match falsely with a single biometric template [9], and $(1 - FMR)^N$ is the probability that the probe does not match falsely with any of the database entries. If FMR is very small then Equation (1.4) can be re-written as

$$FMR_N \cong N \times FMR \tag{1.5}$$

This shows that the probability of false match increases with the database size.

5. Daugman in his research finding has stated that *iris patterns are stable over the lifetime of an individual* [15]. Thereafter this fact is globally accepted by the research community as the universal claim without any experimental proofs thereof. Recently Prof. Kevin Bowyer from University of Notre Dame [16] has claimed that iris patterns are subject to age. The effect of aging in iris is questionable and needs careful investigation.

1.5 Research Objectives

The aforementioned research challenges are addressed to improve the performance of iris biometric system in practical scenarios. The research objectives are—

1. to develop a feature descriptor for iris, which precisely characterises the texture pattern directly from the annular iris image without transformation from Cartesian to polar space.

2. to combine the left and right iris units of an individual to perform recognition. The absence of data from one unit is compensated by the other unit.

3. to reduce the search time during identification by logically partitioning the database into bins. The false matches also improve on dividing N by penetration rate (PR). Substituting the value of N in Equation (1.4) generates

$$FMR_N = 1 - (1 - FMR)^{\frac{N}{PR}}$$

$$\cong \quad \frac{N}{PR} \times FMR \tag{1.6}$$

4. to investigate if iris patterns change over time and affect the performance.

1.6   Thesis Organisation

This thesis is organised into seven chapters where each chapter portrays the contributions specific to a domain. The layout of this thesis is given below.

Chapter 2: Literature Review

The existing literature is explored covering four major domains of biometrics: (a) feature representation, (b) fusion, (c) identification, and (d) effect of aging in iris. For brevity, the tabular comparison of various approaches are presented along with the reported performance.

Chapter 3: F-SIFT based Keypoint Descriptor for Iris

A keypoint descriptor, F-SIFT is presented in this chapter that detects the interest points using Scale Invariant Feature Transform (SIFT) and describes each keypoint using Fourier transform. F-SIFT extracts rich texture details from iris that are invariant to transformations, illumination, and occlusion.

Chapter 4: iGRVM for Multi-unit Iris Fusion

A novel classifier, iGRVM is developed, which incorporates incremental and granular learning into RVM. The proposed classifier is evaluated in context of multimodal biometric score classification, and results are found to be encouraging. Another proposition is to design a fusion framework for multi-unit iris recognition. iGRVM is used to find the class probabilities of individual scores obtained from left and right iris. These probabilities are combined using sum rule to generate a unified decision value.

Chapter 5: Multi-dimensional Tree based Iris Indexing

This chapter proposes efficient indexing schemes for large iris databases using multi-dimensional trees. In this work, indices are generated using local features extracted directly from the annular iris image. The keypoint descriptors are clustered using k-means approach. These cluster centers are used to insert a node into k-d tree. However, k-d tree is not dynamic to the order of insertion of records. The challenges of k-d trees are addressed using k-d-b tree, which is dynamic and considers paging

of secondary memory. Biometrics databases are modeled as spatiotemporal and an efficient data structure R-tree is used for indexing. The tree structure is dynamic, height balanced, considers paging, and is designed to work with data ranges. For efficient retrieval, hybrid coarse-to-fine searching strategy is proposed. The combination of R-tree with coarse-to-fine retrieval approach outperforms existing local feature based indexing approaches.

Chapter 6: Effect of Aging on Iris Performance

This chapter presents an experimental investigation of aging in iris. Template aging databases collected at University of Notre Dame [16] are used to perform the experiments. The matching is performed across years using commercial VeriEye SDK [17] and false non-match cases are obtained at 0% false matches. These cases are studied to find if rejections are attributable to aging or some other covariates are involved.

Chapter 7: Conclusions

This chapter presents the conclusions derived from the proposed work with more emphasis on achievements and limitations. The scope for future research is highlighted at the end.

Chapter 2

Literature Review

Daugman has proposed the first operational iris recognition system in 1993 [10]. This landmark proposition has established iris as a potential biometric modality with many real-time applications [5, 18]. In the recent years, the researchers are trying to reduce the challenges that occur in real-time applications of iris. In this thesis, contributions are made to feature representation, match score level fusion, indexing, and study the effect of aging in iris. Since literature in each direction is independent of the other, the state-of-the-art approaches are explored for each category. The existing literature is explored covering four major domains of biometrics as shown in Figure 2.1. Section 2.1 summarises some well-known *feature representation* approaches for iris. Different *match score based fusion* approaches are discussed in Section 2.2. In Section 2.3, biometric *indexing* approaches are presented for search space reduction. The literature on *iris aging* is given in Section 2.4. The inferences derived from the literature are discussed at the end.
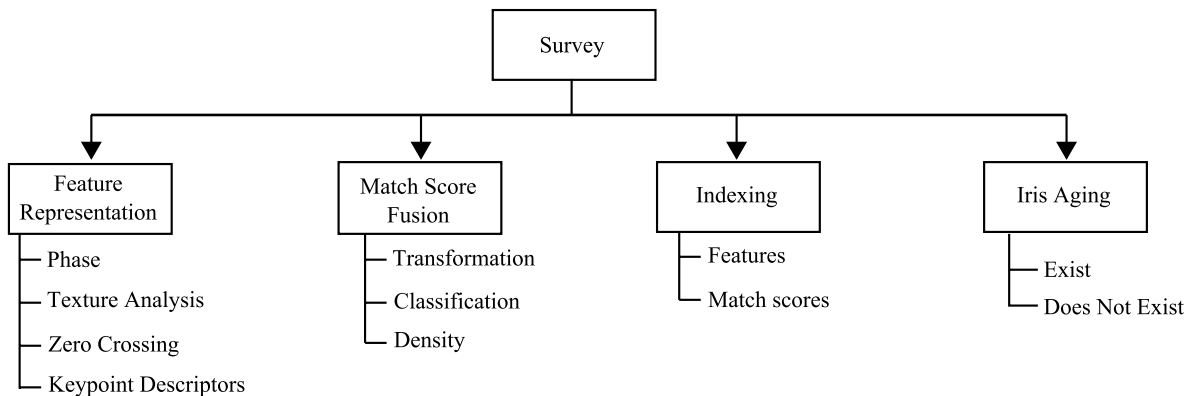
Figure 2.1: Categorisation of literature explored in biometrics into four domains.

2.1 Feature Representation

The randomness in iris patterns is quite high which promotes the research on different ways of representing the iris texture patterns. The existing approaches for iris recognition can be broadly classified into four categories as given in Table 2.1.

2.1.1 Phase-based

Phase information is more popularly used to represent iris texture patterns independent of contrast and illumination. Daugman proposed the first commercially available iris recognition system using phase features [3, 15, 10]. The texture pattern of iris is encoded into a sequence of 2-D Gabor wavelet coefficients whose most significant bits comprise 256 byte iris code. Miyazawa et al. [19] proposed a recognition system using the phase components of 2-D Discrete Fourier Transform (DFT). The phase based image matching is performed using the Phase-Only Correlation (POC) function. Another approach for iris recognition is based on Gabor phase-correlation particularly designed to work for degraded iris images [20]. This approach relies on two important aspects. The first is the combination of local and global information extracted by the correlation measure, and the second one is the joint consideration of correlation peak amplitude and position of the matching score measured in a local manner.

2.1.2 Texture-based

The texture analysis of spatial patterns in iris is used to extract features. Wildes et al. [23] applied Laplacian of Gaussian (LoG) filters to the iris image at multiple scales and Laplacian pyramid is constructed. The iris recognition system proposed in [24] is based on multi-channel Gabor filtering. For filtering, the authors have used 20 Gabor filters corresponding to different frequencies and orientations. Each iris image is divided into eight sub-images after normalisation. This makes total of 160 (8×20) output images from which the iris features are extracted. Ma et al. [25] utilised a Circular Symmetric Filter (CSF) which are based on Gabor filter. The difference between Gabor filter and circular symmetric filter lies in modulating the sinusoidal functions. The authors in [26] defines a bank of spatial filters whose kernels are suitable to clearly discriminate iris texture patterns. The Gabor filter provides image features at certain orientation whereas the spatial filters consider information from different orientations. This marks the superiority of spatial filters over Gabor filter for recognition. Tan et al. [27] proposed an iris recognition algorithm using texture of iris which is regarded as a kind of transient signals and uses the wavelet transform to process such signals.

14

Table 2.1: Feature representation approaches for iris recognition.

Year	First Author	Approach	Database	Results
Phase-based				
1993	Daugman [10]	2-D Gabor wavelet	Iris images from Ophthalmology Associates of Connecticut, Massachusetts and Cambridgeshire	FR: 1 in 128000, FA: 1 in 151000
2008	Miyazawa [19]	2-D Discrete Fourier Transform and POC	CASIA [21] ICE [22]	EER: 0.18% EER: 0.54%
2009	Krichen [20]	Gabor phase-correlation	ICE [22]	FRR: 2%
Texture-based				
1997	Wildes [23]	Laplacian of Gaussian filters	–	–
2000	Zhu [24]	Multichannel Gabor filtering	Self captured (25 subjects)	Acc: 99.09%
2002	Ma [25]	Circular symmetric filters	Self captured (109 subjects)	CRR: 99.85%
2003	Ma [26]	Bank of spatial filters	CASIA [21]	CRR: 99.43%
2004	Tan [27]	Dyadic wavelet transform	CASIA [21]	CRR: 100%
2009	Sun [28]	Multilobe differential filters	BATH [29] CASIAV3 [21] ICE [22]	FRR: 0.94%
2012	Zhang [30]	Perturbation-enhanced feature correlation filter	CASIAV3 [21] CASIA-Iris-Thousand [21] ICE [22]	EER: 0.37% EER: 0.40% EER: 0.24%
Zero-Crossing				
1998	Boles [31]	Wavelet transform	–	–
2002	Sanchez-Avila [32]	Dyadic wavelet transform	Self acquired (20 subjects)	Acc: 97.9%
2005	Sanchez-Avila [33]	Dyadic wavelet transform on an annular region	Self captured (50 subjects)	Acc : 99.6%
2007	Monro [34]	Discrete Cosine Transform	CASIA [21] BATH [29]	CRR: 100%
2012	Ahamed [35]	Curvelet transform	CASIA [21] UBIRIS.vl [36] UPOL [37]	CRR: 99.3%
Keypoint Descriptor				
2009	Belcher [38]	Region-based SIFT	ICE [22] WVU [39]	EER: 5.57% EER: 8.28%
2009	Mehrotra [40]	Harris Corner and Entropy	BATH [29] CASIAV3 [21]	Acc: 87.42% Acc: 92.78%
2009	Mehrotra [41]	SURF	BATH [29] CASIAV3 [21]	Acc: 95.48% Acc: 95.77%
2010	Du [42]	Gabor and SIFT	ICE [22]	EER: 0.026%
2011	Zhang [43]	Deformable DAISY Matcher	CASIA-Iris-Thousand [21] CASIAV3 [21]	EER: 0.21% EER: 0.59%
2013	Sun [44]	SIFT	Self acquired (18 subjects)	Acc: 98.15%

The sharp variations, considered as good indicators of important image structures, are extracted from the set of intensity signals to form discriminating features. The authors in [28] proposed an iris recognition system using ordinal measures for characterising the qualitative relationships between the iris regions rather than precise measurements of its structures. The multilobe differential filters are developed to compute ordinal measures with flexible intralobe and interlobe parameters such as location, scale, orientation, and distance. Zhang et al. [30] proposed a Perturbation-enhanced Feature Correlation Filter (PFCF) for iris recognition. The authors have applied the filters in Gabor feature domain to combine the advantages of Gabor images and correlation filters. This method encodes both local and global iris features for reliable identity verification.

2.1.3 Zero Crossing

Zero crossing approaches seek out those places in the image signal that passes through 0 value and marks them as edge points. Boles et al. [31] presented an algorithm for recognising iris based on the Wavelet transform. This approach makes use of zero crossings of the wavelet transform computed over concentric circles of iris and the resultant 1-D signals are compared with the model features. Wavelet based approach is invariant to translation and rotation of an image. Authors in [32] developed an approach using dyadic wavelet transform. The wavelet function used for feature extraction is the first derivative of cubic spline. The advantage of using this function is that it has smaller number of coefficients compared to second derivative of a smoothing function. Authors in [33] have also extracted zero-crossing representation of the dyadic wavelet transform from two different iris signatures: one based on a single virtual circle of the iris; the other one based on an annular region. From the experiments it is found that the performance of recognition system improves using annular region. Another approach presented in [34] investigates the method of 1-D Discrete Cosine Transform (DCT) as a means of feature extraction. The DCT series of averaged overlapping angular patches are taken from the normalised iris image to form the feature vector. A low complexity iris recognition system is proposed based on Curvelet transform [35]. The zero crossings of curvelet coefficients from the approximation subbands are used as features. Experimental results report that DCT based approach has low computational complexity and high accuracy compared to other approaches.

2.1.4 Keypoint Descriptors

The keypoint descriptors are based on the appearance of an object at particular interest points and are invariant to image scale and rotation. They are also robust to changes in illumination, noise, and minor changes in viewpoint. Scale Invariant Feature Transform is a well known keypoint descriptor for object recognition [45]. SIFT is applied to regions of iris which does not require polar transformation [38]. The idea is to develop a keypoint descriptor that is capable of performing well for iris textures. Mehrotra et al. [40] proposed an iris recognition technique using interest point pairing. The feature set comprises spatial location of each corner point (detected using Harris) and entropy information of window around the corner. The corner points are paired using dual stage approach. At the first stage, the potential corners are obtained by finding Euclidean distance between spatial coordinates. These potential corners are used to find actual corners based on their affinity around a window, which is measured using Mutual Information (MI). The authors in [41] have developed an

iris recognition system by applying Speeded Up Robust Features (SURF) directly on annular iris images. This system performs well for iris because of its capability to distinguish significant texture features from the background. Du et al. [42] proposed an iris recognition system by combining Gabor wavelet with SIFT to generate Gabor descriptor. Both phase and magnitude of Gabor wavelet values are used as features. The Gabor feature descriptor is invariant to scale, deformation, rotation, and contrast of two iris images. This approach performs well for frontal and off-angle iris images taken under non-cooperative scenarios. It is assumed that the rich texture pattern of iris undergoes non-linear deformation due to pupil contraction and dilation. Zhang et al. [43] proposed deformable DAISY matcher for robust iris feature matching. The dense DAISY descriptors are extracted from the normalised iris image for low computational cost. The set of keypoints are localised on the feature map to match using deformation tolerant matching strategy. Sun et al. [44] proposed a recognition system using bovine iris images captured from non-cooperative audiences. The pupil and iris circles are localised using active counters and features are extracted using SIFT. After removing keypoints from pupil region, the keypoint descriptor is generated using bag-of-features and then distance of histogram representations is adopted for matching. Local feature based approaches have shown to improve the iris recognition performance.

2.2 Score Level Fusion

Score level fusion is preferred over other fusion approaches due to the information content and ease of combining scores from different matchers [46]. Nandakumar et al. [47] have mentioned that match score level fusion is challenging because the scores of different matchers may follow different distributions. For instance the scores from two different matchers may be non-homogenous where one represents distance values and other represents similarity scores as shown in Figure 2.2. Existing match score fusion approaches are designed to handle this ambiguity and perform fusion. The score level fusion approaches are divided into following three categories [47]

2.2.1 Transformation-based

As matching scores generated from different modalities are heterogenous, score normalisation is required to transform them to a common domain [48]. In transformation based approaches, the matching scores from different modalities are normalised and then integrated to generate a combined score. Brunelli and Falavigna [49] proposed an integration system which combines acoustic and visual cues

for recognition. The multi-classifier system operates in two steps. In the first step, the input scores are normalised using robust estimators of location and scale. In the second step, the scores are integrated using weighted geometric average. The authors in [50] have proposed a multivariate polynomial model to overcome the tedious recursive learning problems. Kittler et al. [51] developed a theoretical framework for combining the classifiers which includes product rule, sum rule, max rule, min rule, median rule, and majority voting. The most interesting inference from his study is that the sum rule outperforms other combination approaches. Jain et al. [52] used logistic transform to combine scores from three different fingerprint matching algorithms. Experiments performed using large fingerprint database confirms the effectiveness of the integrated system. The performance of multimodal biometric systems are further improved by integrating face and fingerprint modalities using state-of-the-art Commercial Off-The-Shelf (COTS) matchers [53]. Some new normalisation and fusion approaches are proposed and it is found that the combination of Quadric-Line-Quadric (QLQ) normalisation and User Weighting (UW) fusion generates minimum error rates. Jain et al. [48] have studied the performance of various score normalisation approaches and fusion rules using face, fingerprint, and hand-geometry images of a person. The authors also support the study of Kittler et al. [51] that *simple sum rule based fusion performs better compared to other approaches.*

2.2.2 Classifier-based

In classifier based approaches, the *d*-dimensional score vector is taken as input to the classifier and a binary decision regarding acceptance or rejection is taken. Yacoub et al. [56] have evaluated different biometric classifiers like
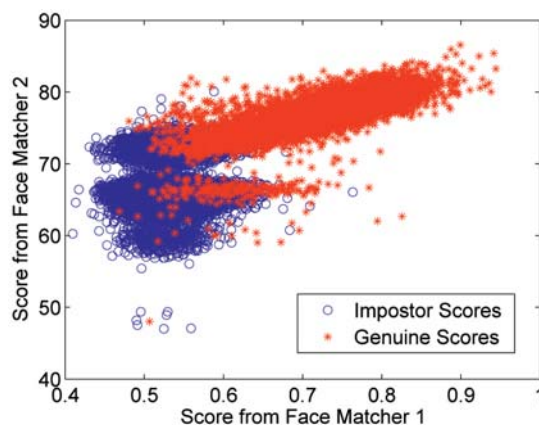
Figure 2.2: Illustrating non-homogenous characteristics in match scores from NIST-Face score set database [54] (this graph is taken from [47]).

Table 2.2: Score level fusion approaches in biometrics.

Year	First Author	Approach	Modality	Database	Results
Transformation-based					
1995	Brunelli [49]	HyperBF networks	Speech and face	Self acquired database	*Acc*: 98%
1999	Jain [52]	Logistic transform	Fingerprint	Self acquired (167 subjects)	*GAR*: $\approx$ 89%
2004	Toh [50]	Multivariate polynomial model	Fingerprint, speech, and hand-geometry	–	*EER*: improved by 50%
2005	Snelick [53]	Normalisation: Quadric-Line-Quadric (QLQ) and Fusion: User Weighting (UW)	Face and fingerprint	FERET [55]	*EER*: 0.63%
2005	Jain [48]	Normalisation: tanh and Fusion: Sum Rule	Face, fingerprint, and hand -geometry	Self acquired	*Acc*: 98.5%
Classifier-based					
1999	Yacoub [56]	SVM, Bayesian classifier, Decision trees, MLP, Fisher Linear Discriminant	Face and voice	XM2VTS [57]	*EER*: 1.00%
2000	Gutschoven [58]	SVM	Face and voice	M2VTS [59]	*FRR*: 2.70%, *FAR*: 0.00%
2003	Lu [60]	RBF Network	Face	ORL [61] Yale [62] AR [63]	*Acc*: 90.2%
2009	Vatsa [64]	Adaptive unification using 2ν-GSVM	Fingerprint	Law enforcement agency	*GAR*: 98.81%
Density-based					
2002	Prabhakar [65]	Likelihood Ratio	Fingerprint	Self acquired (167 subjects)	*EER*: 1.4%
2008	Nandakumar [47]	Likelihood Ratio with GMM	Multimodal	NIST Match Score [54] XM2VTS [66]	*GAR*: 99.1% *GAR*: 98.7%
2010	Vatsa [67]	Likelihood Ratio and SVM	Face	Heterogenous [67]	*GAR*: 94.98%
2013	Tao [68]	Naive Likelihood Ratio via ROC	Face	FRGC [69]	*EER*: $\approx$1.75%

Support Vector Machine (SVM), multilayer perceptron, decision trees, Fisher Linear Discriminant (FLD), and Bayesian classifier for combining match scores. From experimental results it is found that SVM and Bayesian classifier outperforms other approaches. Gutschoven et al. [58] have formulated the fusion problem as classification problem and proposed to solve this problem using SVM. This further substantiates the use of SVM for combining scores from different sources. In [60], the authors have combined three different face matchers using RBF network. The fusion results of RBF network are also compared with traditional sum rule. Vatsa et al. [64] proposed two unification frameworks that dynamically selects most appropriate fusion algorithm. The first framework is rule based approach in which evidence theoretic sum rule or Dezert Smarandache (DSm) function is applied depending upon the scenario. The second unification uses intelligent 2ν-Granular Support Vector Machine (2ν-GSVM) classification to dynamically select the fusion approach.

2.2.3   Density-based

In density based approaches based on Likelihood Ratio (LR) test, the genuine and imposter score densities are computed. These approaches improve the performance provided that densities are estimated carefully. Likelihood ratio fusion is preferred over other approaches like sum rule and SVM. The latter requires careful selection of parameters for instance finding an appropriate normalisation and integration approach in sum rule and choice of kernel and its associated parameters in SVM. Authors in [65] compute LR, which declares a person to be imposter for large values of LR and genuine for small values of LR. This ratio is used to combine four different fingerprint matching algorithms to improve the accuracy of fingerprint verification system. Nandakumar et al. [47] have combined the match scores using likelihood ratio test. The genuine and imposter match score distributions are modelled as finite Gaussian Mixture Model (GMM). The authors have also combined the quality scores within the fusion framework to further improve the performance of multimodal biometrics system. This approach need not care about the density parameters, which are estimated using GMM. A sequential fusion algorithm is proposed in [67] that combines likelihood ratio with support vector machine. Further a dynamic selection algorithm is designed that combines constituent matchers and fusion approaches to optimise the accuracy and computational time. Recently Tao et al. [68] proposed a fusion approach by estimating likelihood ratios of the fused biometric scores through individual ROC curves which construct Naive Bayes classifier. The value of matching scores, generated from an individual matcher, are integrated to find the ratio without explicit computation of densities. This fusion approach reduces the overhead of modeling the distributions and demonstrates higher fusion performance in comparison to SVM and GMM on a small sample size. Table 2.2 summarises various score based fusion approaches.

2.3   Indexing

The search space reduction approaches in biometrics are broadly classified into classification and indexing as shown in Figure 2.3. There exist very little research on classification as the search space is partitioned disproportionately. Existing indexing approaches are categorised into feature based and match score based depending upon the *index design*. Feature based indexing approaches are further classified into local, global, and hybrid categories based on the *type of features* used. Based on the *feature value*, global feature approaches are further sub-divided into real and binary categories. These indexing approaches are discussed in detail in the following sections.

2.3.1 Feature Based Indexing Approaches

These approaches are more reliable as the amount of information required to represent each biometric image is abundant. The biometric features are broadly classified into global and local categories [4]. Some approaches that combine both local and global features for indexing are discussed under hybrid category.

Global Features

In these schemes, the features are extracted without distinguishing an object from the background. This is particularly suitable under scenarios when the complete image describes potential features that can be used for identification. Indexing approaches in primitive stages are developed using global features. Ratha et al. [70] in early 90's proposed a multi-level indexing approach for fingerprint database which unifies the features such as pattern class and ridge density at higher level with elastic structural based matching at lower levels. This approach accelerated the research on indexing using global features as shown in Table 2.3. The global feature based approaches are further sub-divided based on the type of features being used. These approaches are discussed as follows:

Real Valued Features: Orientation or directional field is widely used for fingerprint indexing. Lumini et al. [71] proposed an indexing approach where directional image is registered with reference to its core point. The multi-dimensional feature vector is
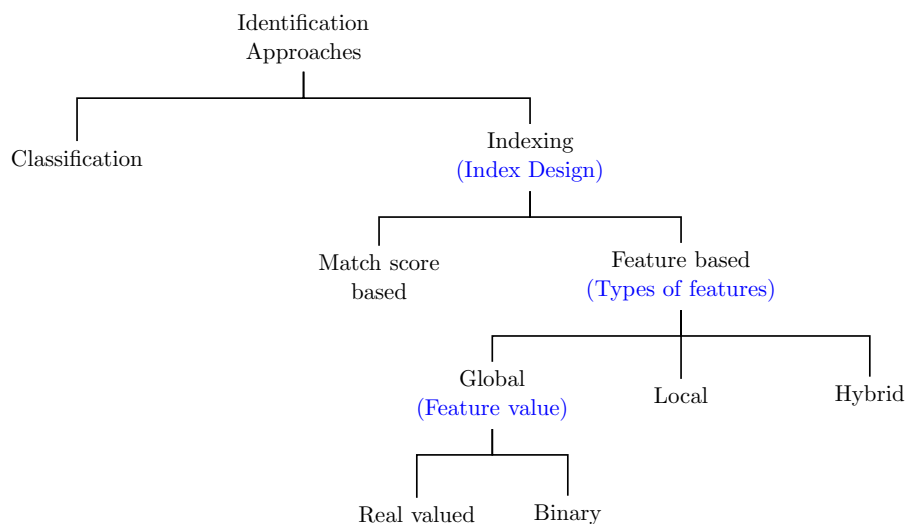
Figure 2.3: Proposed categorisation of indexing approaches that exist in literature. The text in blue indicates the basis of categorisation.

indexed using grid file approach. Some approaches use clustering to group features generated from a biometric trait. Mhatre et al. [72] have proposed a multimodal binning approach using hand geometry and signature biometrics. Liu et al [73] proposed modified form of k-means algorithm to partition the orientation feature space into clusters. For each cluster, the database is further divided into bins using Average Ridge Distance (ARD). The authors in [74] make use of two approaches for iris indexing. In the first approach, the features are extracted using Gabor wavelet [15] to generate the IrisCode. The second approach is based on statistical analysis of pixel intensities and positions of blocks in the iris texture.

Multi-dimensional tree based indexing approaches have gained significant attention recently due to its suitability to biometrics [75, 76]. Some iris specific schemes are developed for search space reduction using eye color [77]. In [78], the authors have proposed an indexing scheme using eye color for noisy iris images. The RGB color image is converted to YC_bC_r color space to generate an index for traversing the tree. Hashing is also used for searching records based on a key value. In [79], the authors have used hashing concept for indexing. They have reported several characteristics inherent to hashing. If collision free hash index is independent of database size then this could be directly used to find person's identity without any underlying algorithm. The hash function is generated from iris code and Kaurnaugh map is constructed for n-bit hashes. The drawback of existing global feature based approaches is that they use high dimensional data which is computationally costly. Dey et al. [80] reduces computational time by extracting Gabor energy features from an iris image at different scale and orientations.

Binary Valued Features: The features extracted from the biometric image are binarised to further speed up searching. An indexing approach for large fuzzy databases is explored by Feng et al. [83] using Beacon Guided Search (BGS). Despite of random bit errors, the iris codes from similar iris pattern are more likely to collide with same beacons. Gadde et al. [12] proposed an indexing approach using Burrows Wheeler Transform (BWT). Their indexing scheme is based on count of occurrence of n-bit binary patterns in normalised iris image.

Local Features

Local features are those patches of an image that differ from its neighborhood. They are extracted around special points or *keypoints*. The features extracted around each detected keypoint are stored as *descriptor*. Local features find correct correspondence between the gallery and probe images irrespective of large variations

Table 2.3: Chronological listing of global feature based indexing approaches.

Year	First Author	Approach	Modality	Database	Results
1996	Ratha [70]	Pattern class, ridge density and elastic structures	Fingerprint	NIST-9 [81]	**Pattern class:** Reduced to 25% and **Ridge density:** Reduces by another 50%
1997	Lumini [71]	Directional features reduced using KL transform and grid files for indexing	Fingerprint	NIST-4 [82]	PR: 6.90% with BM: 0.00%.
2005	Mhatre [72]	Binning features using vector quantisation	Signature and hand geometry	Self captured	PR: 5%, BM: 0%
2007	Liu [73]	Orientation field, ARD and k-means	Fingerprint	NIST-4 [82]	PR: 29.7%, ER: 2.9%
2008	Feng [83]	Beacon Guided Search (BGS)	Iris	UAE database	FAR: 0%, FRR: 0.55%, PR: 0.14%
2008	Mukherjee [74]	IrisCode and SPLDH	Iris	CASIA Version 3.0 (CASIAV3) [21]	IrisCode PR: 17%, HR: 80%, Texture analysis PR: 30%, HR: 84%.
2008	Puhan [78]	Iris color	Iris	UBIRIS [36]	HR: 97%, PR: < 25%
2010	Rathgeb [79]	Hashing and k-map	Iris	CASIA Version 3.0 [21]	PR : $\approx$ 3%, PG : 89.57%
2010	Gadde [12]	Burrows Wheeler Transform	Iris	CASIA Version 3.0 [21]	HR: 99.83%, PR: 17.23%, γ : 90.90%
2012	Dey [80]	Gabor energy features	Iris	Bath Database [29] CASIA Version 3.0 Interval [21] CASIA Version 4.0 Thousand [21] Multimedia University (MMU1) [84] West Virginia University [39]	PR: 14.5%, HR: 91.1%

in transformation, occlusion, and illumination. These features have shown good performance for biometrics recognition [41]. Due to the superiority of these features for recognition, an attempt has been made to apply them for indexing. Chronological listing of various local feature based indexing approaches are shown in Table 2.4.

Local feature based approaches are initially applied to fingerprint biometrics. Minutiae points are extracted from an input fingerprint image and an index is generated using minutiae triplet [85]. Flash approach proposed by Germain et al. [85] uses invariant properties of the minutiae to generate higher dimensional index. This approach has several limitations like triangle length is susceptible to distortions, ridge count, angle is dependent upon the image quality, and the minutiae locations may change. Another work proposed by Bhanu and Tan [87] is an extension of work done by Germain et al. [85]. This scheme generates an index using $H\left(\alpha_{min}, \alpha_{med}, \phi, \gamma, \eta, \lambda\right)$ where triangle's angles $(\alpha_{min}, \alpha_{med})$, triangle's handedness (ϕ), type based on types of

Table 2.4: Chronological listing of local feature based indexing approaches.

Year	First Author	Approach	Modality	Database	Results
1997	Germain [85]	Flash approach with triangle parameters to generate index	Fingerprint	Self constructed reference database of 97, 492 inked dab images	Average query time is 7 microseconds
1999	Bebis [86]	Delaunay triangles from minutiae triplets	Fingerprint	Self captured 300 images (30 persons)	CIP:[a] 93.16%
2003	Bhanu [87]	Parameters from triplets of minutiae	Fingerprint	Self acquired (100 individuals) NIST-4 [82]	CIP: 50%, PR: 0.33%
2005	Mhatre [88]	Pyramid technique	Hand geometry	Self captured images	PR: 8.86%, FRR: 0%
2010	Mehrotra [89]	SIFT and Geometric hashing	Iris	UBIRIS.v1 [36] BATH [29] CASIAV3 [21] IITK [90]	$PR = BM$: 24%
2011	Cappelli [91]	Minutiae cylinder codes and locality sensitive hashing	Fingerprint	NIST-4 [82] NIST-4 (Natural) [82] NIST-14 [92] FVC2000 DB2 [93] FVC2000 DB3 [93] FVC2002 DB1 [94]	PR: 1.59%, Error rate: $\approx 6.5\%$ on NIST-4
2011	Jayaraman [95]	SURF and enhanced geometric hashing	Ear and iris	IITK Ear database [90] UPOL Iris database [37]	HR: 100% for top 5 ranks
2012	Gago-Alonso [96]	Extended Delaunay triangles	Fingerprint	NIST-4 [82] NIST-4 (Natural) [82] NIST-14 [92] FVC2000 DB2 [93] FVC2000 DB3 [93] FVC2002 DB1 [94]	CIP: 99%, PR: 1% on FVC 2002 DB1
2013	Briseo [97]	Extended triplet and Delaunay triangles	Fingerprint	NIST-4 [82] NIST-4 (Natural) [82] NIST-14 (reduced) [92] FVC2000 DB3 [93] FVC2002 DB1 [94]	CIP: 98.5%, PR: 1% on FVC 2002 DB1

[a]Correct Index Power

minutiae (γ), direction of triangle (η), and maximum side (λ) are derived from the triangle formed using non-collinear minutiae points. Bebis et al. [86] proposed another approach for fingerprint identification which is based on the use of Delaunay triangles. For n number of minutiae, the number of Delaunay triangles produced is $O(n)$ in comparison to the number of all possible triangles considered which is $O(n^3)$ [85]. The existing indexing approaches are not capable enough to deal with spurious or missing minutiae and the available approaches are insufficient to handle the effect of noise. Another identification system using minutiae triplets and Delaunay triangles is proposed in [97]. This approach uses new representation of fingerprint based on the extension of Delaunay triangles. Further, a strategy is proposed to dismiss bad quality minutiae triplets which is found to be robust to distortions. In [96], a novel set

of features are introduced based on Delaunay triangles and triangular hulls which are robust to noise. Database indexes are generated using fingerprint features such as ridge contours, minutiae directions and triangle sign. During retrieval, the recommendation score is calculated and an approach to deal with noise is defined. This system performs better in comparison to existing Delaunay triangularisation based indexing approach.

Mhatre et al. [88] have used pyramid technique for indexing biometric databases. The d dimensional data space is divided into $2 \times d$ number of pyramids each having a common tip point and a $(d-1)$ dimensional base. The height and pyramid number is used to form key for indexing the B+ tree. The pyramid technique is specially designed to work with higher dimensional data and is invariant to order of insertion and scalable. Recently, Cappelli et al. [91] have proposed an indexing scheme using Minutiae Cylinder Codes (MCC). MCC features are invariant to translation, rotation, and robust against skin distortions. For index creation, Locality Sensitive Hashing (LSH) scheme is used.

Geometric Hashing is an indexing technique for model based object recognition. This is ab initio applied to biometrics by Mehrotra et al. [89]. The authors developed an indexing approach for iris using geometric hashing of SIFT keypoints. This approach is invariant to all possible transformations, occlusion, and non-uniform illumination. During iris retrieval, geometric hashed location from query iris image are obtained to access appropriate bin of the hash table and top matches are retrieved by majority voting as shown in Figure 2.4. An enhanced geometric hashing approach is proposed in [95]. In this approach, to handle all possible rotations each object is aligned using principal components of the feature points. Thus, each keypoint is inserted exactly once into the hash table. This reduces the space and time required to compute geometric invariants using basis pair [89].

Hybrid Approaches

Some approaches for indexing are developed that combines the merits of both global as well as local features. Since local and global features select independent characteristics, in certain cases it is advisable to perform indexing by combining both the features. This is done to belittle the limitations of either feature extraction approaches and simultaneously combine the merits of both. Hybrid approaches for indexing are listed in Table 2.5. Boer et al. [98] proposed an indexing approach using three features i.e., directional field estimate, fingercode, and minutiae triplets. In [99], a fingerprint retrieval approach is developed that combines the level-1 features (local ridge line orientation and frequencies) with level-2 features (minutiae). Li et al. [100] proposes palmprint retrieval approach using a layered scheme to filter the database where global

(a) Detected keypoints   (b) Select basis pair   (c) Keypoints after transformation   (d) After $\binom{n}{2}$ transformations

(e) Hash table occupancy   (f) Hash table after rehashing
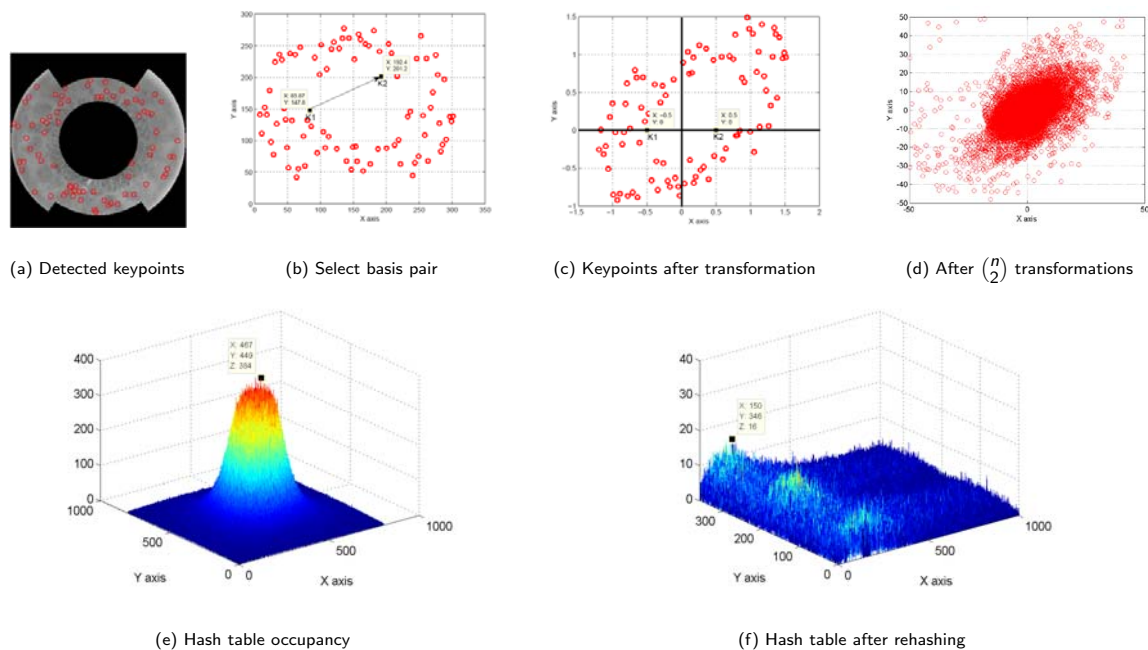
Figure 2.4: Geometric hashing based indexing approach using SIFT features [89].

Table 2.5: Hybrid feature based indexing approaches.

Year	First Author	Approach	Modality	Database	Results
2001	Boer [98]	Directional field estimate, fingercode and minutiae triplets	Fingerprint	FVC2000 DB2 [93]	*PR*: 18%, *HR*: 100%
2005	Li [100]	Texture energy features	Palmprint	Self acquired	*Acc*: 94.5%
2012	Cappelli [99]	Level-1 and Level-2 features	Fingerprint	NIST-4 [82] NIST-4 (Natural) [82] NIST-14 [92] FVC2000 DB2 [93] FVC2000 DB3 [93] FVC2002 DB1 [94]	*PR*: 20%, *BM*: 0.1%

features are used for filtering at coarse level followed by matching using local features at fine level.

2.3.2   Match Score based Indexing Approaches

Several approaches exist to biometrics database indexing using features. However, very little literature exist on indexing the biometrics database using match scores. This is primarily due to the need to generate and process score matrices which may increase an additional overhead. Match score based approaches on the other hand avoids the need to develop a trait specific feature extraction routine. The first attempt for database indexing using match score is proposed by Maeda et al [101]. This technique stores the matrix of all scores and is updated on addition of a new user. The main drawback of

Table 2.6: Match score based indexing approaches.

Year	First Author	Approach	Modality	Database	Results
2007	Gupta [102]	Wavelet transform and B+ Tree	Ear	IITK [90]	*HR*: 95.8%, *PR*: 34%
2009	Gyaourova [103]	Reference image and union fusion rule	Multimodal	FERET face database [55] WVU Multimodal [39]	*PR*: 3%, *HR*: 99%
2010	Paliwal [104]	SURF and VA+ file	Palmprint	PolyU [105]	*HR*: 98.01%

this approach is working with database of million users can be prohibitive. To reduce the dimensionality of features required for matching, anchor model based indexing approaches are proposed. Gupta et al. [102] proposed a scheme with only four match score values. The coefficients are generated from preprocessed biometric image using wavelet transform. The binarised approximation coefficients at second level is divided into four equal sized quadrants and Hamming Distance (HD) for each quadrant with respect to reference template of all ones is measured. This HD value is used to traverse the B+ tree for indexing. In [103], the modality specific index code is generated by computing match scores between the biometric image and fixed set of reference images as shown in Figure 2.5. During identification, the index code of probe image is compared against the enrolled identities. The output of potential matches are fused to further narrow down the list and increase the hit rate. Vector Approximation (VA+) file is used to index high dimensional match score database in [104]. The match score vectors are obtained by comparing each image in the database with all images in the training set. The match scores of all images in the database are indexed using VA+ file. This approach is found to be the most powerful match score based indexing approach. The summary of various match score based indexing approaches are shown in Table 2.6.
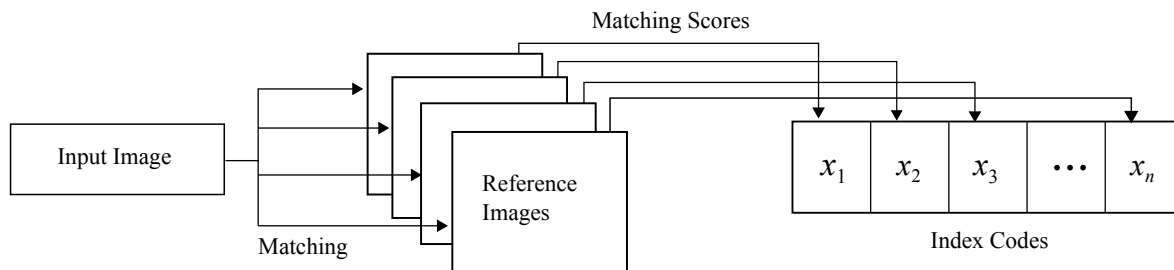
Figure 2.5: Index code generation using match scores [103].

2.4 Effect of Aging in Iris

Daugman mentioned that *iris is well protected from the environment and stable over time* [3, 106]. This fact is also supported with the case study of Sharbat Gula[1], the Afghan girl whose iris templates were matched after the age difference of 18 years. Owing to these characteristics of iris recognition, it is now used for authentication in several large scale government identification projects [5, 14]. However, recent research has claimed that iris recognition accuracy degrades over time [107, 108, 109, 110, 111]. Tome-Gonzalez et al. [107] studied the effect of time on the BiosecureID database with time lapse of maximum four months. The authors used Masek's iris matcher [112] to investigate the effect of aging and analysed that the intra-class variability increased over time with very little change in the impostor distribution. However, the time lapse considered for this study is very short (four months) and it is not justifiable to attribute aging to be the cause of performance reduction. Baker et al. [113] analysed aging in iris recognition for multi-year time lapse. 6,797 iris images of 23 subjects were captured using the LG2200 iris camera. To evaluate the FNMR across time, images were collected from the same subjects first at an interval of less than 120 days and then at an interval of more than 1200 days. The images used in this study were manually screened for quality checks. The performance was evaluated using Neurotechnology VeriEye SDK [17] along with two other matchers. The authors inferred that factors such as pupil dilation, contact lens, occlusion, and sensor aging could not account for increase in false non match rates. Fairhurst et al. [114] studied aging on 79 users with 632 images. They modified Masek's iris segmentation to reduce the segmentation errors and improve iris recognition accuracy. The authors concluded that dilation decreases with age and thus matching performance also reduces over time. Fenker and Bowyer [111, 16, 115] performed experiments with images pertaining to 322 subjects captured over a period of three years. They concluded that false non-match rate increases with time because of template aging.

Ellavarason and Rathgeb [116] re-investigated the two year time lapse database used by Fenker and Bowyer [109] with six different iris feature extraction algorithms. They also observed that change in FNMR from short to long time lapse is attributable to template aging. Sazonova et al. [117] examined the effect of elapsed time on iris recognition utilising 7628 images from 244 subjects acquired over time lapse of 2 years at Clarkson university. The authors also considered the impact of quality factors such as local contrast, illumination, blur, and noise on the iris recognition performance. The modified Masek's algorithm and VeriEye SDK were used for generating match

---

[1]Afghan Girl. http://en.wikipedia.org/wiki/Afghan_Girl

Table 2.7: Existing literature that supports aging in iris.

Year	First Author	Approach	Database	Time Lapse
2008	Gonzalez [107]	Masek [112]	BiosecureID	4 months
2011	Fairhurst [114]	Modified Masek [112]	79 subjects (632 images)	3 months
2012	Fenker [16, 111, 115]	VeriEye SDK [17]	322 subjects	3 years
2012	Sazonova [117]	Modified Masek's algorithm [112] and VeriEye SDK [17]	244 subjects (7628 images)	2 years
2012	Rankin [110]	Local and non-local operators	119 subjects	6 months
2013	Baker [113]	VeriEye SDK [17]	23 subjects (6,797 images)	4 years
2013	Ellavarason [116]	6 different matchers	86 subjects	2 years
2013	Czajka [118]	3 different matchers	58 subjects (571 images)	8 years

scores and the significance of quality factors for recognition were also demonstrated. They observed that the performance of both the matchers degrade with time. One recent research on aging by Czajka [118] used dataset of 571 images collected from 58 eyes with up to eight years of time lapse acquired from 2003 to 2011. The results obtained using three different matchers and genuine scores exhibit template aging. The authors claimed that more accurate matchers are highly vulnerable to aging. Rankin et al. [110] performed another study for aging using visible spectrum images in which the images were acquired from both the eyes of 119 subjects. Even for a short time difference of six months, 32 out of 156 comparisons resulted in false rejections. This performance was obtained by applying both local and non-local operators. These error rates are very high compared to other studies. The brief description of existing literature on iris aging is listed in Table 2.7. In response to Rankin et al. [110], Daugman and Downing [119] pointed out that their error rates were constant at all points in time studied, namely about 20%, showing no change in recognition accuracy over time. Recently, on two time-lapse datasets collected by law enforcement agencies, National Institute of Standards and Technology (NIST) IREX report [120] suggests that *population-averaged recognition metrics are stable, consistent with the absence of iris ageing.*

2.5   Observations

The existing literature has offered new insights into the domain of iris. Some key observations from the existing literature are:

- Several feature representation approaches of iris characterises the texture pattern using global features. Few approaches are developed using local features like SIFT and SURF. These approaches have shown to yield good results with the scope

for improvement.

- The transformation based fusion approaches fail to achieve accurate separation for the conflicting cases [51].

- The classifier based fusion approaches becomes biased towards the imposter class which is generally overpopulated. Performing fusion using density based approaches require careful estimation of the density parameters [47].

- Indexing approaches developed using global features fail to possess invariance to transformations [75, 76]. The local feature based indexing approach proposed in [89] performs with high bin miss rate of 24%.

- The match score based indexing approaches are independent of the modality. However, there is a need to generate and process score matrices which may increase an additional overhead [103].

- Researchers do not have a consensus on iris template aging. A proper analysis is required to understand the impact of aging on iris.

In this thesis, an endeavour has been made to address the aforementioned issues. The contributions span across different domains of iris biometrics as shown in Figure 2.6. To characterise iris pattern using local features, a keypoint descriptor is proposed that suitably describes texture. Further, a classifier is proposed for the fusion of left and right units of iris. The proposed classifier is designed to handle class imbalance in the training data. Local feature based indexing approaches are developed using multi-dimensional trees. The idea is to reduce the bin miss rate and penetration rate during the search process. Finally, an investigation is made to study the effect of aging in iris. The propositions of this thesis are discussed in detail in the subsequent chapters.
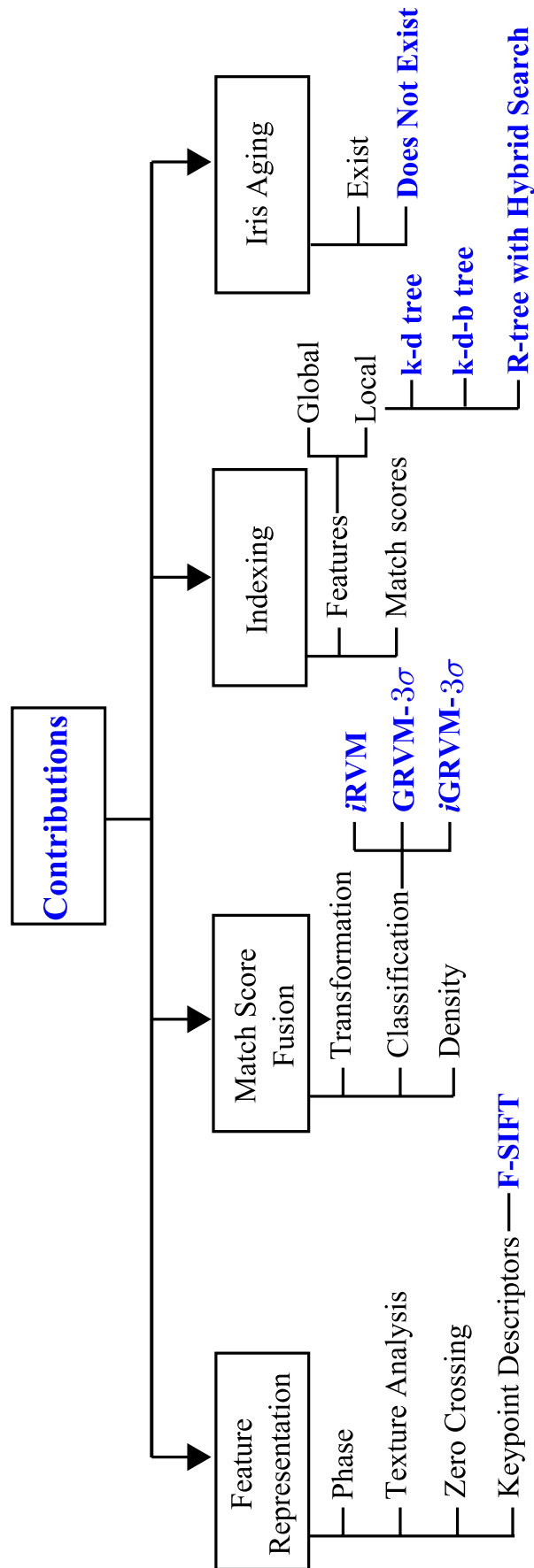
Figure 2.6: Contributions of this thesis (highlighted in blue).

Chapter 3

F-SIFT based Keypoint Descriptor for Iris

Traditional iris biometric systems perform recognition under controlled imaging scenarios where the subject is asked to gaze at the camera to acquire iris images illuminated with infrared light source [121]. Several real-time iris recognition systems like UIDAI [5] and UAE [18] also acquire images using the controlled setup. Traditional approaches have shown to yield good performance on real-time iris databases. However, existing feature representations suffer from few challenges like:

1. The texture patterns in iris are subject to change due to expansion and constriction of pupil for varying illumination as shown in Figure 3.1. This change in pattern can be visualised from the normalised iris images on the right. Once the pupil constricts (refer Figure 3.1(a)), the iris patterns are rendered more clearly whereas these patterns contract when iris image is dilated as shown in Figure 3.1(b). Such deformations in texture degrades the performance of iris.

2. The relative position of iris patterns change due to cyclotorsion which cannot be mapped to the same location in the polar coordinates. The change in gaze also deforms the pattern along its own axis which in turn transforms the texture pattern of iris as shown in Figure 3.2.

3. As reported in [13], the transformation of iris from Cartesian to polar space introduces aliasing artifacts.

The idea is to extract features directly from the annular iris image. Existing global feature extraction approaches cannot be applied directly to annular iris image. Local features find correct correspondences between the gallery and probe images irrespective of large variations. The well-known keypoint descriptors for local feature extraction are SIFT [45] and SURF [122]. The performance of these keypoint descriptors are

(a) Pupil constriction

(b) Pupil dilation
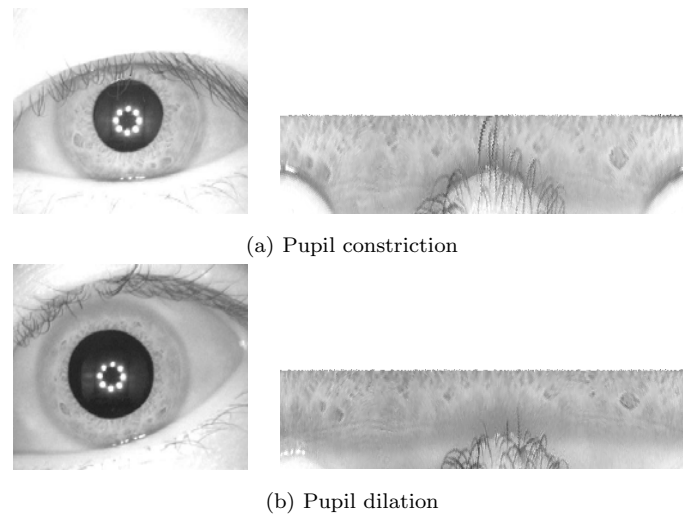
Figure 3.1: Effect of illumination on iris texture.

found to be encouraging as reported in [123]. The only limitation of existing keypoint descriptors is that, sometimes they wrongly pair two different regions of iris that possess texture similarity as shown in Figure 3.3. In this chapter, an endeavour has been made to develop a keypoint descriptor coined Fourier SIFT (F-SIFT) which combines the attributes of Fourier transform and SIFT. The input iris image is preprocessed to extract features directly from annular region of iris as explained in Section 3.1.

(a)

(b)
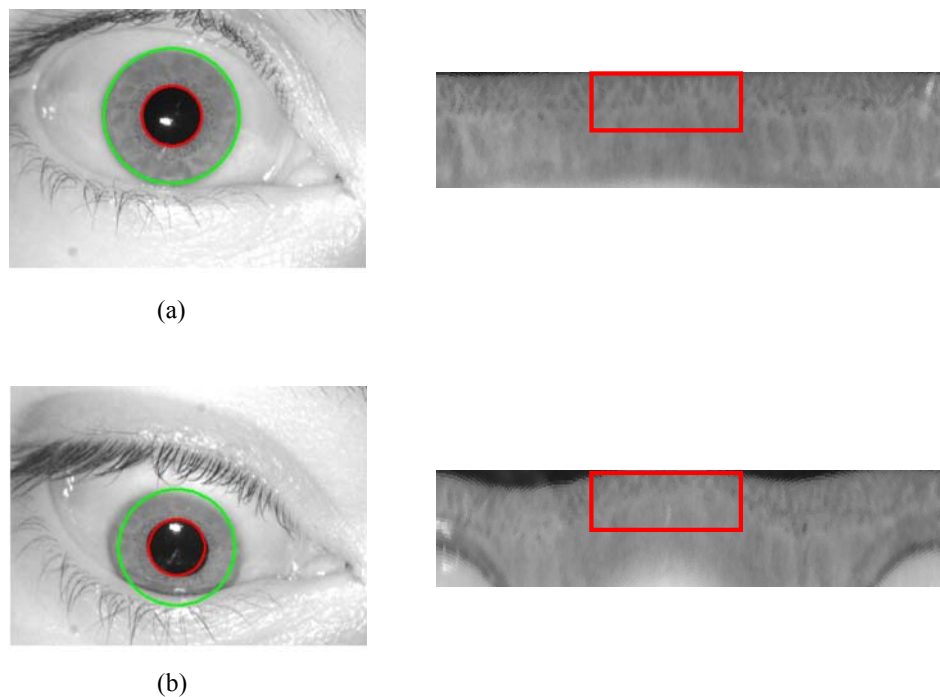
Figure 3.2: Iris images of a subject for change in gaze. The normalized iris images the demonstrate deformation of texture pattern.

Local feature extraction using F-SIFT is explained in Section 3.2. The keypoints described using Fourier transform are paired using Phase-Only Correlation (POC). The combination of SIFT with Fourier transform for feature extraction, and matching using Phase-Only Correlation performs better compared to state-of-the-art approaches as substantiated by the experimental results given in Section 3.3.
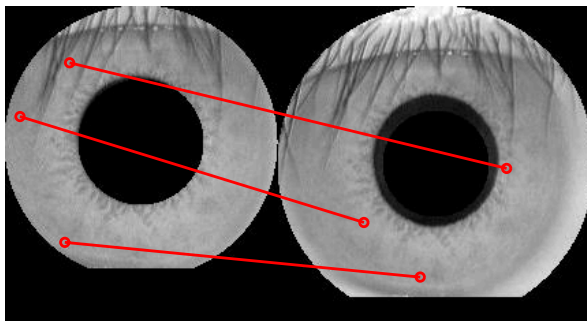
Figure 3.3: Sample impairments using SIFT due to texture similarity.

3.1 Preprocessing

The input iris image is preprocessed to detect annular region of iris for feature extraction. In the proposed approach, iris segmentation is performed using non-parametric spectrum image approach based on image morphology. This approach is preferred over existing segmentation approaches due to its simplicity, accuracy, and speed. The input iris image is binarised using adaptive threshold. Further, the pupil boundary is localised using spectrum image approach and iris circle is delineated using circular summation of intensities. For feature extraction, annular region underlying pupil and iris boundaries are considered after removing eyelids. The block diagram of proposed preprocessing approach is given in Figure 3.4.

Input Image　　Adaptive Threshold　　Pupil Detection　　Iris Detection　　Eyelid Detection　　Annular Iris
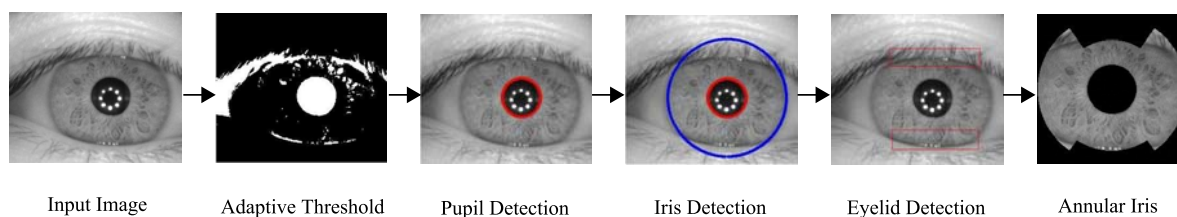
Figure 3.4: Block diagram of proposed preprocessing approach.

3.1.1 Adaptive Thresholding

Static value of threshold may fail for different images acquired under varying illumination conditions [124]. To find an adaptive threshold, the binary images are obtained for the range of thresholds (τ) which are further considered for removing specular highlights (holes). Morphological region filling approach is used to fill holes in the image. Each hole filled image is used to find the number of connected components (η) that changes for the change in value of threshold (τ). The value of τ corresponding to minimum non-zero η is chosen as adaptive value of threshold for binarisation [125].

3.1.2 Pupil Detection

A fast approach is used to find pupil circle without any pre-estimation of radius range as input unlike Circular Hough Transform [126]. The binary image is re-complemented to form the spectrum image [127]. The distance of every pixel in the binary image is obtained with nearest non-zero pixel. By computing the distance between non-zero pixels, the spectrum showing the largest filled circle can be formed within the set of foreground pixels. Since pupil is the largest filled circle in an iris image the overall intensity of the spectrum peaks in the center as shown in Figure 3.5.

3.1.3 Iris Detection

The contrast enhanced image is used to find the outer iris boundary by drawing concentric circles of different radii from the pupil center and the intensities lying over the perimeter of the circle are summed up. Among the candidate iris circles, the circle having maximum change in intensity with respect to the previous drawn circle is the outer iris boundary.

3.1.4 Sector based Annular Iris

Hugo et al. [13] have raised the problem of aliasing that occurs during transformation of iris from Cartesian to polar space. In this thesis, the problem of aliasing is addressed by directly considering the *annular region* of iris without normalisation. Further, the annular region contains noise due to eyelids and eyelashes that should be detected and removed. In a normal gaze, the edge of the upper eyelid intersects the sclera and approximately half of the upper iris circle whereas lower eyelid covers one-fourth of the lower iris circle. However, the left and the right regions are independent of

such occlusions. The proposed sector based approach consider these regions free from occlusions [89] [123].

(a)   (b)   (c)   (d)

(e)   (f)   (g)   (h)
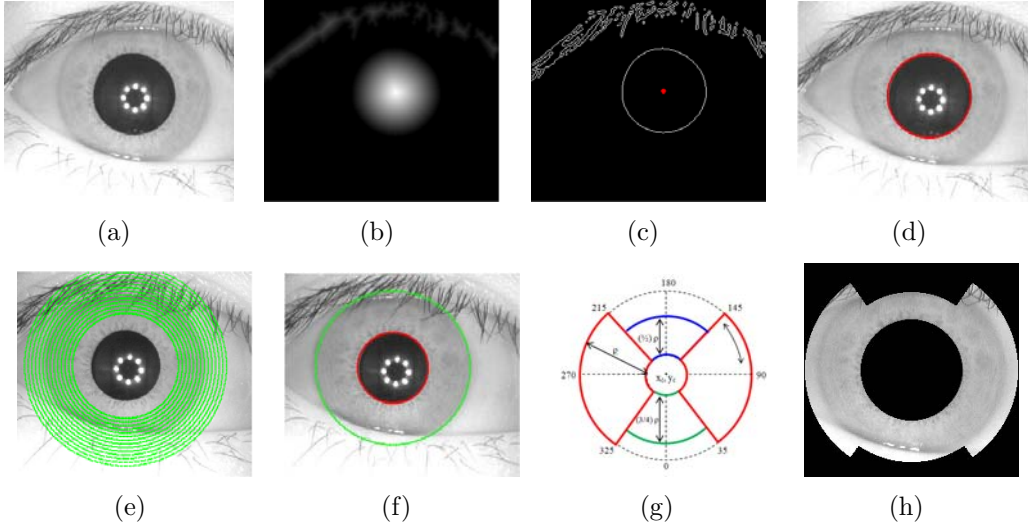
Figure 3.5: Steps involved in proposed preprocessing approach. (a) input iris image, (b) spectrum image, (c) edge detected image with center, (d) pupil localised image, (e) concentric circles of different radii, (f) iris localised image, (g) geometrical representation of sectors, and (h) noise independent annular iris.

3.2 Proposed Fourier-SIFT

The impairments in SIFT pairing can be minimised by extracting features suitable to iris texture. Fourier transform has the property of describing periodic function such as texture that contains repetitive patterns [128]. Further, SIFT is robust to various possible transformations, occlusion, and illumination. This motivates the unique combination of SIFT with Fourier transform for efficient iris recognition. In the proposed F-SIFT approach, the keypoints are detected using SIFT and each keypoint is described using Fourier transform. The pairing of keypoints using phase information of Fourier transform further improves the performance. The block diagram of proposed F-SIFT approach is shown in Figure 3.6. The steps involved in iris recognition using F-SIFT are explained in the sequel.

3.2.1 Keypoint Detection using SIFT

The first step is to find potential keypoints that are invariant to scale and orientation. For each detected keypoint a detailed model is fit to determine location and scale. The
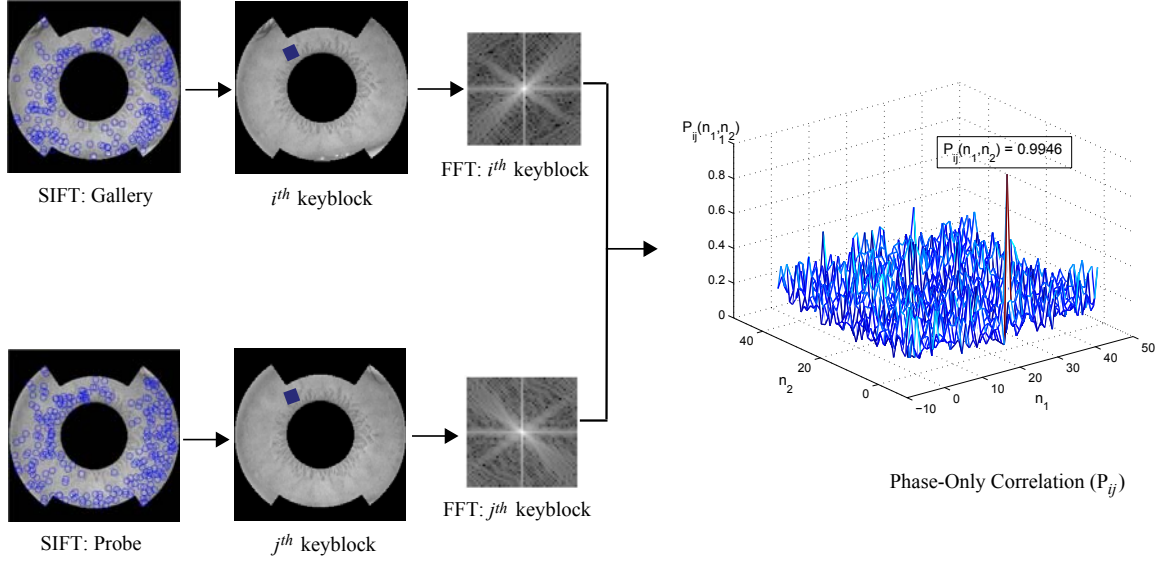
Figure 3.6: Block diagram of proposed F-SIFT approach.

orientation is assigned to each location based on image gradients. The steps involved in keypoint detection are explained in this section.

Detection of Scale Space Extrema For keypoint detection, there is a need to identify stable locations that can be assigned with change in viewpoint and scale. Such locations, invariant to scale change, can be found by searching stable features across all possible scales using a continuous function known as scale space [45]. The only possible scale space function is Gaussian function. Therefore, scale space of an image is defined as:

$$L(x, y, \sigma) = G(x, y, \sigma) * I(x, y) \tag{3.1}$$

where $I(x, y)$ is an input image and $*$ is the convolution operation.

$$G(x, y, \sigma) = \frac{1}{2\pi\sigma^2} e^{-\frac{(x-y)^2}{2\sigma^2}} \tag{3.2}$$

To detect stable keypoint locations in the scale space, Difference of Gaussian (DOG) function is convolved with the image. The DOG for two nearby scales of an iris image I is computed as

$$
\begin{aligned}
D(x, y, \sigma) &= (G(x, y, k\sigma) - G(x, y, \sigma)) * I(x, y) \\
&= L(x, y, k\sigma) - L(x, y, \sigma)
\end{aligned}
\tag{3.3}
$$

where k is a constant multiplicative factor used for changing the scale. This scale invariant technique is found to be suitable for annular iris image because the size of

iris texture changes due to expansion and contraction of pupil as shown in Figure 3.1.

Keypoint Localisation DOG images are used to detect interest points with the help of local maxima and minima across different scales. Each pixel in DOG image is compared to 8 neighbours in the same scale and 9 neighbours in the neighbouring scales. The pixel is selected as a candidate keypoint if it is local maxima or minima in 3×3×3 region as shown in Figure 3.7(a). Once the keypoints are detected the next step is to perform the detailed fit to the nearby data for location, scale, and ratio of principal curvature. The basic idea is to reject keypoints with low contrast. In [45] it is stated that keypoints with low contrast are sensitive to noise or poorly localised, hence they should not be considered. The stable set of keypoints detected using SIFT, are essentially required for matching iris images with non-centered gaze as shown in Figure 3.2.

Orientation Assignment Orientation is assigned to each keypoint location to achieve invariance to image rotations as the descriptor can be represented relative to orientation. To determine keypoint orientation, a gradient orientation histogram is computed in the neighbourhood of keypoint. The scale of the keypoint is used to select Gaussian smoothed image L. For each Gaussian smoothed image $L(x, y)$, magnitude $(m(x, y))$ and orientation $(\theta(x, y))$ are computed as

$$m(x,y) = \sqrt{(L(x+1,y) - L(x-1,y))^2 + (L(x,y+1) - L(x,y-1))^2} \qquad (3.4)$$

$$\theta(x,y) = \tan^{-1}\left(\frac{(L(x,y+1) - L(x,y-1))}{(L(x+1,y) - L(x-1,y))}\right) \qquad (3.5)$$

Orientation histogram is then formed for gradient orientation around each keypoint. The histogram has 36 bins for 360 orientations, and each sample is weighted by gradient magnitude and Gaussian weighted circular window with σ of 1.5 times of scale of the keypoint before adding it to the histogram. Peaks in the histogram correspond to orientation and any other local peak within 80% of the largest peak is used to create keypoint with the computed orientation. This is done to increase stability during matching [45].

3.2.2 Keypoint Descriptor using Fourier Transform

The descriptor vector is formed by taking a window $(W \times W)$ around each detected keypoint centered at (x, y) relative to the direction of orientation (θ). The local descriptor is defined for each keyblock (refer Figure 3.7(b)) using Fourier transform. As
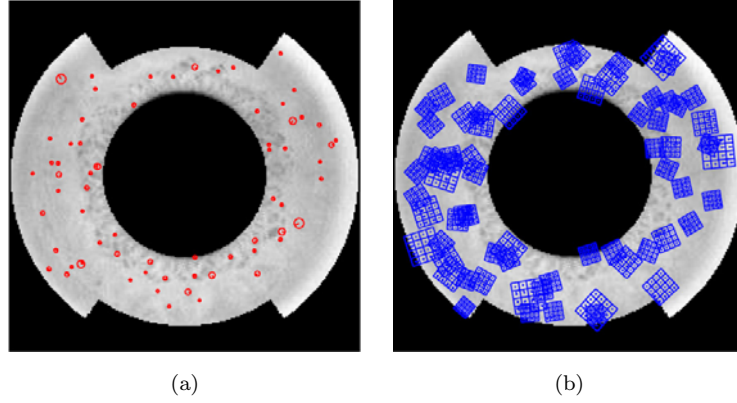
Figure 3.7: Application of SIFT on annular iris image (a) detected keypoints, (b) feature descriptor.

iris has abundant texture information, the Fourier transform efficiently describes the global frequency content of each block. The basic idea is to use phase information of the Fourier transform to robustly define texture pattern. Descriptor of each keyblock is obtained using

$$
\begin{aligned}
K_i(u,v) &= \frac{1}{W^2} \sum_{n_1=(x-\frac{W}{2})}^{(x+\frac{W}{2})} \sum_{n_2=(y-\frac{W}{2})}^{(y+\frac{W}{2})} I(n_1,n_2) e^{-i2\pi(\frac{n_1 u}{W}+\frac{n_2 v}{W})} \\
&= A(u,v) e^{i\theta(u,v)}
\end{aligned} \tag{3.6}
$$

where $u > 0$ and $(x - \frac{W}{2}) \leq u \leq (x + \frac{W}{2})$, $v > 0$ and $(y - \frac{W}{2}) \leq v \leq (y + \frac{W}{2})$. Here $A(u,v)$ are the amplitude components of each keyblock and $\theta(u,v)$ are the phase components for each keyblock.

3.2.3 Keypoint Pairing using POC

The keypoints are paired between gallery and probe iris images using phase based image matching. The phase information between i^{th} keyblock in the probe image is paired to j^{th} keyblock in gallery image using Phase-Only Correlation (POC) function [129]. This approach has already been applied to normalised iris image and its subregions [19]. In this chapter, the local descriptors of two keypoints are paired using POC. Let, $A_i(u,v)$ and $\theta_i(u,v)$ be the amplitude and phase components of Fourier transform from i^{th} keyblock. Similarly, $A_j(u,v)$ and $\theta_j(u,v)$ be the amplitude and phase components from j^{th} keyblock. Thus, cross phase spectrum between K_i and K_j is obtained using

$$
R_{ij}(u,v) = \frac{K_i(u,v)\overline{K_j(u,v)}}{|K_i(u,v)K_j(u,v)|} \tag{3.7}
$$

(a) P_{ij}: Similar region   (b) P_{ij}: Dissimilar region
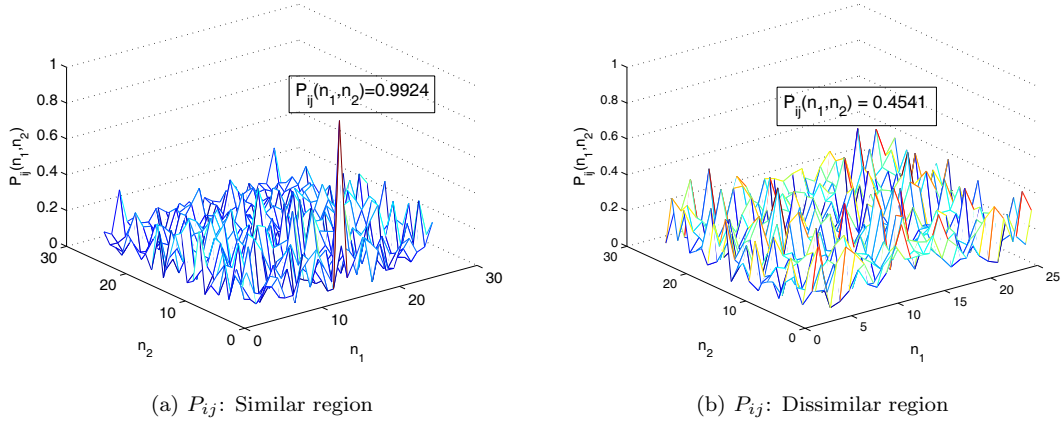
Figure 3.8: Phase-Only Correlation between (a) similar and (b) dissimilar keyblocks from iris.

$$= e^{i\{\theta_i(u,v) - \theta_j(u,v)\}}$$

where $\overline{K_j(u,v)}$ denotes the complex conjugate. The POC function (P_{ij}) is the inverse Fourier transform of cross phase spectrum (R_{ij}) which is defined as

$$P_{ij}(n_1, n_2) = \frac{1}{W^2} \sum_{u=(x-\frac{W}{2})}^{(x+\frac{W}{2})} \sum_{v=(y-\frac{W}{2})}^{(y+\frac{W}{2})} R_{ij}(u,v) e^{i2\pi(\frac{n_1 u}{W} + \frac{n_2 v}{W})} \tag{3.8}$$

This POC function helps to define the similarity between two keyblocks. If keyblocks are from similar texture regions of iris, their POC function gives a distinct sharp peak as shown in Figure 3.8(a). However, if keyblocks (i, j) are taken from two dissimilar regions of iris the peak drops significantly (refer Figure 3.8(b)). The height of the peak can be taken as a good similarity measure for pairing the keyblocks. If the peak in P_{ij} is greater than the threshold, the corresponding keyblocks (i, j) are paired and removed from the list of keypoints left to be paired. This process is iterated for the remaining keypoints in the probe set. Here, the value of threshold is empirically chosen to attain the highest performance.

3.3 Experimental Results

The experiments are performed to compare the proposed F-SIFT descriptor with existing SIFT and SURF descriptors [123]. Table 3.1 shows the accuracy values along with error rates for the different approaches. From the accuracy values it can be observed that F-SIFT performs better than the traditional SIFT on annular iris image. The traditional SIFT is performing with an accuracy of 92.08% and 85.19% on BATH

and CASIAV3 databases. The accuracy using F-SIFT improves to 97.13% and 97.95% for BATH and CASIAV3 databases respectively. F-SIFT is also capable of achieving FNMR of 0.0% on CASIAV3 database. F-SIFT performs comparable to SURF on BATH database whereas, it outperforms SIFT and SURF on CASIAV3 databases. The texture discrimination is quite high for CASIAV3 database which results in enhanced performance using F-SIFT. This supports the use of texture features for iris to improve recognition accuracy. The ROC curves for BATH and CASIAV3 databases are shown in Figure 3.9(a) and Figure 3.9(b) respectively. The distribution of genuine and imposters matching scores using various keypoint descriptors are shown in Figure 3.10 and Figure 3.11 for BATH and CASIAV3 databases respectively. From the histogram plot of F-SIFT for CASIAV3 it is graphically evident that no genuine individual is rejected by the system (refer Table 3.1).

Table 3.1: Recognition performance (in %) for SIFT, SURF, and F-SIFT.

Database →	BATH			CASIAV3		
Approach ↓	ACC	FMR	FNMR	ACC	FMR	FNMR
SIFT	92.08	7.01	8.82	88.76	8.80	13.67
SURF	**98.24**	1.44	2.06	96.52	2.16	4.78
F-SIFT	97.13	0.72	5.00	**97.95**	4.09	**0.00**
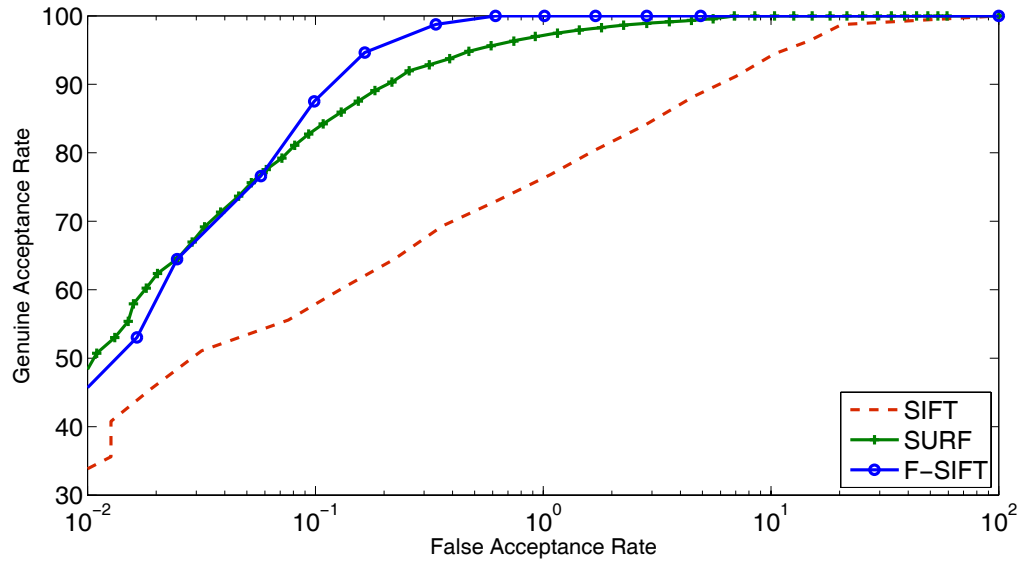
(a) **BATH**
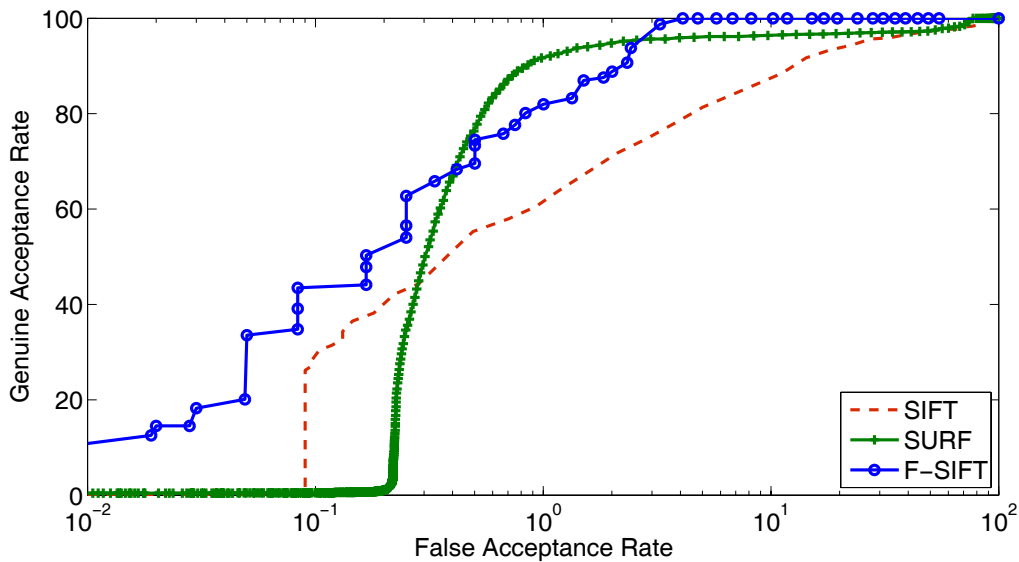
(b) **CASIAV3**

Figure 3.9: Receiver operating characteristic curves comparing SIFT, SURF, and F-SIFT approaches.

3.4 Summary

In this chapter, a keypoint descriptor is proposed that effectively describes the iris texture. The keypoints are detected from annular iris image using conventional SIFT. Each keypoint is described using Fourier transform. The phase information of Fourier transform is used for pairing the keypoints. This helps to minimise the impairments that occur due to SIFT. As iris has abundant texture details hence characterising

42
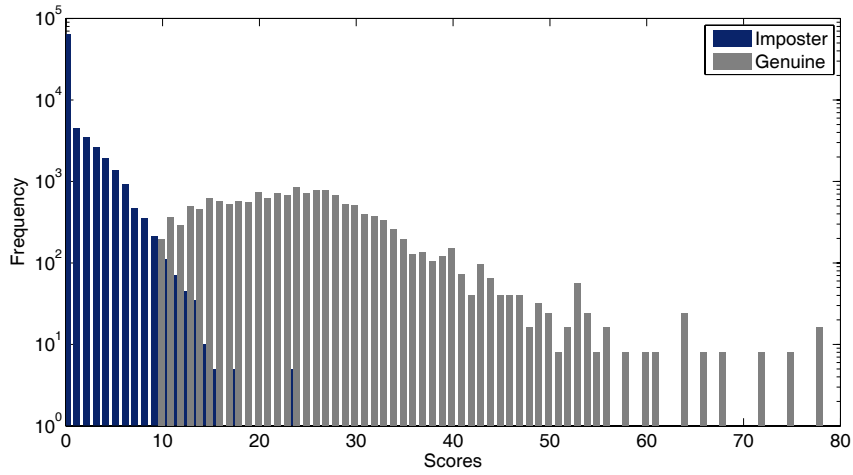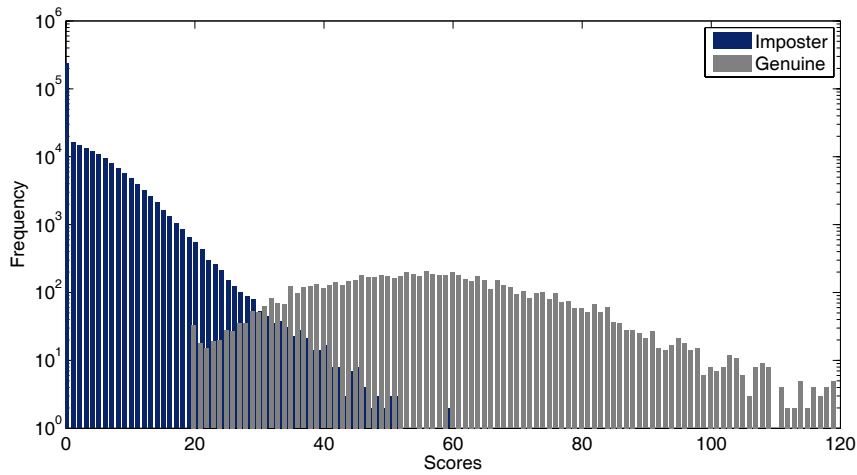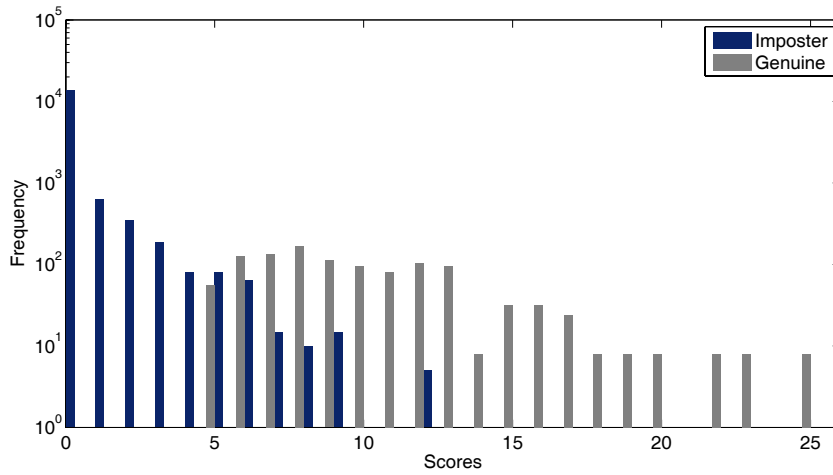
(a) **SIFT**

(b) **SURF**

(c) **F-SIFT**

Figure 3.10: Distribution of genuine and imposter scores on BATH database.
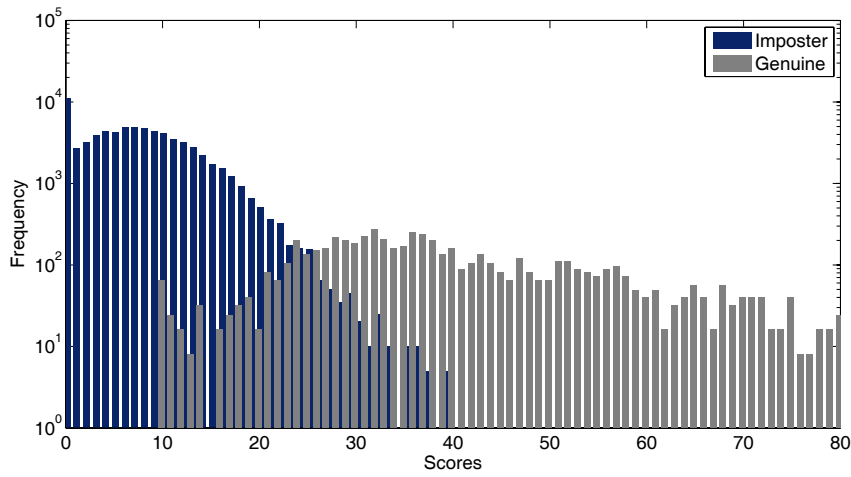
(a) **SIFT**
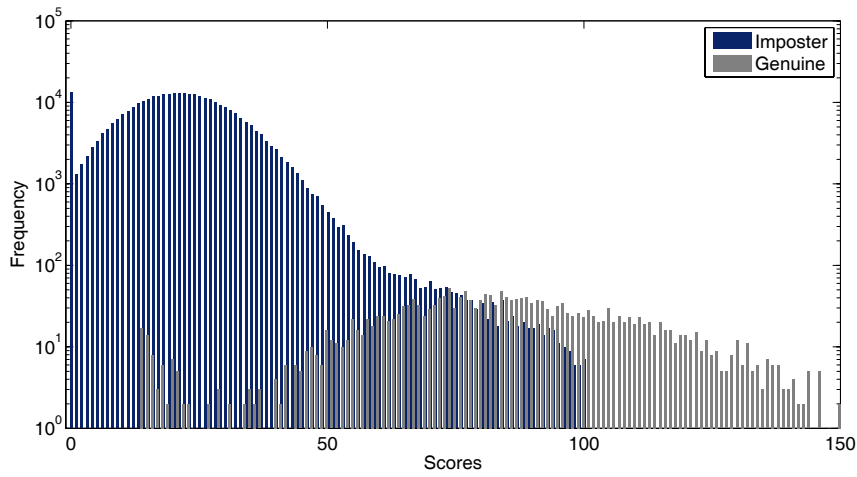
(b) **SURF**
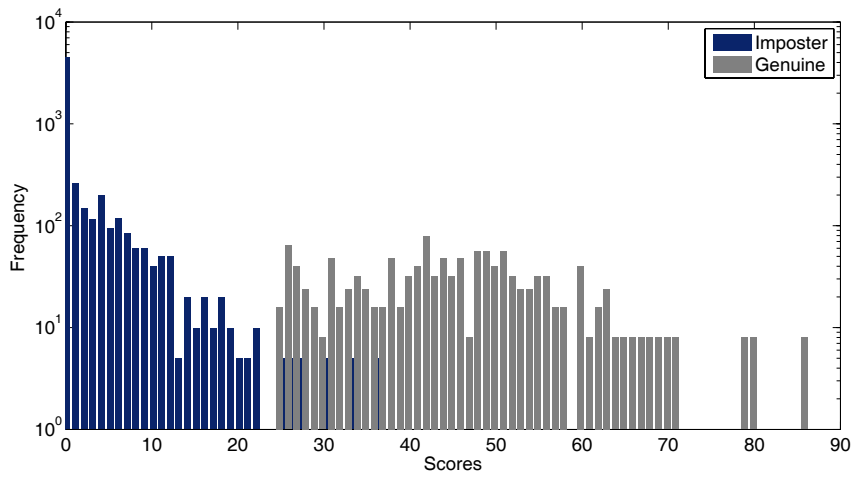
(c) **F-SIFT**

Figure 3.11: Distribution of genuine and imposter scores on CASIAV3 database.

iris using Fourier transform enhances the performance. Empirically it is found that the proposed approach outperforms other keypoint descriptors on CASIAV3 database whereas the performance is comparable to SURF on BATH iris database.

Chapter 4

*i*GRVM for Multi-unit Iris Fusion

Iris recognition using single instance may suffer from various challenges such as noisy sensor data, mis-localisation, occlusion due to eyelids, effect of disease like cataract, and spoof attacks. Figure 4.1 shows instances where the use of only one iris may cause incorrect classification whereas the use of both the iris images may provide correct and improved classification performance. In the first row, the iris boundary of left unit is incorrectly detected due to the presence of reflection. The left image in the second row could not be segmented but the right image is segmented properly. Similar observation can be made in the third row with the effect of dilation and occlusion in the right iris image. These limitations are addressed by combining left and right units of iris which is useful when data from one unit is noisy or unavailable.

In this chapter, *classifier-based* match score level fusion approaches are developed due to its suitability to biometrics [47, 58, 130]. Generally, a classical pattern recognition application relies on a classifier which predicts the class label of the probe data. For example, in a two class biometrics verification (class labels being *genuine* and *imposter*), match scores generated by matching gallery and probe images has to be classified correctly. Generally, it is assumed that the representative training data is available during the development stage and in such cases, the trained classifier yields high classification accuracy. There are certain limitations to this assumption:

- there exists the possibility that the entire training data is not available simultaneously. For example, in the case of India's Aadhaar project [5] or US-VISIT program [131], users are enrolled on a continuous basis. In such a scenario, training data is available only in an incremental manner. Training the classifiers in batch mode with every incremental update can be computationally expensive.

- training databases can be highly unbalanced where data from one class is

Left   Right
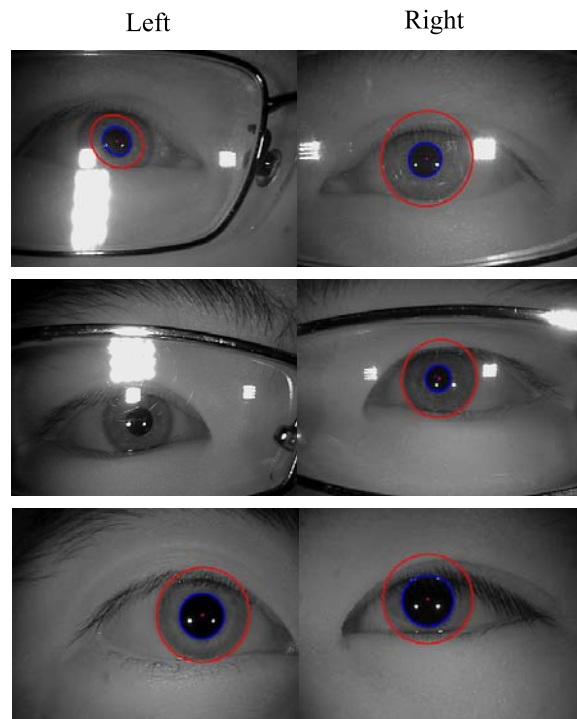
Figure 4.1: Sample instances where authentication using single iris may fail, however using both the irises can solve the problem.

over-populated compared to other class(es). In biometrics, the number of genuine scores available for training is under-represented in comparison to impostor scores.

- some classifiers are inherently computationally expensive, they perform well if the training size is small but on large training data they may require significant time or become intractable.

Different classifiers such as linear threshold, Bayesian network, and Support Vector Machine [132] require labeled training data to learn the decision boundary. Support Vector Machine has shown to yield good results in several pattern classification problems including biometrics. It avoids overfitting and leads to good generalisation by finding the separating hyperplane that maximises the margin width. The subset of training data points used to represent the hyperplane are denoted as support vectors. However, SVM suffers from the following limitations [133]:

1. the number of support vectors required for classification is relatively large,

2. in classical SVM, there is a need to tune the regularisation parameter during the training phase,

3. the kernel function must satisfy the Mercer condition.

Relevance Vector Machine (RVM) [133], on the other hand, is a fully probabilistic classifier which introduces a prior over each weight governed by the set of hyper-parameters. RVM is a sparse linearly parameterised model like SVM and it has been shown that the generalisation performance of RVM is comparable to that of SVM with significantly fewer relevance vectors [133]. Lower number of relevance vectors leads to reduced testing time. Further, RVM requires very few parameters to be optimised for training the classifier. However, RVM has the following challenges owing to which it has not been well explored particularly in biometrics.

1. Conventional RVM cannot work with very large training data as the formulation requires expensive matrix inverse operation. Further, the amount of memory required to store the product of basis functions limits its utilisation for considerably large training databases.

2. RVM is trained in batch mode and if new batch of training data arrives, the classifier has to be re-trained with new as well as old data. This is not feasible for many real-time applications such as biometrics where it may be required to continuously update the classifier to adjust the changes (in data and template) that happen over time.

3. RVM may not be suitable to handle large class imbalance in the training data and may get biased towards the class with more number of training samples.

In this chapter, incremental granular RVM is proposed that can be trained with large unbalanced training data to perform efficient classification. As shown in Figure 4.2, the learning process starts by considering batches of training data which are divided into granules. The RVM is trained on each granule independently and the results are amalgamated to obtain a robust boundary for classification. The knowledge from the previous training is carried forward to the next learning batch. The major contributions of this research are:

1. **Incremental RVM** (*i*RVM) is proposed which is scalable to new enrollments and also reduces the training size.

2. **Granular RVM** (GRVM) handles the class imbalance problem by training the classifier locally for each granule.

3. **Incremental Granular RVM** (*i*GRVM) combines the advantages of incremental and granular learning into RVM.
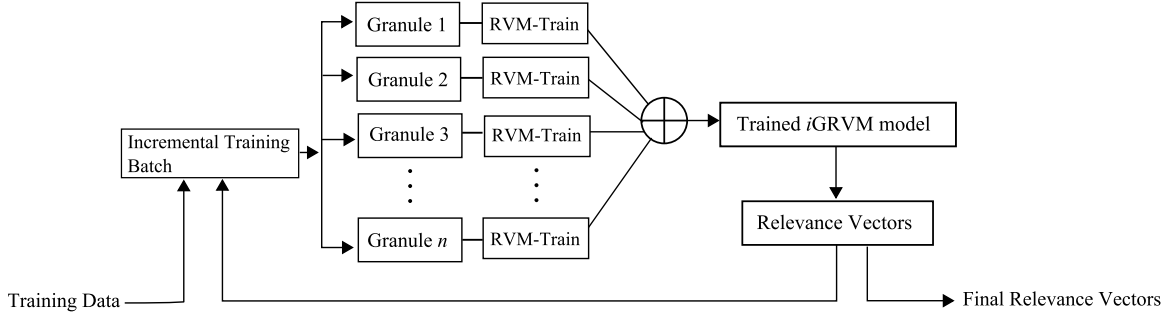
Figure 4.2: Block diagram of Incremental Granular Relevance Vector Machine (*i*GRVM).

4. **Efficient fusion approach** for multi-unit iris recognition using proposed *i*GRVM.

This chapter is organised as follows— Section 4.1 provides the formulation of conventional RVM for classification. The description of proposed incremental granular RVM is given in Section 4.2. The performance of *i*GRVM is evaluated using a case study on multimodal biometrics with two classes (genuine and imposter) as given in Section 4.3. The results obtained encouraging which promotes the application of *i*GRVM for multi-unit iris fusion as presented in Section 4.4. Section 5.4.5 analyses the results obtained on multi-unit iris databases.

4.1 Relevance Vector Machine for Classification

This section briefly discusses the formulation of RVM [133]. Let $\{\mathbf{x}_n, t_n\}_{n=1}^N$ be the pair of input data $(\mathbf{x}_n)$ with scalar valued target label (t_n). RVM by design follows a Bayesian probabilistic model for learning and the predictions are based on the function

$$y = \boldsymbol{\Omega}^T \Phi(\mathbf{x}) \tag{4.1}$$

where $\boldsymbol{\Omega} = (\omega_0, \omega_1, \omega_2, \ldots, \omega_N)^T$ is the weight matrix, $\Phi(\mathbf{x}) = [\phi(\mathbf{x}_1), \phi(\mathbf{x}_2), \ldots, \phi(\mathbf{x}_N)]^T$ is a set of basis functions, for $\phi(\mathbf{x}_n) = [1, K(\mathbf{x}_n, \mathbf{x}_1), K(\mathbf{x}_n, \mathbf{x}_2), \ldots, K(\mathbf{x}_n, \mathbf{x}_N)]$ with $K(*, *)$ is the kernel function which can be of the form Gaussian, Euclidean, Laplacian, etc. The output of RVM (y) is a linear combination of weighted basis functions. The weights $(\boldsymbol{\Omega})$ are computed during training and the training samples corresponding to non-zero weights are called *relevance vectors* (RVs). The objective of learning the classifier is to predict the posterior probability of class membership for the given input $\mathbf{x}$. The linear model in Equation (4.1) is generalised by applying the logistic sigmoid link function

49

$\sigma(y) = 1/(1 + e^{-y})$ to y and adopting the Bernoulli distribution to define the likelihood as

$$P(\mathbf{t}|\boldsymbol{\Omega}) = \prod_{n=1}^{N} \sigma\{y(\mathbf{x}_n, \boldsymbol{\Omega})\}^{t_n} [1 - \sigma\{y(\mathbf{x}_n, \boldsymbol{\Omega})\}]^{1-t_n} \tag{4.2}$$

To obtain the marginal likelihood analytically, Mackay's iterative procedure [134] is used which is based on the Laplace's method. Let α be the vector of hyperparameters and each individual α value is associated with every weight value. For the fixed values of α, the most probable weights $\mathbf{w}$ are found, giving location of the mode of posterior distribution [133]. Since

$$p(\boldsymbol{\Omega}|\mathbf{t}, \alpha) \propto P(\mathbf{t}|\boldsymbol{\Omega})p(\boldsymbol{\Omega}|\alpha), \tag{4.3}$$

this is equivalent to finding the maximum of

$$\log\{P(\mathbf{t}|\boldsymbol{\Omega})p(\boldsymbol{\Omega}|\alpha)\} = \sum_{n=1}^{N} [t_n \log y_n + (1-t_n)\log(1-y_n)] - \frac{1}{2}\boldsymbol{\Omega}^T\mathbf{A}\boldsymbol{\Omega} \tag{4.4}$$

over $\boldsymbol{\Omega}$, where $y_n = \sigma\{y(\mathbf{x}_n, \boldsymbol{\Omega})\}$. Equation (4.4) is differentiated twice to obtain

$$\nabla_{\boldsymbol{\Omega}}\nabla_{\boldsymbol{\Omega}} \log p(\boldsymbol{\Omega}|\mathbf{t}, \alpha)|_{\mathbf{w}} = -(\Phi^T\mathbf{B}\Phi + \mathbf{A}) \tag{4.5}$$

where $\mathbf{A} = \text{diag}(\alpha_0, \alpha_1, \alpha_2, \ldots, \alpha_N)$ and $\mathbf{B} = \text{diag}(\beta_1, \beta_2, \ldots, \beta_N)$ with $\beta_n = \sigma\{y(\mathbf{x}_n)\}[1 - \sigma\{y(\mathbf{x}_n)\}]$. The covariance matrix Σ and the posterior over weights centered at $(\mathbf{w})$ are defined as

$$\Sigma = (\Phi^T\mathbf{B}\Phi + \mathbf{A})^{-1} \tag{4.6}$$

$$\mathbf{w} = \Sigma\Phi^T\mathbf{B}\mathbf{t} \tag{4.7}$$

Using Σ and $\mathbf{w}$, the hyper-parameters are updated using

$$\alpha_i = \frac{\gamma_i}{\mathbf{w}_i^2} \tag{4.8}$$

where $\mathbf{w}_i$ is the ith posterior weight computed using Equation (4.7), $\gamma_i \equiv 1 - \alpha_i\Sigma_{ii}$ and Σ_{ii} is the ith diagonal element of Σ. Similarly, β is updated using

$$\beta = \frac{N - \sum_i \gamma_i}{\|\mathbf{t} - \Phi\mathbf{w}\|^2} \tag{4.9}$$

The convergence criteria for the above iterative procedure is defined as

$$\delta = \sum_{i=1} \alpha_i^{n+1} - \alpha_i^n \tag{4.10}$$

Re-estimation stops when $\delta < \delta_\tau$, where δ_τ is the threshold value for change of α between iterations. The training samples corresponding to $\mathbf{\Omega} \neq 0$ are termed as relevance vectors ($\mathbf{R}$). The weights and relevance vectors obtained from Algorithm 1 are used to find an estimate of the target value pertaining to the new input x'

$$y' = \mathbf{w}^T \phi(x') \tag{4.11}$$

where y' is the probabilistic class value predicted by the trained model. This classification algorithm is provided in Algorithm 2.

Algorithm 1: RVM-Train

Input: $\mathbf{x}$: Input matrix of N scores with dimension d, $\mathbf{t}$: corresponding target values

Output: $\mathbf{R}$: model of relevance vectors, $\mathbf{w}$: weight matrix

1 Generate $\Phi = [\phi(\mathbf{x}_1), \phi(\mathbf{x}_2), \ldots, \phi(\mathbf{x}_N)]$

2 Initialise δ_τ `// Threshold for convergence`

3 Initialize α, β `// Initialisation of hyper-parameters`

4 **repeat**

5     $\mathbf{A} = \text{diag}(\alpha), \mathbf{B} = \text{diag}(\beta)$

6     $\Sigma = (\Phi^T \mathbf{B} \Phi + \mathbf{A})^{-1}$

7     $\mathbf{w} = \Sigma \Phi^T \mathbf{B} \mathbf{t}$

8     $\gamma_i \equiv 1 - \alpha_i \Sigma_{ii}$

9     $\alpha_i = \frac{\gamma_i}{\mathbf{w}_i^2}$

10     $\beta = \frac{N - \sum_i \gamma_i}{\|\mathbf{t} - \Phi \mathbf{w}\|^2}$

11     $\delta = \sum_{i=1} \alpha_i^{n+1} - \alpha_i^n$

12 **until** $\delta < \delta_\tau$

13 $\mathbf{R} = \mathbf{x}(\mathbf{w}_{\text{index}})$ `// Training samples corresponding to non-zero weights`

Algorithm 2: RVM-Classify

Input: x': Test data for classification, $\mathbf{R}$: Relevance vectors, $\mathbf{w}$: Weight matrix

Output: y': Predicted class membership

1 Generate $\phi(x')$ using $\mathbf{R}$

2 $y' = \mathbf{w}^T \phi(x')$

4.2 Proposed Incremental Granular Relevance Vector Machine

There is a need to handle frequent insertions in training samples that happen over time. Further, for unbalanced dataset, there is a possibility for any classifier to

become easily biased towards the majority class. A real-time classifier has to be continuously updated to enrollments. Thus, RVM learning is modified to incorporate imbalanced nature of large training databases. Incremental learning [135] and granular computing [136] approaches are unified with RVM to design an efficient classifier. This section describes the formulation of *i*GRVM for data classification. The classifier is designed to incrementally update the decision boundary for new batch of training data. Training RVM using data divided into granules may further boost the performance. Our hypothesis is that this unique combination of granulation and incremental learning when applied to RVM, can improve the performance. The proposed variant of RVM is more focussed towards developing an adaptive and unbiased learning framework.

4.2.1   Incremental Relevance Vector Machine (*i*RVM)

For many real-time applications, since the data arrives in batches, it is important to introduce incremental learning strategies. Traditional RVM performs training in offline (batch) mode. Further, training RVM requires matrix inverse operation (Equation (4.6)) that performs $O(N^3)$ computations [133], where N is the size of training data. Therefore, RVM is not suitable for learning if the size of N is very large.

Researchers have proposed some modifications to train RVM classifier for large number of training data. Tipping proposed to reduce the training time of traditional RVM using fast marginal likelihood maximisation [137]. This learning approach helps to achieve speed-up by considering an empty model and sequentially adding basis vector to increase marginal likelihood. Tzikas et al. proposed a modification to fast marginal likelihood maximisation approach which also learns the location and scale parameters of kernel during training [138]. These approaches [137, 138] focus on dynamically adding or deleting the relevance vectors from the complete batch of training data. However, as mentioned earlier in many real-time applications, the complete training samples are not available simultaneously [135]. Very large scale biometric applications such as UIDAI [5] of India and US-VISIT [131] programs continuously enroll new subjects and new training data is obtained incrementally. In this research, traditional RVM is extended to make it scalable to new enrollments via incremental learning on encountering every new batch of data. Incrementally learning a classifier helps to keep memory and time computations (Hessian inverse) simple. This also facilitates updating the classifier with the availability of new enrollment data.

The proposed incremental RVM (*i*RVM) considers only relevance vectors from the previous training batch with a new batch of data for re-training. This approach is

based on the assumption that only RVs are essential for making predictions and all other training samples pertaining to the previous batches can be safely removed. This concept is similar to Tipping's constructive training approach [133] which reduces the total number of basis functions and the computational complexity. The steps involved in *i*RVM learning are:

Step 1: Initial training data ($\mathbf{T}_1$) is provided as input to the RVM and relevance vectors ($\mathbf{R}_1$) are obtained for the first batch.

Step 2: RVM is re-trained using the new batch of training data ($\mathbf{T}_i$) along with the relevance vectors from the previous iteration ($\mathbf{R}_{i-1}$). RVM-Train($\mathbf{T}_i \oplus \mathbf{R}_{i-1}$) on the aggregated set generates the new relevance vectors $\mathbf{R}_i$ along with the weights ($\mathbf{w}_i$), where $\oplus$ denotes the concatenation operation.

Step 3: The previous step is repeated on encountering new training samples in $\mathbf{T}_i$ for $i = 2, 3, 4, \ldots, m$, where m is the number of incremental training batches.

The learning strategy of *i*RVM is given in Algorithm 3. The relevance vectors from the last iteration ($\mathbf{R}_m$) are finally considered for making predictions until the new batch of training data arrives as shown in Figure 4.3. The formulation of *i*RVM is given by

$$y = \mathbf{w}^T \Phi(\mathbf{T}_m \oplus \mathbf{R}_{m-1}) \tag{4.12}$$

The classification algorithm for *i*RVM is same as RVM-Classify (Algorithm 2). It is interesting to note that, on encountering every new batch of data, the objective of the proposed *i*RVM is to adapt to new enrollments via incremental learning. Therefore, it can be viewed as a classical example of *lifelong machine learning* approach [139].

Algorithm 3: *i*RVM-Train

Input: $\mathbf{T}_m$: Training data, $\mathbf{t}_m$: Equivalent target values.
Output: $\mathbf{R}_m$: Relevance vectors, $\mathbf{w}_m$: Most probable weight matrix
1 foreach *Batch m of training* **do**
2 $\mathbf{T}_m \leftarrow \mathbf{T}_m \oplus \mathbf{R}_{m-1}$ `// combine training data with RVs from the last iteration`
3 $[\mathbf{R}_m, \mathbf{w}_m] = \text{RVM-Train}(\mathbf{T}_m, \mathbf{t}_m)$
4 end

4.2.2   Granular Relevance Vector Machine (GRVM)

In several applications, training is performed with highly imbalanced data. For instance in biometric applications, positive/genuine class contains lesser samples
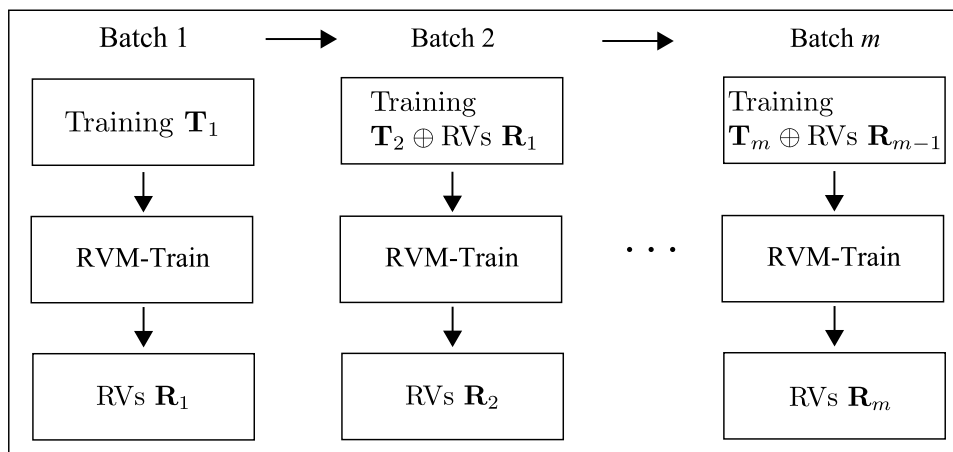
Figure 4.3: Training of Incremental Relevance Vector Machine (*i*RVM). The relevance vectors from the last iteration ($\mathbf{R}_{i-1}$) are used to perform training with new batch of data ($\mathbf{T}_i$).

and negative/impostor class contains large number of samples. This imbalance problem can be handled by considering various strategies such as oversampling the genuine scores (minority class) and undersampling the imposter scores (majority class). However, random data sampling may lead to information loss, for instance some informative samples may be lost. An alternative approach is to split the training data into segments and train the classifier on each segment locally; i.e., in granulation manner. Granular computing [140] solves the problem in each information granule locally while not compromising global generalisation. There are two approaches to granular computing: the first approach performs granule split using divide and conquer strategy whereas the second approach is based on granule shrink. In this thesis, two variants of granular RVM are studied each using the *split* and *shrink* approaches.

Granular RVM using Repetitive Undersampling (GRVM-*ru*)

Tang et al. [141] have applied repetitive undersampling (granule shrink) approach to SVM to address the class imbalance problem. The results obtained are encouraging [141] which motivates the application of this undersampling approach to RVM. As already stated that for classification, only relevance/support vectors are required for making predictions. In this work, only RVs are used to sample the data without loss of information. The process of learning granular RVM based on repetitive undersampling (henceforth termed as GRVM-*ru* for convenience) is shown in Figure 4.4. The steps involved in this undersampling approach are

Step 1: From the initial training data ($\mathbf{T}_1$), all the training samples pertaining to
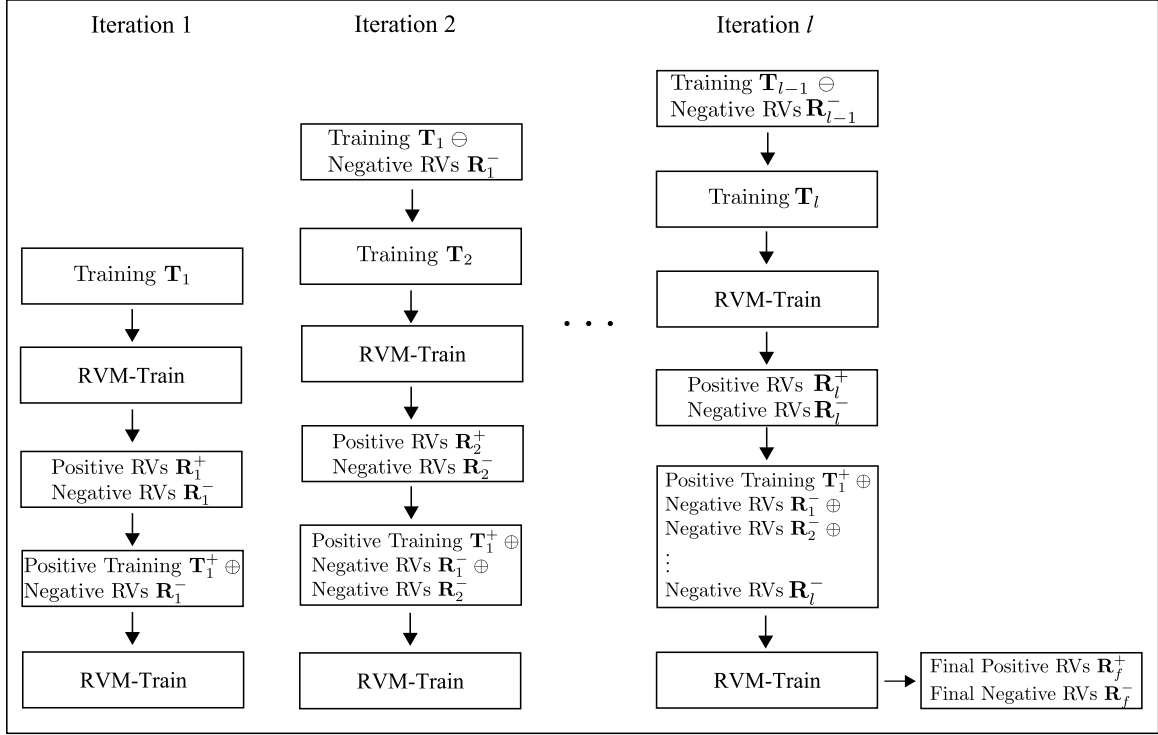
Figure 4.4: Training of Granular Relevance Vector Machine using repetitive undersampling (GRVM-*ru*). Here $\oplus$ denotes the concatenation and $\ominus$ denotes removing data from the set.

the genuine class ($\mathbf{T}_1^+$) are considered informative and hence form the positive information granule.

Step 2: Since the number of samples in the imposter class is very large only the relevance vectors from the imposter class ($\mathbf{R}_1^-$) form the negative information granule.

Step 3: To generate another negative granule, RVM is retrained on the training data ($\mathbf{T}_1$) after removing negative relevance vectors from the previous iteration ($\mathbf{R}_1^-$). This reduces the training data to $\mathbf{T}_2 = \mathbf{T}_1 \ominus \mathbf{R}_1^-$ by *granule shrink*, where $\ominus$ denotes removing elements from the set.

Step 4: On training ($\mathbf{T}_2$), the relevance vectors from the negative class ($\mathbf{R}_2^-$) are the ones which were left undetected at the very first training of RVM. These RVs are considered important and form the second negative granule. The process of granulation terminates on meeting the convergence criteria.

Step 5: Negative granules are combined with the positive granule using the aggregation operation ($\mathbf{T}_1^+ \oplus \mathbf{R}_1^- \oplus \mathbf{R}_2^- \oplus \ldots \oplus \mathbf{R}_l^-$).

Step 6: The aggregation set is initialised to positive class ($\mathbf{T}_1^+$). At the outset, the classifier is assumed to classify every score as negative.

Step 7: A new negative granule is extracted and combined with the aggregation set. RVM is trained on this aggregated set, and if the classification performance improves, next negative granule is extracted otherwise the undersampling process stops.

The relevance vectors ($\mathbf{R}_f^+, \mathbf{R}_f^-$) obtained from the final aggregation set is used to predict the class label of the probe sample. The formulation of GRVM-*ru* is given by

$$y = \mathbf{w}^T \Phi(\mathbf{T}_1^+ \oplus \mathbf{R}_1^- \oplus \mathbf{R}_2^- \oplus \ldots \oplus \mathbf{R}_l^-) \tag{4.13}$$

where l is the number of iterations used until GRVM-*ru* converges. The initial learning of GRVM-*ru* requires complete training data. In RVM, the Hessian matrix becomes ill-conditioned for large values of N [142]. Thus, the problem to train highly unbalanced data still remains unaddressed.

Granular RVM using 3σ rule (GRVM-3σ)

As mentioned earlier, the data from positive (under-represented) class is small and hence considered without sampling. However, the negative class has to be divided into granules using the *granule split* before applying RVM. It has been observed that imposter scores in biometrics follow Gaussian distribution. According to the 3σ rule of Gaussian distribution, approximately 99.73% values lie within the data covered by $\pm3\sigma$ as shown in Figure 4.5. Let $\mathbf{x}$ be the samples from the population that follow a Gaussian distribution with mean μ and standard deviation σ. The percentage of data covered can be given by

$$
\begin{aligned}
p\left(\mu - \sigma \leq \mathbf{x} \leq \mu + \sigma\right) &\approx 0.6827 \\
p\left(\mu - 2\sigma \leq \mathbf{x} \leq \mu + 2\sigma\right) &\approx 0.9545 \\
p\left(\mu - 3\sigma \leq \mathbf{x} \leq \mu + 3\sigma\right) &\approx 0.9973
\end{aligned}
\tag{4.14}
$$

This statistical property of Gaussian distribution is adopted to subsample the data of majority class. Figure 4.6 illustrates the steps involved in the proposed granular approach using 3σ subsampling which is explained below.

Step 1: This approach assumes positive (minority) class to be all informative and hence form the positive granule ($\mathbf{T}^+$).
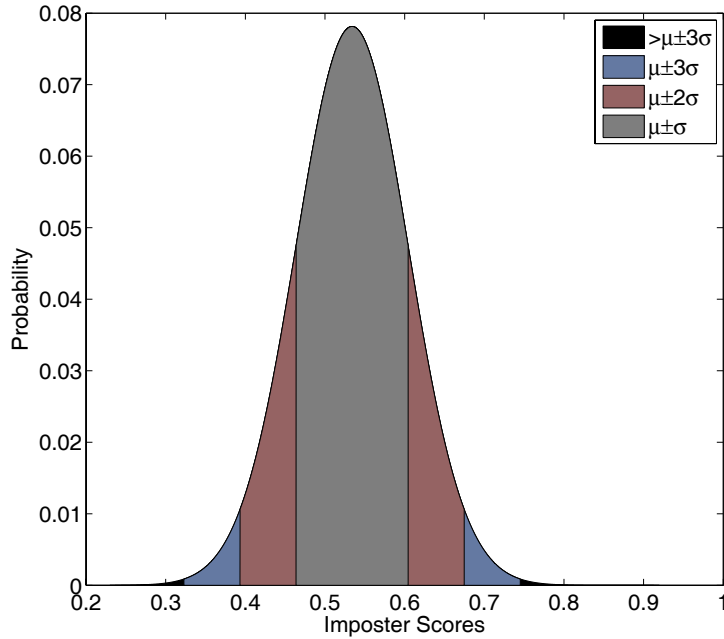
Figure 4.5: An example showing that impostor score distribution in biometrics follows Gaussian. This figure shows the percentage of data covered using the 3σ rule. This graph is generated using NIST BSSR Face Matcher 2 [54].

Step 2: All the data from the negative class is represented by $\mathbf{T}^-$ with mean μ and standard deviation σ.

Step 3: The first negative granule ($\mathbf{NG}_1$) is formed by considering only those samples from the negative (majority) class that are covered by

$$\mathbf{NG}_1 = \left\{ \mathbf{T}^- | \mathbf{T}^- \in \mu \pm \sigma \right\} \tag{4.15}$$

This covers approximately 68% of the values. For large class imbalance there may be further difficulty in training RVM with 68% of the negative samples. This issue is further resolved by randomly undersampling the data from each negative granule. The sampling is performed in the ratio of $1 : 2 : 3 : 4$ for $\mu \pm \sigma : \mu \pm 2\sigma : \mu \pm 3\sigma : > \mu \pm 3\sigma$ respectively. This choice of ratios is made to handle the class imbalance problem by selecting equal amount of data from each negative granule. This ensures that the relevance vectors are not biased towards any one part of the negative class.

Step 4: RVM (RVM$_1$) is then trained using the positive granule and the first negative granule ($\mathbf{NG}_1$). To find the training accuracy with this model, RVM$_1$ is tested

on all the negative data prior to undersampling that is covered within $\mu \pm \sigma$. The misclassifications ($\mathbf{M}_1$) that arise out of RVM$_1$ training are taken further to improve the performance of the classifier.

Step 5: The second negative granule ($\mathbf{NG}_2$) is formed by considering those samples that fall outside $\mu \pm \sigma$ but within $\mu \pm 2\sigma$. This can be given by the values of $\mathbf{T}^-$ that fall in the range of

$$\mathbf{NG}_2 = \left\{ \mathbf{T}^- | \mathbf{T}^- \in (\mu \pm 2\sigma) \ \& \ \mathbf{T}^- \notin (\mu \pm \sigma) \right\} \tag{4.16}$$

However, as mentioned earlier only 20% of the samples in this bracket are selected for RVM training. $\mathbf{NG}_2$ is further combined with the negative relevance vectors ($\mathbf{R}_1^-$) from RVM$_1$ and the mis-classifications from the last iteration ($\mathbf{M}_1$). The combined $\mathbf{NG}_2$ with positive granule is used to train RVM$_2$.

Step 6: This process is repeated for $\mathbf{NG}_3$ that contains negative samples as shown in Equation (4.17). Subsampled $\mathbf{NG}_3$ along with the misclassifications of RVM$_2$ ($\mathbf{M}_2$) and $\mathbf{R}_2^-$ are used to train RVM$_3$.

$$\mathbf{NG}_3 = \left\{ \mathbf{T}^- | \mathbf{T}^- \in (\mu \pm 3\sigma) \ \& \ \mathbf{T}^- \notin (\mu \pm 2\sigma) \right\}. \tag{4.17}$$

Step 7: The final negative granule ($\mathbf{NG}_4$) contains all the remaining 0.3% of the samples that lie outside the range of $\mu \pm 3\sigma$. Thus, a final RVM (RVM$_4$) is trained on positive granule with $\mathbf{NG}_4$, misclassifications ($\mathbf{M}_3$) and negative relevance vectors ($\mathbf{R}_3^-$) of RVM$_3$.

Algorithm 4 outlines the steps involved in training granular RVM using 3σ rule (GRVM-3σ). The model trained with this data is finally used to perform classification. The formulation of GRVM-3σ is given by

$$y = \mathbf{w}^T \Phi(\mathbf{T}^+ \oplus \mathbf{NG}_4 \oplus \mathbf{R}_3^- \oplus \mathbf{M}_3) \tag{4.18}$$

The proposed granular RVM (GRVM-3σ) is capable of training highly imbalanced data. Note that the mis-classifications that arise from the previous iteration are carried forward to re-train RVM with improved decision boundary. At the same time, use of RVs helps to avoid over-fitting. Unlike repetitive undersampling, 3σ approach is relatively faster as RVM is trained using a smaller size of data. Also, assuming that the negative samples can be approximated with Gaussian distribution does not impact the performance of the training algorithm because essentially, all the training data is either validated or included during learning.
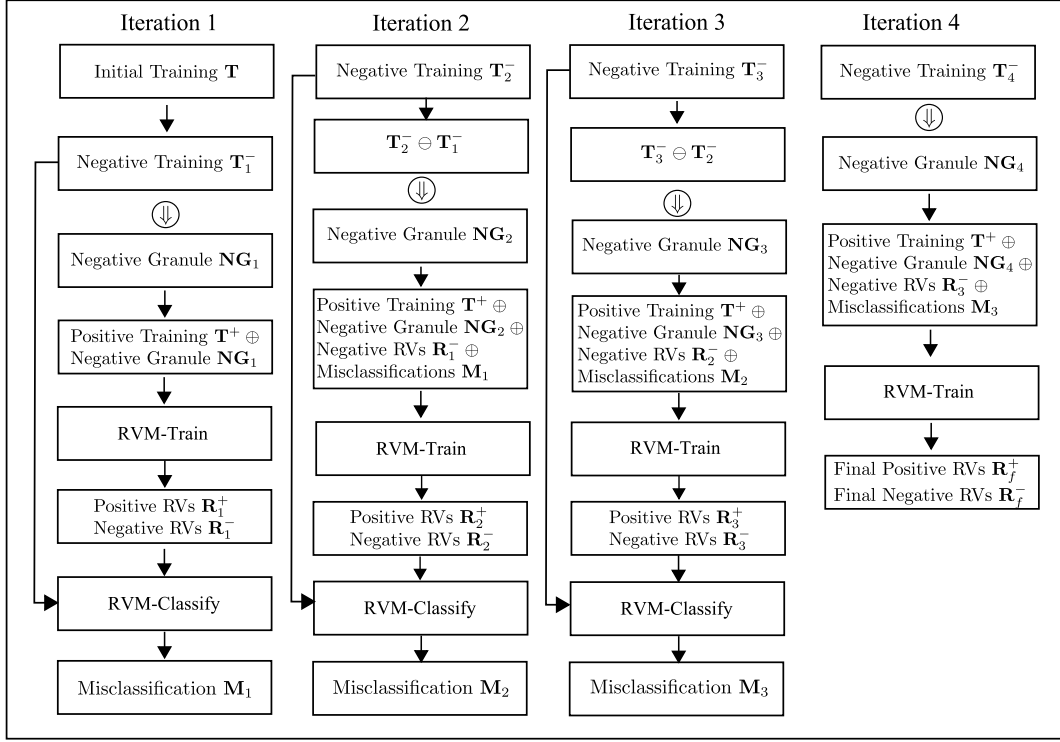
Figure 4.6: Steps involved in training Granular Relevance Vector Machine using 3σ rule (GRVM-3σ). Here $\Downarrow$ denotes the subsampling operation.

4.2.3 Incremental Granular Relevance Vector Machine (iGRVM-3σ)

The previous two sections propose algorithms to address the problem of large data and class imbalance individually. However, they cannot solve both the problems together. Therefore this section proposes the Incremental Granular Relevance Vector Machine (iGRVM-3σ) to address both the problems using a single classifier.

Incremental RVM (iRVM) and granular RVM (GRVM-3σ) are fused hierarchically to generate a novel classifier- iGRVM-3σ. This classifier is robust to updates and handles large class imbalance problem as well. iGRVM-3σ functions hierarchically where for each new batch of training data, granular RVM is used to find the relevance vectors. Here experiments are performed using both GRVM variants but GRVM-3σ is preferred due to its ability to handle large unbalanced training data. The steps involved in iGRVM-3σ are:

Step 1: The process starts with incremental learning of the initial batch of training data ($\mathbf{T}_1$). The negative granule ($\mathbf{NG}_{11}$) is generated by retaining samples from $\mu \pm \sigma$.

Step 2: RVM is trained with the positive granule ($\mathbf{T}_1^+$) and the subsampled negative

59

Algorithm 4: GRVM-3σ-Train

Input: $\mathbf{T}$: Training data, $\mathbf{t}$: Equivalent target values.

Output: $\mathbf{R}$: Relevance vectors, $\mathbf{w}$: Most probable weight matrix

1   $\mathbf{T}^+ = \{\mathbf{T}|\mathbf{T} \in \text{positive class}\}$

2   $\mathbf{T}^- = \{\mathbf{T}|\mathbf{T} \in \text{negative class}\}$

3   $n \leftarrow |\mathbf{T}^+|$

4   $PC \leftarrow 0$ `// Percentage of data covered`

5   $\mu \leftarrow \mathbf{mean}(\mathbf{T}^-)$

6   $\sigma \leftarrow \mathbf{sigma}(\mathbf{T}^-)$

7   $i \leftarrow 1$

8   **while** $PC < 1$ **do**

9        $s \leftarrow n \times \frac{i}{10}$

10     $l_i \leftarrow \mathbf{random}(s)$

11     $\mathbf{T}_i^- = \{\mathbf{T}^-|\mathbf{T}^- \in \mu \pm i\sigma\}$

12   **if** $i == 1$ **then**

13        $\mathbf{NG}_i \leftarrow \mathbf{T}_i^-(l_i)$ `// Undersampling negative granule`

14   **else**

15        $\mathbf{NG}_i \leftarrow \left[\mathbf{R}_{i-1}^- \oplus \mathbf{M}_{i-1} \oplus (\mathbf{T}_i^- \ominus \mathbf{T}_{i-1}^-)(l_i)\right]$

16   **end**

17     $\mathbf{T}_i \leftarrow \mathbf{T}^+ \oplus \mathbf{NG}_i$

18     $[\mathbf{R}_i, \mathbf{w}_i] = \text{RVM-Train}(\mathbf{T}_i, \mathbf{t}_i)$

19     $\mathbf{T}' \leftarrow \mathbf{T}^+ \oplus \mathbf{T}_i^-$

20     $y = \text{RVM-Classify}(\mathbf{T}', \mathbf{R}_i, \mathbf{w}_i)$

21     $\mathbf{M}_i = y \neq t'$

22     $\mathbf{R}_i^- = \{\mathbf{R}_i|\mathbf{R}_i \in \text{negative class}\}$

23     $PC \leftarrow |\mathbf{T}_i^-|/|\mathbf{T}^-|$

24     $i \leftarrow i + 1$

25   **end**

---

granule ($\mathbf{NG}_{11}$). The trained model is used to check for mis-classifications ($\mathbf{M}_{11}$) that arise after learning.

Step 3:   The next negative granule ($\mathbf{NG}_{12}$) covers data in the range of $\mu \pm 2\sigma$ exclusive of values from $\mu \pm \sigma$. The RVM is trained with $\mathbf{T}_1^+$ along with $\mathbf{R}_{11}^-$ and $\mathbf{M}_{11}$.

Step 4:   This process is iterated until the complete impostor training data is covered.

Step 5:   The relevance vectors ($\mathbf{R}_{1f}^+, \mathbf{R}_{1f}^-$) after final training from $\mathbf{T}_1$ are taken as input to the next batch of training ($\mathbf{T}_2$) to learn incrementally. The new training batch is thus represented as $\mathbf{T}_2 = \mathbf{T}_2 \oplus \mathbf{R}_{1f}^+ \oplus \mathbf{R}_{1f}^-$.

Step 6:   RVM is re-trained with this new unified training set ($\mathbf{T}_2$). The learning process of iGRVM-3σ is iterated for $i = 2, 3, \ldots, m$ until the new batch for training arrives.

Step 7: The RVs from the latest enrolled batch of iGRVM-3σ ($\mathbf{R}_{mf}^{+}, \mathbf{R}_{mf}^{-}$) are finally used to make predictions using Equation (4.11).

iGRVM-3σ provides the stable set of relevance vectors with significantly reduced training time. The steps involved in training the proposed iGRVM-3σ approach are summarised in Figure 4.7 and Algorithm 5. The formulation of iGRVM-3σ can also be shown using the following equation[1]

$$y = \mathbf{w}^{T}\Phi\left(\mathbf{T}_{m} \oplus \mathbf{R}_{(m-1)f}^{+} \oplus \mathbf{R}_{(m-1)f}^{-}\right) \tag{4.19}$$

The proposed iGRVM-3σ has the following attributes

1. **Sparse:** It holds the property of RVM which has been proved to be a relatively sparser model with generalisation capability in accordance with SVM [133]. The number of relevance vectors required for classification are considerably less in comparison to SVM.

2. **Scalable:** iGRVM-3σ performs re-training on encountering a new batch of training data. Hence the classifier is adaptive to environmental dynamics, which makes it scalable to new enrollments as well.

3. **Faster:** RVM requires matrix inverse operation for covariance computation (Equation 4.6) which is a costly operation for very large training databases. iGRVM-3σ performs training recurrently on subsampled granules, thus the learning is faster compared to conventional RVM.

4. **Unbiased:** iGRVM-3σ handles class imbalance problem by subsampling the data from the over-populated class using granular computing. The model trained on the positive and subsampled negative data is unbiased in nature.

Algorithm 5: iGRVM-3σ-Train

    Input: $\mathbf{T}_{m}$: Training data, $\mathbf{t}_{m}$: equivalent target values.
    Output: $\mathbf{R}_{m}$: relevance vectors, $\mathbf{w}_{m}$: most probable weight matrix
1 foreach *Batch m of training* **do**
2 $\mathbf{T}_{m} \leftarrow \mathbf{T}_{m} \oplus \mathbf{R}_{m-1}$
3 $[\mathbf{R}_{m}, \mathbf{w}_{m}] = \text{GRVM-3}\sigma\text{-Train}(\mathbf{T}_{m}, \mathbf{t}_{m})$
4 end

---

[1]As the training of each RVM variant is different so the weight matrix ($\mathbf{w}$) is also different.
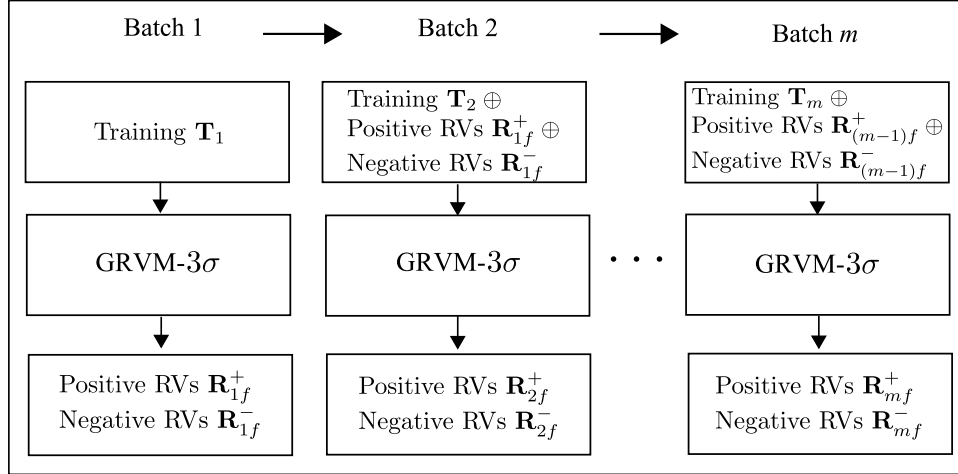
Figure 4.7: Steps involved in training of *i*GRVM-3σ.

4.3 *i*GRVM-3σ Case Study: Multimodal Biometric Match Score Classification

The proposed incremental granular RVM learning algorithm is applied for biometric score classification and the results highlight that it can be used as an effective alternative that can optimise computational time. The steps involved in d-dimensional biometric score vector classification using *i*GRVM-3σ are:

- Training *i*GRVM-3σ: The training set $(\mathbf{x}, \mathbf{t})$ consists of $\{x_{i1}, x_{i2}, \ldots, x_{id}, t_i\}_{i=1}^{N}$ for N scores from d different sources with the corresponding class labels in t_i. The objective is to apply a function to $\mathbf{x}$ that provides a clear separation between the genuine and impostor classes. The proposed *i*GRVM-3σ-Train$(\mathbf{x}, \mathbf{t})$ is called for training score vectors to generate the most probable weights $\mathbf{w}$ along with relevance vectors $(\mathbf{R})$.

- Classification: The trained *i*GRVM-3σ model is used to predict the class of d-dimensional probe multimodal score vector given by x' using Equation (4.11). The output from *i*GRVM-3σ is a probabilistic value which is used to make final decision.

4.3.1 Databases and Algorithms

The databases utilised for this case study are standard and commonly used for testing the classifiers [47]. NIST Biometrics Score Set - Release 1 (BSSR1) [54] and Biosecure DS2 [143] are used to perform experiments. BSSR1 and Biosecure DS2 are match score database, so no feature extraction approach is required. The match scores from

Table 4.1: Databases used to perform iGRVM-3σ case study.

Database	Modalities	Subjects	Scores	
			Genuine	Imposter
BSSR1 (Set 1)	Face, Finger	517	517	266772
BSSR1 (Set 2)	Fingerprint	6000	6000	35994000
BSSR1 (Set 3)	Face	3000	6000	17994000
Biosecure DS2	Face, Finger, Iris	51	Sessions 1 and 2	

BSSR1 are normalised using min-max approach and used for classification. Table 4.1 summarises the details of the databases used. The proposed iGRVM-3σ is compared to some existing classification approaches that have already been applied to biometrics fusion. A brief description of each of the approaches are given below:

- Likelihood ratio [47]. In this approach, match scores are classified using the likelihood ratio (LR) test. The distribution of genuine and imposter scores are modeled using Gaussian Mixture Model (GMM).

- Support Vector Machine for classification [132]. It takes vector of scores as input which are classified to generate a binary decision. The experiments for SVM are performed using Matlab version of LIBSVM library[2].

- Relevance Vector Machine [133] is used to classify the d-dimensional vector of scores into one of the two classes.

4.3.2 Protocol

Two case studies are performed with three times random cross validation to study the performance of iGRVM-3σ under different scenarios.

- Case Study 1 is performed to study the performance of iGRVM-3σ over other classifiers such as LR, SVM, and RVM. In this experiment all three sets of BSSR1 database are used. Table 4.2 shows the number of training samples used from each class for learning the classifiers. From the complete batch of training data, 10% of the genuine and imposter scores are used for incrementally learning the classifier in batches.

- Biometrics databases are generally unbalanced and not all the classifiers yield good results for such databases. Case Study 2 is used to study the performance

---

[2]LIBSVM - A Library for Support Vector Machines. http://www.csie.ntu.edu.tw/~cjlin/libsvm/. The Matlab code uses mex files to provide an interface between C and Matlab.

Table 4.2: Experimental protocol for Case Study 1 and 2.

Database	Case Study 1				Case Study 2			
	Training		Testing		Training		Testing	
	Genuine	Imposter	Genuine	Imposter	Genuine	Imposter	Genuine	Imposter
BSSR1 (Set 1)	52	2668	465	264104	52	26677	465	240095
BSSR1 (Set 2)	600	3599	5400	35990401	600	3599400	5400	32394600
BSSR1 (Set 3)	600	3599	5400	17990401	600	1799400	5400	16194600
Biosecure DS2	-	-	-	-	51	21012	102	21012

of iGRVM-3σ for highly unbalanced training datasets. Table 4.2 shows the experimental protocol followed for this imbalance study. The databases used in this case study are BSSR1 and Biosecure DS2. Biosecure DS2 by design is highly unbalanced, whereas for BSSR1, the datasets are partitioned to showcase the unbalanced nature and classification performance.

4.3.3   Case Study 1: i**GRVM-**3σ **Performance**

This experiment is performed to measure the performance of the proposed classifier as well as LR, SVM and RVM classification. The classifiers are trained using the experimental protocol mentioned in Table 4.2. The Receiver Operating Characteristic (ROC) curve for Case Study 1 is shown in Figure 4.8. Table 4.3 illustrates Genuine Acceptance Rate (GAR) at 0.01% False Acceptance Rate (FAR). The key results and observations are

- For BSSR1 (all three sets), the proposed GRVM-3σ and iGRVM-3σ classifier yields comparable results as other classifiers (LR and SVM) in terms of accuracy (Table 4.3). GRVM-3σ divides the database into granules following the statistical property of Gaussian distribution. As imposter scores from biometric database are assumed to be Gaussian, this confirms the effectiveness of GRVM-3σ over GRVM-ru. Further, GRVM-ru requires the complete database for initial training, so problems inherent to large training persist whereas GRVM-3σ performs training on such large data using the divide and conquer approach. The amalgamation operation is performed at each stage of granulation so the training errors are considered simultaneously which further improves the performance in comparison to GRVM-ru.

- RVM training is costly since it requires matrix inversion operation. Training SVM requires minimum time for all the databases as shown in Table 4.4[3]. As stated by

---

[3]The testing time reported in this chapter is for complete testing samples as given in experimental protocol (Table 4.2).

Tipping and Faul [137], SVM is a C implementation whereas RVM is written using Matlab, so a comparison of time across platforms is not reasonable. In practical applications, there is always an effort to minimise testing time as training is an offline process. Table 4.4 shows the number of SVs/RVs required by individual classifiers. Testing time is directly proportional to the number of non-zero vectors used for making predictions. RVM generates significantly reduced number of relevance vectors and hence preferred over SVM due to sparsity. However, iGRVM-3σ performs iterative training to minimise the training error. RVs generated using GRVM-3σ are more compared to RVM but significantly less compared to SVM. As shown in Table 4.4, the testing time on the entire testing set of the proposed variants of RVM are significantly less compared to SVM. While one can argue that the performance should also be compared with online SVM, the objective of this research is not to showcase superiority of the proposed algorithm over SVM but to show that the modification over RVM makes it applicable to biometrics.

- All incremental variants of RVM performs equivalent to its offline/batch mode. The incremental learning approaches facilitates to learn very large training set in batches which cannot otherwise be enrolled in offline mode. Therefore, incremental variants provide added advantage that can be useful in biometrics.

Table 4.3: Genuine acceptance rate at 0.01% false acceptance rate for Case Study 1.

Algorithm	NIST BSSR1		
	Set 1	Set 2	Set 3
Face Matcher 1	74.27	-	71.22
Face Matcher 2	68.28	-	64.06
Finger Left	77.18	75.52	-
Finger Right	85.30	83.13	-
LR	98.06	90.26	**76.39**
SVM	98.92	91.05	74.58
RVM	98.70	89.74	75.85
iRVM	98.27	90.77	75.89
GRVM-ru	98.49	89.74	73.38
iGRVM-ru	98.92	90.78	75.61
GRVM-3σ	**99.35**	**91.10**	75.21
iGRVM-3σ	99.14	90.98	75.70

(a)

(b)

(c)
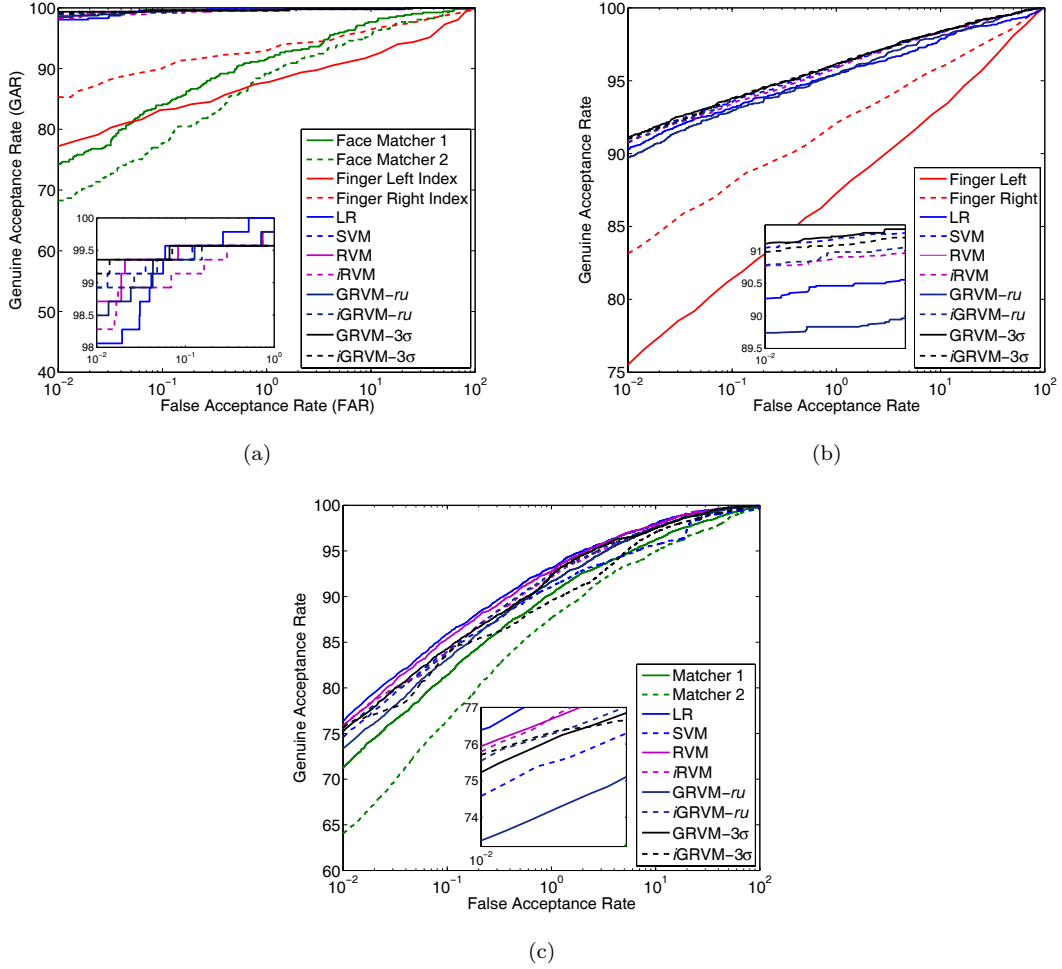
Figure 4.8: Performance of various classifiers on (a) NIST Multimodal (Set 1), (b) NIST Fingerprint (Set 2), and (c) NIST Face (Set 3) under Case Study 1.

Table 4.4: Time taken (in seconds) by various learning based approaches on complete training and testing samples from BSSR1 for Case Study 1.

Approach	Set 1			Set 2			Set 3		
	Training	Testing	# SV/RV	Training	Testing	# SV/RV	Training	Testing	# SV/RV
LR	0.81	0.72	G:3, I:3	0.45	69.78	G:3, I:3	1.48	50.42	G:2, I:5
SVM	0.02	0.23	54	0.27	1068.77	1200	0.94	242.44	576
RVM	84.46	0.09	4	425.19	471.43	4	361.54	138.47	10
*i*RVM	2.92	0.05	4	149.76	8.74	4	22.75	147.77	20
GRVM-*ru*	350.16	0.06	3	405.22	358.17	4	1101.70	118.24	4
*i*GRVM-*ru*	9.82	0.13	4	253.72	441.54	14	113.13	77.52	4
GRVM-3σ	6.90	0.20	22	554.21	673.41	48	7.27	121.31	9
*i*GRVM-3σ	2.48	0.34	19	31.07	374.08	10	11.23	126.14	4

4.3.4   Case Study 2: Unbalanced Databases

This case study is performed to understand the nature of these classifiers on highly unbalanced databases. The experimental protocol followed for highly unbalanced database is shown in Table 4.2. As mentioned previously for incremental learning 10% of training data is used. The ROC plots for unbalanced database is shown in Figure 4.9. The key observations from this study are:

- Table 4.5 shows the accuracy of different classifiers on highly imbalanced data. LR outperforms other approaches in this study. In most of the cases, LR is designed to handle imbalance in the training database [47]. The performance of $GRVM-3\sigma$ and iGRVM-3σ is comparable to LR. Classification accuracy improves for more data but the performance of some classifiers such as iRVM and iGRVM-ru reduces due to biased distribution of data.

- The training database is very large so some offline classifiers such as RVM and GRVM-ru cannot not be trained. As explained earlier, these approaches require complete data for initial training. If training database is large enough as given in Table 4.2, RVM and GRVM-ru generates memory error and classifier fails to learn.

- In almost all the experiments of unbalanced nature it is observed that the proposed GRVM-3σ performs comparable to LR and SVM. This approach samples the database following the statistical property of Gaussian and is preferred over random data sampling. The information loss is minimal and hence the classifier performs well for highly unbalanced biometric databases.

- Testing time required by iGRVM-3σ is less compared to SVM (Table 4.6). Thus, iGRVM-3σ is comparable to other existing classifiers in terms of time and performance. This approach can be taken as an alternative to existing learning based approaches.

- Biosecure DS2 is the most challenging database in terms of class imbalance. This database is utilised to study the performance of iGRVM-3σ under such large variations. Table 4.5 shows that iGRVM-3σ performs as good as LR and SVM with an accuracy of 94.12%. However, it requires minimum testing time on this database due to significantly reduced number of relevance vectors.
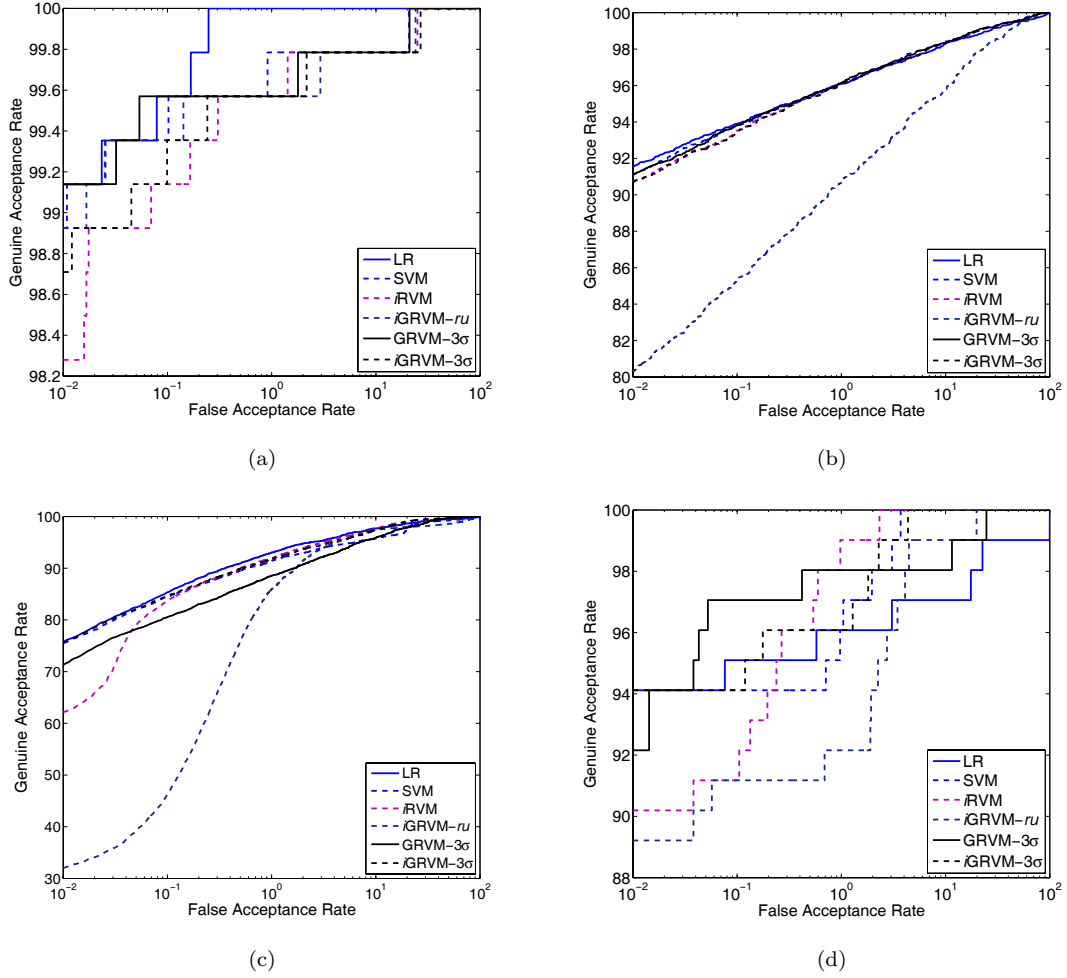
Figure 4.9: Performance of various classifiers on highly skewed training data (Case Study 2) for (a) NIST Multimodal, (b) NIST Fingerprint, (c) NIST Face, and (d) Biosecure DS2 databases.

Table 4.5: Genuine acceptance rate (GAR) at 0.01% false acceptance rate (FAR) for highly skewed databases.

Algorithm	Databases			
	Set 1	Set 2	Set 3	Biosecure DS2
LR	99.14	91.54	75.76	94.12
SVM	98.92	91.10	75.50	94.12
iRVM	98.28	90.74	62.15	90.20
iGRVM-ru	98.92	80.33	32.07	89.22
GRVM-3σ	99.14	91.11	71.30	92.36
iGRVM-3σ	98.71	90.71	75.59	94.12

Table 4.6: Training and testing time taken (in seconds) by various learning based classification approaches for highly unbalanced data.

Approach	Set 1			Set 2		
	Training	Testing	#SV/RV	Training	Testing	#SV/RV
LR	3.40	0.75	G:3, I:10	227.96	24.84	G:3, I:3
SVM	0.06	0.41	58	391.75	1552.39	1200
iRVM	51.25	0.12	4	16395.50	411.44	7
iGRVM-ru	167.49	0.09	3	72409.20	250.48	4
GRVM-3σ	11.31	0.13	4	251.70	426.01	378
iGRVM-3σ	18.66	0.06	3	298.51	203.36	11
Approach	Set 3			Biosecure DS2		
	Training	Testing	#SV/RV	Training	Testing	#SV/RV
LR	122.97	10.88	G:3, I:5	4.50	0.03	G:2, I:2
SVM	1113.71	546.30	1200	0.06	0.03	46
iRVM	27.25	100.84	5	235.19	0.01	8
iGRVM-ru	6650.31	71.49	10	2568.83	0.03	20
GRVM-3σ	23.86	151.40	39	2.09	0.003	5
iGRVM-3σ	24.39	82.47	55	6.49	0.006	3

4.4   *i*GRVM-3σ for Multi-unit Iris Recognition

The performance of proposed iGRVM-3σ classifier motivates its application for multi-unit iris recognition. The left and right iris images are combined to improve the performance without adding any extra hardware cost to the existing iris recognition system. As discussed earlier, recognition using single unit (left/right) may not perform well for iris images acquired under noisy conditions or failure to capture cases. In this chapter, an effort has been made to develop a multiple unit iris recognition system that performs fusion at match score level. Kittler et al. [51] have shown that the fusion of match scores from one or more classifier gives better performance over a single classifier. In the proposed fusion framework, the match scores from individual modalities are passed as an input to the classifiers and the posterior probabilities are combined using sum rule. The training set consists of $\{x_{n1}, x_{n2}, \ldots, x_{nd}, t_n\}_{n=1}^{N}$ for N scores from d different sources with the corresponding class labels in t_n, where d denotes the number of modalities, units or algorithms used. A classifier is trained using match scores from an independent modality along with the corresponding class labels. This process is iterated d times which generates d sets of relevance vectors and weights.

The match scores (S^{Left} and S^{Right}) are obtained from left and right units of iris using SIFT (please refer Chapter 5). The classifier is used to find the probabilistic values of the scores obtained. The left scores from N iris images are used to train the classifier. Similarly training is done using scores from the right iris images. This

generates two sets of relevance vectors and weights as defined by

$$\{\mathbf{R}^d, \mathbf{w}^d\} = \text{Train}(\mathbf{S}^d, \mathbf{t}) \tag{4.20}$$

where $d \in \{Left, Right\}$ denotes the left and right iris images respectively. Training of the proposed fusion approach is explained in Algorithm 6. Each set of relevance vectors and weights are used to approximate the corresponding output values for the multi-unit probe score x^d.

$$y^d = \text{Classify}(\mathbf{R}^d, \mathbf{w}^d, x^d) \tag{4.21}$$

The proposed unification approach is a variant of classification approaches discussed earlier and performs fusion over classification of scores generated from individual classifiers. Finally, the fusion of the outputs are done using weighted sum rule given by

$$y_{final} = \frac{1}{d} \sum_{j=1}^{d} y^j \tag{4.22}$$

where y^j is a probabilistic value whose weighted sum ranges between 0 and 1. The block diagram of proposed fusion framework for multi-unit iris recognition is shown in Figure 4.10.

Algorithm 6: Train-Fusion

    Input: $\mathbf{T}$: Training data, $\mathbf{t}$: Equivalent target values.
    Output: $\mathbf{R}^d$: Relevance vectors for d sources, $\mathbf{w}^d$: Most probable weight
           matrices

  1 **for** $i=1$ **to** d **do**
  2 $\mathbf{S}^i \leftarrow \mathbf{T}^i$ `// Match scores for `d` dimension`
  3 $\{\mathbf{R}^i, \mathbf{w}^i\} = \text{Train}(\mathbf{S}^i, \mathbf{t})$
  4 **end**

4.5   Experimental Results

The case study on match score databases is encouraging which supports the application of iGRVM-3σ to improve the iris recognition performance. From the total number of genuine scores available 10% scores are taken to form the training set and remaining 90% scores are assigned to the test set. The imposter scores are partitioned into 1% and 99% to generate train and test sets respectively. The first experiment is performed to evaluate the classifier performance on the available iris recognition databases followed by fusion in the second experiment.
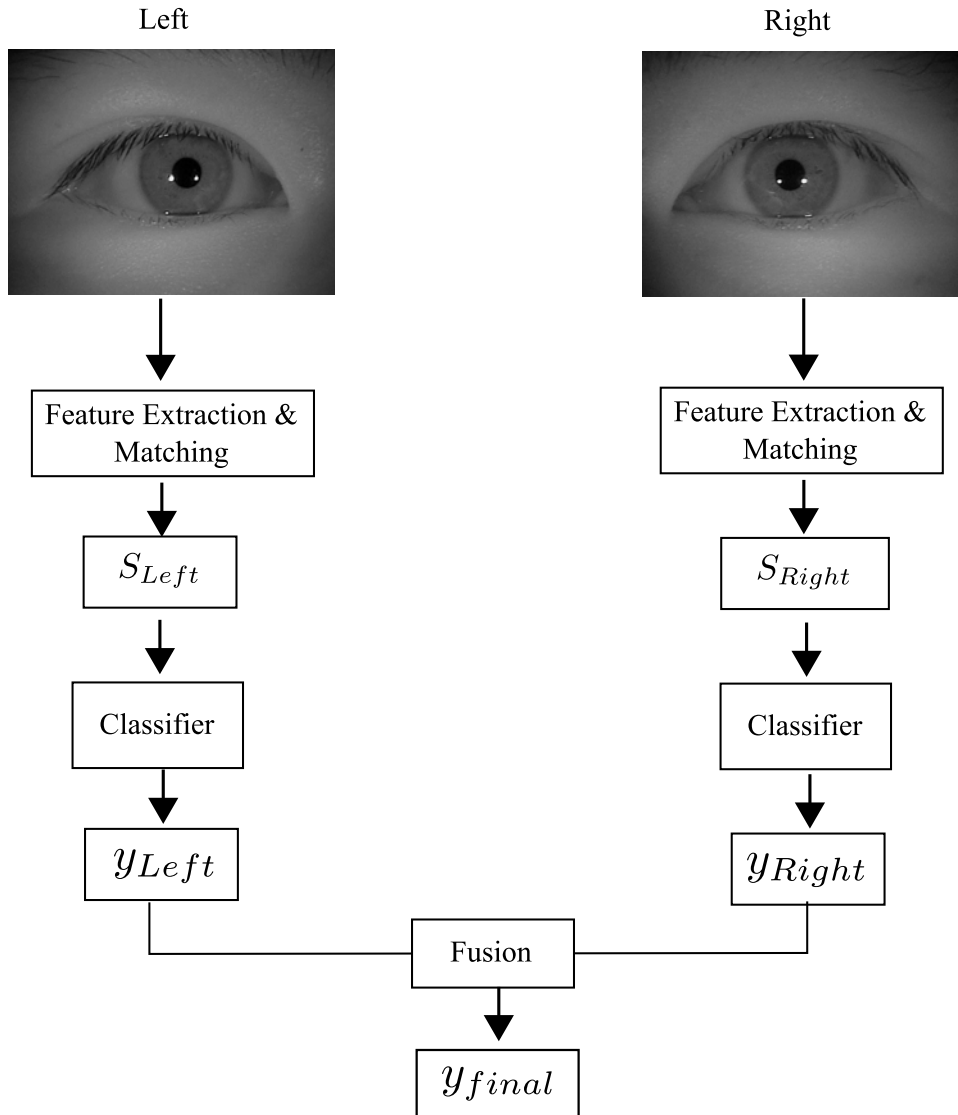
Figure 4.10: Steps involved in multi-unit iris recognition algorithm using the the proposed fusion approach.

4.5.1 Experiment 1: Classification

In this experiment, the performance of various classifiers are evaluated. ROC curves are shown in Figure 4.11(a) and Figure 4.11(b) for BATH and CASIAV3 databases respectively. Following inferences are made from the results obtained:

- The accuracy of proposed iGRVM-3σ is relatively high for BATH database as shown in Table 4.7. The performance is comparable to SVM with significant improvement in testing time (Table 4.8). As discussed earlier, the testing time is dependent upon number of relevant/support vectors used for making predictions. The number of support vectors required are considerably high for SVM in

comparison to *i*GRVM-3σ which in turn reduces the testing time (Table 4.8).

- For CASIAV3 database, GRVM-3σ outperforms existing classifiers. The time required to perform classification is lowest among its contenders. This is particularly useful when iris is deployed for real-time identification applications.

- The number of relevance vectors required by *i*GRVM-3σ increases due to data distribution with an equivalent increase in time for CASIAV3 database as shown in Table 4.8. The testing time increases in comparison to other RVM variants. However, the testing time is significantly low compared to SVM and comparable to LR.
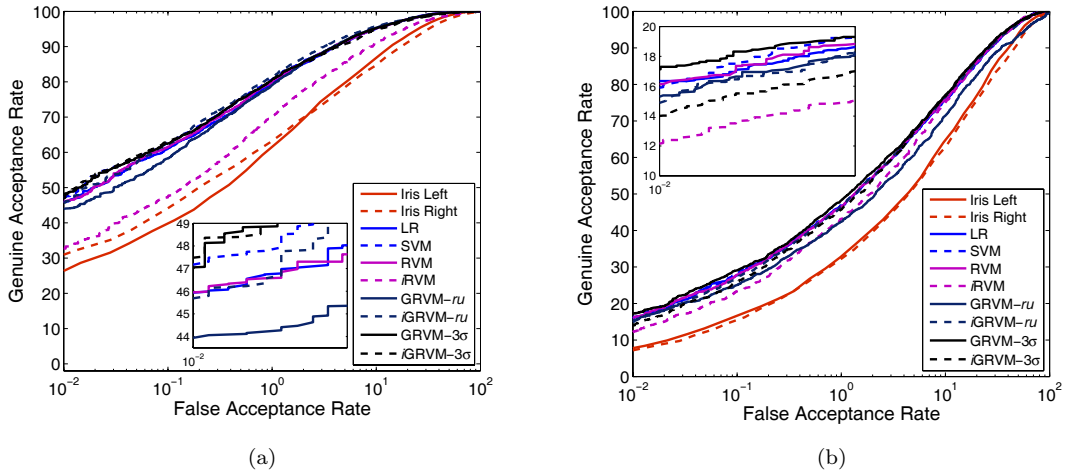
Figure 4.11: Performance of various classifiers on (a) BATH and (b) CASIAV3 databases.

Table 4.7: Genuine acceptance rate at 0.01% false acceptance rate for BATH and CASIAV3 databases using different classifiers.

Algorithm	BATH	CASIAV3
Left	26.32	07.74
Right	30.79	07.12
LR	45.95	16.35
SVM	47.22	15.98
RVM	46.01	16.14
*i*RVM	32.80	12.27
GRVM-*ru*	43.94	15.30
*i*GRVM-*ru*	45.77	14.92
GRVM-3σ	47.51	**17.28**
*i*GRVM-3σ	**47.83**	14.02

Table 4.8: Training and testing time taken (in seconds) by various learning based classification approaches on BATH and CASIAV3 databases.

Approach	BATH			CASIAV3		
	Training	Testing	#SV/RV	Training	Testing	#SV/RV
LR	0.24	0.08	G:3, I:3	0.24	0.12	G:3, I:3
SVM	0.19	1.88	488	0.09	4.51	662
RVM	307.44	0.03	9	167.44	0.04	8
iRVM	9.07	0.02	2	13.44	0.03	4
GRVM-ru	1467.24	0.02	3	621.44	0.03	5
iGRVM-ru	13.13	0.02	2	65.96	0.03	4
GRVM-3σ	3.29	0.02	7	2.11	0.01	3
iGRVM-3σ	9.35	0.06	2	10.27	0.15	22

4.5.2   Experiment 2: Fusion

In this experiment, the proposed fusion approach is used to combine the probabilistic decision values obtained after classifying individual scores. These scores are combined using weighted sum rule. The key observations of the proposed model are:

- Figure 4.12 shows the ROC curves of different fusion approaches. Using the proposed fusion framework, GRVM-3σ outperforms other classifiers. However, iGRVM-3σ fails to achieve the desired performance for single unit of iris and hence the fusion results after combination are not promising.

- Table 4.9 highlights the improvement in fusion accuracy over classification. A single classifier may not be appropriate to perform fusion for conflicting cases [67]. Thus the accuracy improves after combining the classification results using linear sum rule.

- The testing time also reduces significantly using GRVM-3σ based fusion (Table 4.10). This is particularly due to less number of vectors required for making predictions.
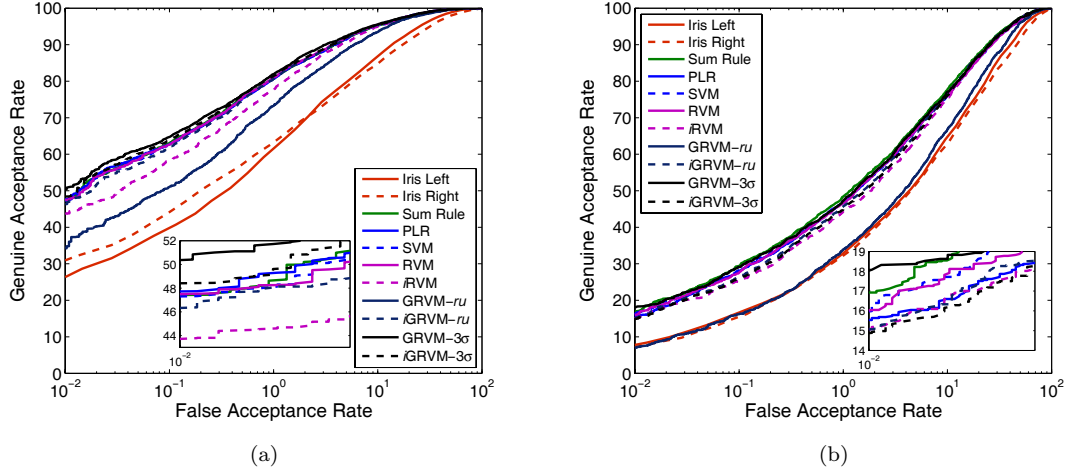
Figure 4.12: Performance of various fusion approaches for (a) BATH and (b) CASIAV3 databases.

Table 4.9: Genuine acceptance rate at 0.01% false acceptance rate for BATH and CASIAV3 databases using different fusion approaches.

Algorithm	BATH	CASIAV3
Sum Rule	47.44	16.96
PLR	47.72	15.62
SVM	47.29	16.20
RVM	47.49	16.02
*i*RVM	43.72	15.14
GRVM-*ru*	34.48	07.08
*i*GRVM-*ru*	46.44	15.11
GRVM-3σ	**50.55**	**18.07**
*i*GRVM-3σ	48.41	14.90

Table 4.10: Training and testing time taken (in seconds) by various fusion approaches on BATH and CASIAV3 databases.

Approach	BATH				CASIAV3			
	Training	Testing	#SV/RV		Training	Testing	#SV/RV	
			Left	Right			Left	Right
PLR	0.65	0.10	G:3	I:5	0.35	0.12	3	3
SVM	0.21	4.44	616	612	0.23	10.59	838	794
RVM	80.49	0.03	2	3	321.99	0.47	6	62
*i*RVM	36.90	0.03	2	3	51.80	0.29	2	39
GRVM-*ru*	226.60	0.04	3	3	542.97	0.14	2	17
*i*GRVM-*ru*	89.61	0.03	3	2	145.92	0.05	3	4
GRVM-3σ	4.51	0.008	2	2	10.53	0.009	2	2
*i*GRVM-3σ	7.16	0.11	4	6	15.61	0.06	4	8

4.6 Summary

The main contribution of this chapter is to propose incremental and granular learning into RVM and develop a novel classifier- *i*GRVM. The proposed classifier not only preserves the *sparse* property of original RVM, but it is also *scalable*, *faster*, and can be trained with *unbalanced* large data. The case study on biometric match score classification highlights that *i*GRVM outperforms original RVM classifier and is comparable to LR and SVM. The key advantage of the proposed classifier comes from testing time which is significantly reduced compared to SVM. This case study motivates the application of *i*GRVM for boosting the performance of iris recognition systems. The 2-dimensional scores from left and right units of iris are classified using proposed *i*GRVM classifier. The results showcase an improvement in performance using multi-unit iris over recognition using single unit.

The second contribution is an efficient fusion approach that combines the decisions from different biometric classifiers using *i*GRVM. The probabilistic decision from individual classifiers are combined using sum rule. Iris recognition performance further improves using the proposed fusion framework. The results of fusion are obtained using different classifiers like LR, SVM, and RVM. From the experiments it is inferred that the proposed *i*GRVM can be considered as an attractive alternative to well-known classifiers such as LR and SVM.

Chapter 5

Multi-dimensional Tree based Iris Indexing

Recent deployment of biometrics for various real time applications has led to the creation of some large biometric databases. FBI database (IAFIS) is one of the largest biometric database in the world [144]. This database includes criminal histories of more than 66 million subjects in the criminal master file with 25 million fingerprints from civilians. UAE has launched a national border crossing security initiative. Presently 27 land, air, and sea ports of entry are equipped with this system [4]. In India, a large scale project Aadhaar [5] is undertaken to issue unique identification number to each individual across the country using face, fingerprint and iris [5]. In UK, Iris Recognition Immigration System (IRIS) is used to enter through automated barriers at certain airports [14].

On such large biometric databases, identifying an individual with limited computation resource becomes challenging. Performing an exhaustive search against the already enrolled templates in the database is not pragmatic. As discussed earlier, the size of the database has severe implications on speed as well as performance [88]. Logically partitioning the database reduces the number of comparisons required to find the identity of the probe. Databases can be partitioned using classification or indexing approaches. Classification schemes partition the database into some *supervised* classes. For instance classifying the face database into male and female classes having unbiased distribution, reduces the search space by approximately half. However, the performance of classification approaches is greatly affected by the number of classes (ascertained priori). Further, classification reduces the size of search database disproportionately which results in unbalanced distribution of identities [103].

The aforementioned issues are resolved by continuous classification approaches also known as indexing. Indexing logically partitions the database such that images
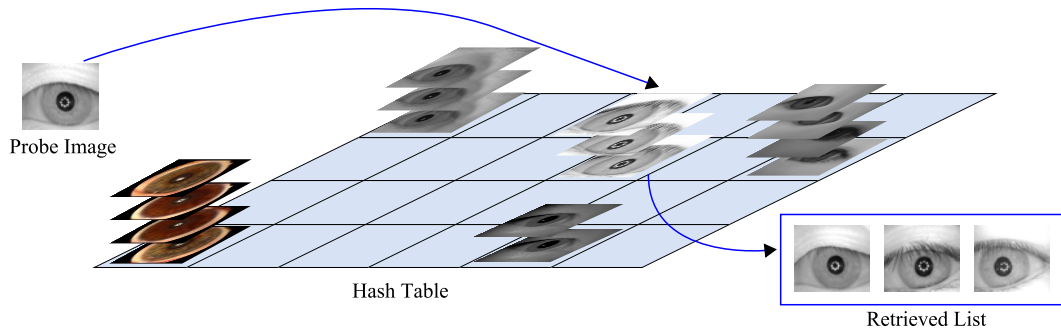
Figure 5.1: Illustrating search space reduction using indexing.

possessing similar characteristics share the similar index as shown in Figure 5.1. In indexing, each image is characterised by a numerical vector. Based on similarity preserving transformation, similar biometric images fall in close proximity of the multi-dimensional space. In continuous classification approaches, the system performance can be enhanced by regulating the number of neighbors considered. The main objective of indexing is to significantly reduce the number of candidates to be considered by the underlying matching algorithm. Tan et al. [145], have performed an empirical investigation to compare the performance of classification over indexing. Experimentally it is found that at specific GAR during identification, only 5% of the database is searched by indexing whereas classification may need to search approximately 20% of the entire search space. This substantiates the application of continuous classification (indexing) approaches for biometrics.

Indexing biometric databases is not simple as data is unstructured and cannot be easily sorted into alphabetical or numerical order [72]. An ideal biometric indexing approach must satisfy the following characteristics:

i. *Scalable* to new insertion, as many real time biometric applications like Aadhaar [5] continuously enroll the data. The cost of re-indexing the entire database for each new enrollment is not pragmatic.

ii. The index space should be *balanced* and insertion order invariant. On arrival of sorted data, the index structure generally becomes skewed. However, an ideal indexing approach avoids such imbalance.

iii. The index generated should possess *invariance* to various possible transformations that happen due to change in acquisition setup, environmental dynamics etc.

iv. The index should be *multi-dimensional* by design. As biometric features are multi-dimensional in nature so the indexing approach should be designed to handle multi-dimensional features.
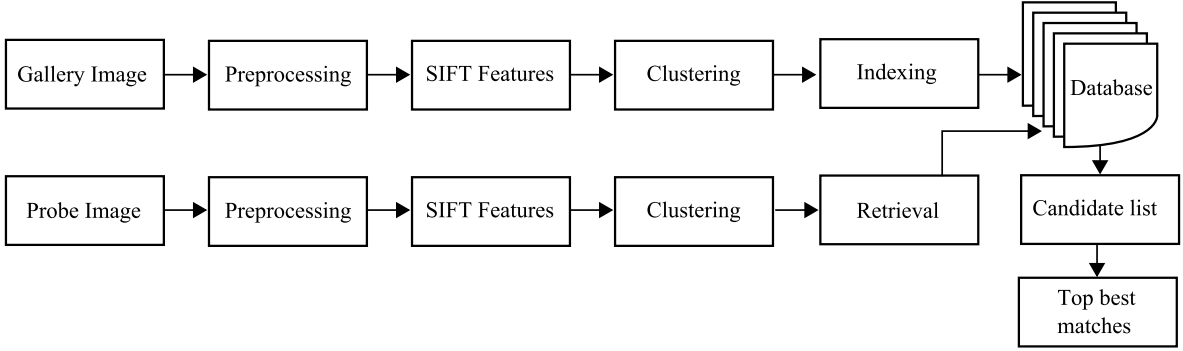
Figure 5.2: Block diagram of proposed indexing approaches.

Spatial data structures are popularly used for indexing multi-dimensional databases [146]. The primary objective is to design an index which is scalable, balanced, invariant to transformations, and multi-dimensional in nature. In this chapter, an effort has been made to index iris biometric database using multi-dimensional trees. The features extracted using SIFT are clustered into m groups as discussed in Section 5.1. Clustered features are used to index the database using **k-d tree** as given in Section 5.2 (please refer Figure 5.2). Some issues specific to k-d tree supports the application of **k-d-b tree** for indexing iris databases as discussed in Section 5.3. Application of **R-tree** for iris database indexing (refer Section 5.4) improves performance compared to other two proposed approaches. For R-tree retrieval, hybrid coarse-to-fine searching strategy is proposed that combines the merits of local as well as global features. The detailed description of proposed indexing approaches are explained in sequel.

5.1 Clustering Keypoint Descriptors

The number of SIFT keypoints (n) vary across iris images in the database of size N. The traditional approaches to database indexing becomes unsuitable for change in value of n. K-means clustering is used to group the number of keypoints sharing similar descriptor property. The idea is to have transformation from variable number of keypoints (n) to fixed number of clusters (m), already ascertained. Clustering is done by representing each keypoint descriptor in k-dimensional (k=128) space. To begin with k-means clustering, centroids are chosen analytically at equal intervals from the descriptor set. The choice of centers can be randomised but this may lead to variation in results. The process starts with assigning each keypoint i to jth cluster center with

minimum squared error given by

$$ed_j = ||D_i - c_j||^2 \tag{5.1}$$

where $1 \leq i \leq n$ and $1 \leq j \leq m$, D is the keypoint descriptor matrix of size $(n \times k)$ and c stores the cluster centers. The keypoints sharing similar descriptor properties are grouped together and cluster centers are re-calculated to obtain new centers. After m new centers are calculated, the re-association is done between the original keypoints and the nearest new centroid using Equation (5.1). This process is iterated until cluster centers gets fixed. The clustered keypoints are shown in Figure 5.3 for change in value of m, marked using colors. The choice of m is crucial and ascertained experimentally. Algorithm 7 outlines the steps involved in k-means clustering approach.

Algorithm 7: K-means

    Input: D: Keypoint descriptor matrix of size $(n \times k)$
    Output: c: Cluster centroids of size $(m \times k)$
1 Initialise cluster centers $[c_1; c_2; \ldots c_m]$ at uniform intervals
2 **repeat**
3   **foreach** *keypoint descriptor i* **do**
4   **foreach** *cluster center j* **do**
5 $ed_j = ||D_i - c_j||^2$
6   **end**
7   Assign each keypoint i to the cluster j that has minimum ed
8   **end**
9   **foreach** *cluster j* **do**
10   Recompute centers c_j
11   **end**
12 **until** *cluster centers gets fixed*

5.2   K-d Tree

K-d tree is a multi-dimensional binary search tree for indexing higher dimensional databases [147]. The application of k-d tree for indexing various large scale real-time databases is promising [146]. In this thesis, local feature based indexing approach is proposed using k-d trees. The merits of proposed indexing approach over existing indexing approaches are outlined as follows:

1. The approach in [75] constructs a single k-d tree using *global* features whereas the proposed indexing constructs multiple k-d trees (m) using *local* features.
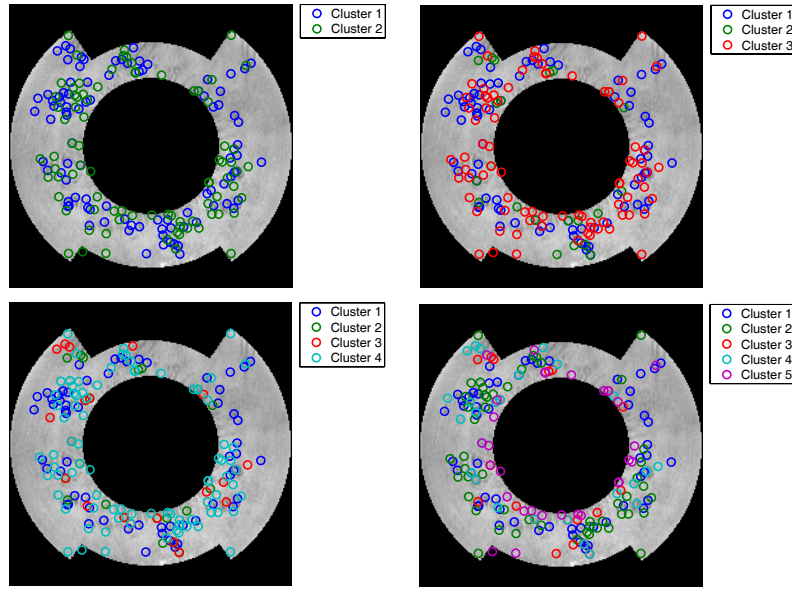
Figure 5.3: Clustered keypoint descriptors using k-means for change in value of m.

2. Local feature based indexing approach proposed in [89] is invariant to various possible transformations. However, the time required for single probe identification is high which is reduced significantly using the proposed k-d tree based indexing approach.

The cluster centers obtained using k-means are used to construct k-d tree as explained in Section 5.2.2. For m cluster centers, m such k-d trees are constructed. During retrieval, cluster centers are obtained for probe iris image. The k-d tree corresponding to probe cluster center is traversed and K Nearest Neighbors (KNN) are retrieved as explained in Section 5.2.3. The nearest neighbors from m trees are combined using union operation to form a candidate set. The block diagram of proposed indexing approach is given in Figure 5.4. To summarise, the keypoints are clustered using **k**-means. The clustered keypoints are inserted into **k**-d tree during indexing and retrieved using **k**nn approach. Thus, there is a need to have an in depth study of the parameter **k** used by clustering, indexing and retrieval modules. For the sake of clarity, few conventions are renamed and used subsequently in this thesis. These notations are defined as:

Approach	Convention		Description
	Original	Used	
k-means	k	m	m is the number of clusters
k-d tree	k	k	k is the data dimensionality
KNN	k	p	p is the number of nearest neighbors
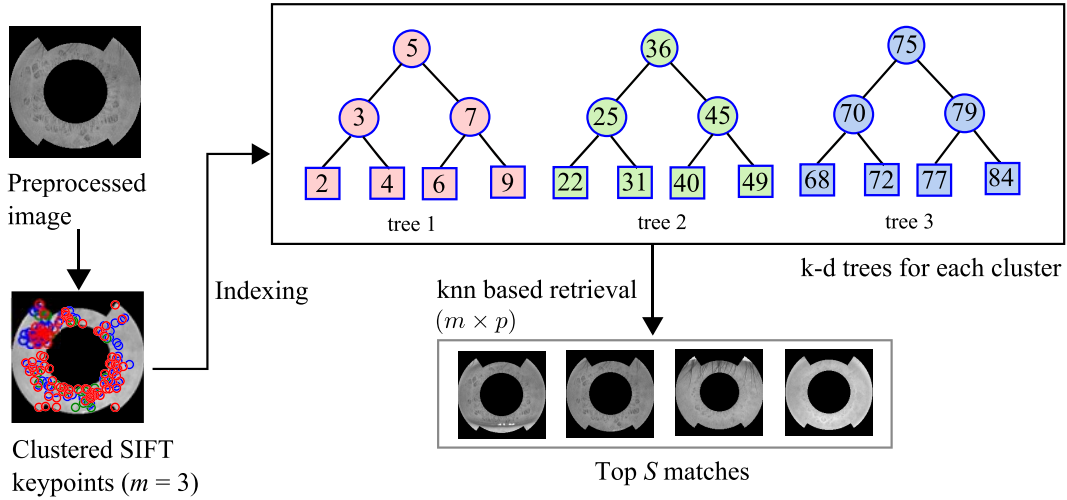
Figure 5.4: Block diagram of the proposed k-d tree based indexing approach.

5.2.1   Structure of k-d tree

Each node is represented as k-dimensional (k is dimensionality of each node) point (P) in the tree. The k-dimensional features of node P are denoted as $\{k_0(P), k_1(P) \ldots k_{k-1}(P)\}$. Each node in the tree has two pointers, *left(P)* and *right(P)*. During tree construction, the discriminator that is used for partitioning the feature space is given by *split-dim(P)*. Let, $j \leftarrow$ *split-dim(P)*, then for any point Q in $left(P)$, $k_j(Q) < k_j(P)$. Similarly for any point R stored as a node in $right(P)$, $k_j(R) > k_j(P)$. All nodes in the same level have same split dimension. The root node has discriminator 0 and its immediate level has discriminator 1. The discriminator at level i is calculated as $split - dim(P) = i$ mod k. The planar graph representation for 2-d tree is shown in Figure 5.5(a). The operation performed along split dimension j are defined as j-median which finds the median along the *jth* dimension among all the records. The 2-d space representation of k-d tree is shown in Figure 5.5(b). Here non-leaf nodes are represented as circles ($\bullet$) and leaf nodes are represented as squares ($\blacksquare$). Each node is bounded by a rectangle to define its geometric range.

5.2.2   Indexing

In k-d tree indexing, the space representing points are partitioned into two subspaces. Following the concept of binary search trees, each record should have equal probability of being on either side. The split value for each level is chosen to be the median value of marginal distribution of features for a particular dimension. Points on the left subtree are less than the split value and points on the right are greater than the split value. In this approach, iris database is indexed using k-d trees constructed from cluster centers.

(a) planar graph   (b) 2-d space
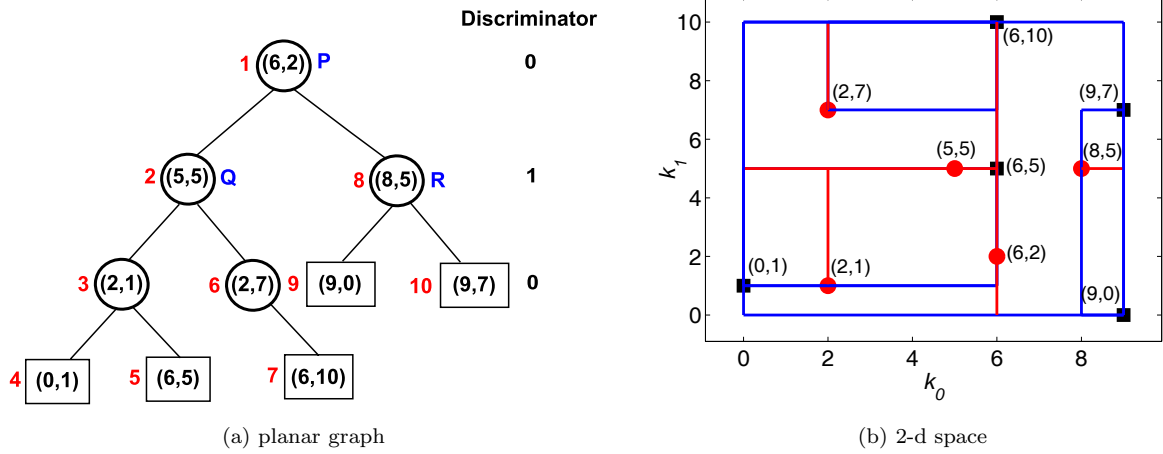
Figure 5.5: 2-d tree representations of sample points. In (b) ● represents non-leaf node and ■ represents leaf node.

Figure 5.6: Proposed k-d tree structure for N iris images.

Each cluster center from an iris image is denoted by C_{xy} for $1 \leq x \leq N$ and $1 \leq y \leq m$ where N is the total number of iris images and m being the number of cluster centers for each image. A group (G_y) is build for yth cluster center from all iris images in the gallery set. An independent k-d tree is constructed (denoted as t_y) for group G_y using Algorithm 8. Thus, m such k-d trees are constructed for m cluster centers. The mapping of cluster centers for k-d tree construction is shown in Figure 5.6. The k-d tree construction starts by finding the j-median element of G_y for the *jth* discriminator. This median element is used to create a node P, which is root of the tree. Further, those elements in G_y which are j-less than P are stored in G_L (left subtree). Similarly, elements of G_y which are j-greater than P are stored in G_R (right subtree). The tree construction process is iterated with two new lists G_R and G_L. The $left(P)$ is pointer to subtree generated using G_L and $right(P)$ is the pointer to subtree generated using G_R. The split dimension for the next level is found by $(j + 1) \bmod k$. The k-d tree construction is a recursive process and stops when the lists are empty.

Algorithm 8: k-d_Insert

Input: G_y: Group of *yth* cluster centers, j: discriminator
Output: T_y: k-d tree from *yth* group

1 if $G_y = \phi$ **then**
2 $\quad$ **return** NULL
3 end
4 $P = j$-median element of G_y
5 $G_L = \{a \in G_y | a \text{ is } j\text{-less than } P\}$
6 $G_R = \{b \in G_y | b \text{ is } j\text{-greater than } P\}$
7 $split - dim(P) = j$
8 $M = (j + 1) \bmod k$
9 $left(P) = \text{k-d\_Insert}(G_L, M)$
10 $right(P) = \text{k-d\_Insert}(G_R, M)$
11 return P

5.2.3   KNN Retrieval

The gallery iris images that have close proximity with probe iris are retrieved using k nearest neighbor (KNN) search algorithm [148] . KNN is defined by taking a circle of radius r centered at query node (Q) and finding all nearest neighbors (p) that must lie within the circle. The search process begins by traversing the k-d tree in depth first order to reach the leaf node depending upon the value at split dimension. After encountering the leaf node, the distance of Q is obtained with the leaf. A priority queue (QD) is maintained in non-increasing order of distance values and the image identifier (id) corresponding to the tree node are stored in form of a list ($List$). The radius (r) of circle is equal to distance of *pth* closest element from Q. For illustration, let us consider k-d tree in Figure 5.5(a). To retrieve 3nn corresponding to query $Q(1, 1)$, the tree is traversed in depth first order and distance of Q is obtained with leaf node as shown in Figure 5.7(a). Whenever an element of tree node in the active partition is found to be more closer than *pth* distant element of priority queue (stored at $QD[1]$), the $\{List, QD\}$ is updated as shown in Figure 5.7(b). If the node under investigation is non-leaf node, the recursive procedure is called for the node on same side of the partition as Q. However, if the number of elements in $List$ is less than p then the other side of the partition is explored. In case the size of $List$ is equal to p then a decision is taken to search parent's other child to find more closer neighbors. If the circle centered at Q intersects with geometric boundaries of the other subtree then the partition is considered on the other side as shown in Figure 5.7(a-b). The side opposite to active partition is considered to further find the neighbors based on distance from Q. However, if the geometric boundaries do not overlap, then the opposite subtree

is left unexplored as marked by gray colored nodes in Figure 5.7(b-c). Figure 5.7(c) highlights final neighbors in green color after traversing the k-d tree using KNN. The 2-d space representation of query and its three nearest neighbors marked by green $*$ are shown in Figure 5.7(d).

Due to the algorithmic efficiency and applicability to k-d tree [148], KNN is used to retrieve p nearest neighbors corresponding to the probe iris template. The keypoint descriptors from probe iris are divided into m clusters and the *yth* cluster center is used to traverse corresponding tree (t_y) for finding p neighbors. The algorithm for finding nearest neighbor for probe cluster (Q_y) is given in Algorithm 9. For m cluster centers, $(m \times p)$ neighbors are obtained. The set union operation is used to combine the neighbors into a comprehensive candidate list. At refined stage, the probe feature descriptor is compared with each element of the candidate list to rank the retrieved identities. Top S matches are taken to claim the identity of probe, where $\{S \subseteq (m \times p)\}$.

5.2.4   Experimental Results

In this section, the efficiency of proposed indexing approach is measured experimentally. The results are obtained for change in number of clusters (m) and nearest neighbors (p). The optimal choice of these parameters is obtained experimentally.

Databases Used

The experiments in this thesis are performed using two publicly available databases:

- **BATH Iris** (BATH) [29]: This database comprises images from 50 subjects. For each subject both left and right iris images are acquired (100 eyes), each containing 20 images of the respective eyes. This makes total of 1000 iris images to perform experiments.

- **CASIA Iris Version 3** (CASIAV3) [21]: This database is acquired in an in-door environment. The images have been captured in two sessions, with an interval of at least one month. The database comprises 249 subjects (498 irises) with total of 2655 images from the left and right eyes.

To measure the identification accuracy, each database is divided into mutually exclusive gallery and probe sets. In order to reduce the response time during identification, the gallery set is partitioned into bins. This reduces the number of comparisons required to find the identity of the probe.
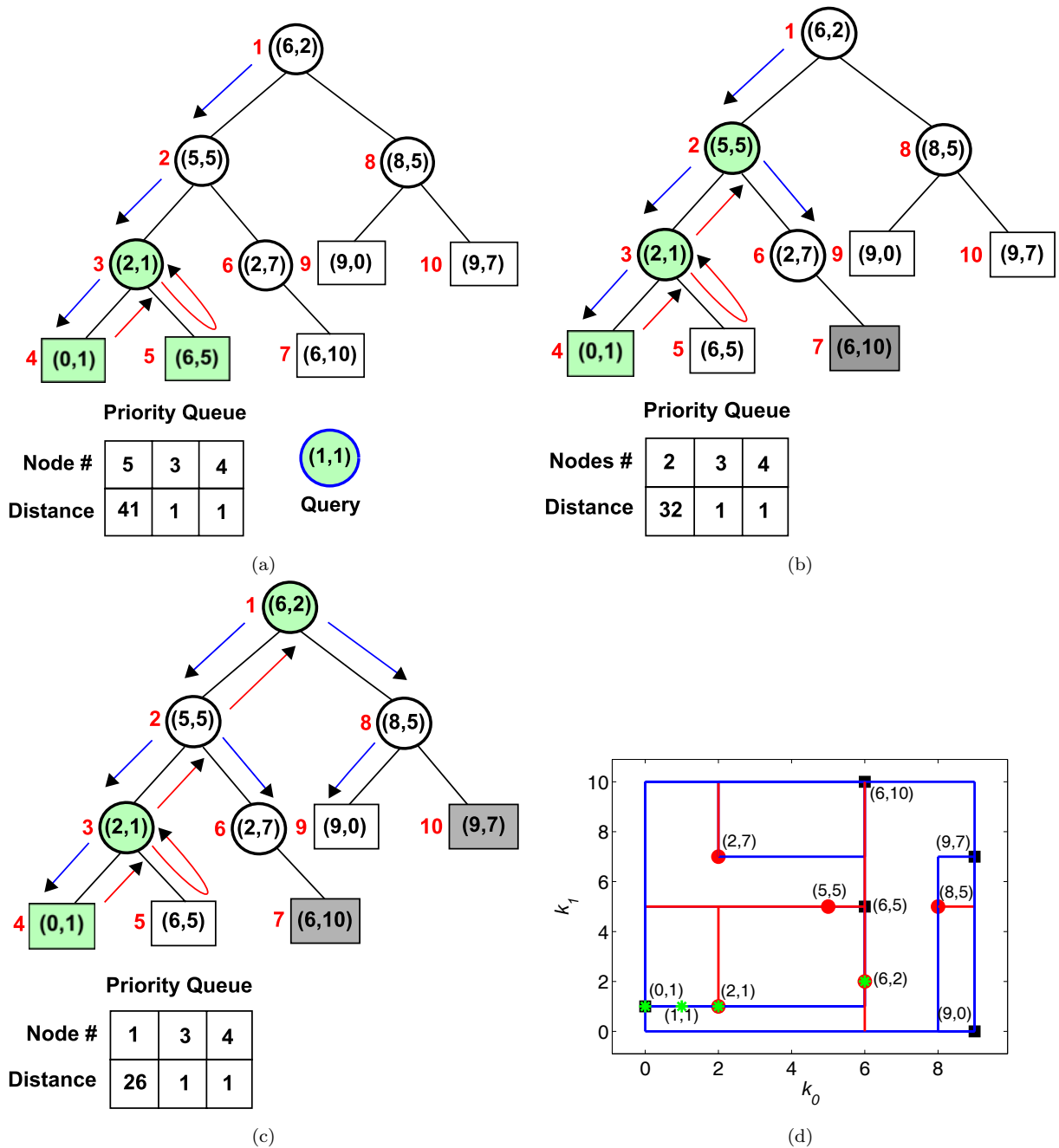
Figure 5.7: Query retrieval using KNN from 2-d tree, (a)-(c) illustrates search process of KNN and (d) spatial representation of tree where query node and its retrieved neighbors are marked by green *.

Design of Experiments

The experiments are carried out for change in two significant parameters as discussed earlier. The first and most influential parameter is decision regarding number of cluster centers m and the second is number of nearest neighbors p. The choice of m and p are dependent upon rank-k identification. Thus, results are obtained by varying values of

---

Algorithm 9: KNN_Search

Input: Q: *yth* cluster center from probe features, T: *yth* k-d tree
Output: *List*: List of gallery *ids* for p best matches

1 $d = split - dim(T)$
2 $p = T[data_d]$ `// Data value of tree node at dth dimension`
3 if T *is leaf* **then**
4 $\quad \{List, QD\} = $ Update_List(Q, T) `// QD is priority queue of p`
$\quad$ distances
5 $\quad$ **return** $List$
6 end
7 if $Q[d] \leq p$ **then**
8 $\quad List = $ KNN_Search$(Q, T(left))$
9 else
10 $\quad List = $ KNN_Search$(Q, T(right))$
11 end
12 if **length**$(List) < p$ **then**
13 $\quad flag = true$
14 else
15 $\quad flag = $ Search_Otherside(Q, QD, T)
16 end
17 if $flag$ **then**
18 $\quad \{List, QD\} = $ Update_List(Q, T)
19 $\quad$ **if** $Q[d] \leq p$ **then**
20 $\quad\quad List = $ KNN_Search$(Q, T(right))$
21 $\quad$ **else**
22 $\quad\quad List = $ KNN_Search$(Q, T(left))$
23 $\quad$ **end**
24 end
25 return $List$

---

m and p. CMC curves for change in m are shown in Figure 5.9(a) and Figure 5.9(b) for BATH and CASIAV3 databases respectively. Each sub-figure shows curves for some selected nearest neighbors {5, 10, 20, 40, 50}. The reason for showing selected curves of p is to achieve visual clarity in graphs. Table 5.1 and Table 5.2 shows the values of pi for change in m and p on BATH and CASIAV3 databases respectively. From the results it is evident that as the number of nearest neighbors increases, pi improves. The reason for increase in pi with p is that the number of neighbors increases which in turn increases probability of finding the correct match. The penetration rate for the proposed system is a monotonically increasing function of p and m. Thus, PR is obtained using

$$PR = \frac{m \times p}{N} \tag{5.2}$$

Algorithm 10: Update_List(Q, T)

Input: Q: *yth* cluster center from probe, T: *yth* Tree

Output: *List*: List of gallery *ids* for p best matches, QD: Priority queue of p closest distances encountered

1 $point = T[data]$

2 $distance = \sqrt{\sum_{i=1}^{k}(Q[i] - point[i])^2}$

3 **if** $length(List) = p$ *and* $QD[1] > distance$ **then**

4 $QD[1] = distance$

5 $List[1] = T[id]$ `// image id corresponding to tree node`

6 **else if** $length(List) < p$ **then**

7   **shift** elements of $\{List, QD\}$ one to right

8 $QD[1] = distance$

9 $List[1] = T[id]$

10   **sort** $\{List, QD\}$ in non-increasing order

11 **return** $\{List, QD\}$

Algorithm 11: Search_Otherside(Q, QD, T)

Input: Q: *yth* cluster center from probe, QD: Priority queue of p distances, T: *yth* tree

Output: $flag$: Logical value to determine if the boundaries overlap

1 $sum = 0$

2 $LB = $ lower boundary of T `// defined during node creation`

3 $UB = $ upper boundary of T

4 $r = QD[1]$ `// distance of pth nearest neighbor`

5 $flag = $ true

6 **for** $d = 1$ **to** k **do**

7   **if** $Q[d] < LB[d]$ **then**

8 $sum = sum + \sqrt{(Q[d] - LB[d])^2}$

9   **if** $sum > r$ **then**

10 $flag = $ false

11   **break**

12   **end**

13   **end**

14   **else if** $Q[d] > UB[d]$ **then**

15 $sum = sum + \sqrt{(Q[d] - UB[d])^2}$

16   **if** $sum > r$ **then**

17 $flag = $ false

18   **break**

19   **end**

20   **end**

21 **end**

22 **return** $flag$

Table 5.1: Probability of identification for change in m and p at different values of R for BATH database using k-d tree based indexing.

$R \downarrow p \rightarrow$	$m = 2$					$m = 3$					$m = 4$				
	5	10	20	40	50	5	10	20	40	50	5	10	20	40	50
1	0.70	0.74	0.70	0.81	0.83	0.74	0.78	0.83	0.83	0.83	0.79	0.75	0.79	0.83	0.83
2	0.77	0.79	0.77	0.85	0.85	0.78	0.80	0.85	0.87	0.87	0.79	0.83	0.83	0.92	0.92
5	0.77	0.81	0.81	0.89	0.87	0.83	0.83	0.91	0.89	0.91	0.79	0.88	0.92	0.92	0.92
10	0.81	0.83	0.81	0.91	0.91	0.85	0.89	0.91	0.91	0.93	0.79	0.88	0.92	0.92	0.92
20	0.81	0.83	0.83	0.91	0.96	0.87	0.89	0.98	0.96	0.96	0.79	0.88	0.92	0.92	0.92
40	0.81	0.83	0.85	0.94	0.98	0.87	0.91	0.98	1.00	1.00	0.79	0.88	0.96	0.92	0.92
80	0.81	0.83	0.85	0.96	0.98	0.87	0.91	0.98	1.00	1.00	0.79	0.88	0.96	0.96	0.96
100	0.81	0.83	0.85	0.96	0.98	0.87	0.91	0.98	1.00	1.00	0.79	0.88	0.96	0.96	0.96
$R \downarrow p \rightarrow$	$m = 5$					$m = 6$					$m = 7$				
	5	10	20	40	50	5	10	20	40	50	5	10	20	40	50
1	0.81	0.88	0.94	0.94	0.94	0.85	0.88	0.91	0.91	0.91	0.89	0.89	0.96	0.96	0.96
2	0.84	0.94	1.00	0.97	0.94	0.88	0.91	0.94	0.94	0.94	0.93	0.89	0.96	0.96	0.96
5	0.91	0.94	1.00	1.00	1.00	0.91	0.94	0.94	0.94	0.94	0.96	0.93	0.96	0.96	0.96
10	0.94	0.97	1.00	1.00	1.00	0.91	0.94	0.97	0.97	0.97	0.96	0.93	0.96	0.96	0.96
20	0.94	0.97	1.00	1.00	1.00	0.97	0.94	0.97	1.00	1.00	0.96	0.96	1.00	0.96	0.96
40	0.94	0.97	1.00	1.00	1.00	0.97	0.97	1.00	1.00	1.00	0.96	0.96	1.00	1.00	1.00
80	0.94	0.97	1.00	1.00	1.00	0.97	0.97	1.00	1.00	1.00	0.96	0.96	1.00	1.00	1.00
100	0.94	0.97	1.00	1.00	1.00	0.97	0.97	1.00	1.00	1.00	0.96	0.96	1.00	1.00	1.00
$R \downarrow p \rightarrow$	$m = 8$					$m = 9$					$m = 10$				
	5	10	20	40	50	5	10	20	40	50	5	10	20	40	50
1	0.93	1.00	0.96	0.96	0.96	0.93	0.96	1.00	1.00	1.00	0.91	0.95	0.95	1.00	1.00
2	0.93	1.00	0.96	1.00	1.00	0.93	1.00	1.00	1.00	1.00	0.95	0.95	0.95	1.00	1.00
5	0.96	1.00	0.96	1.00	1.00	0.96	1.00	1.00	1.00	1.00	0.95	1.00	1.00	1.00	1.00
10	0.96	1.00	1.00	1.00	1.00	**1.00**	1.00	1.00	1.00	1.00	0.95	1.00	1.00	1.00	1.00
20	0.96	1.00	1.00	1.00	1.00	1.00	1.00	1.00	1.00	1.00	0.95	1.00	1.00	1.00	1.00
40	0.96	1.00	1.00	1.00	1.00	1.00	1.00	1.00	1.00	1.00	0.95	1.00	1.00	1.00	1.00
80	0.96	1.00	1.00	1.00	1.00	1.00	1.00	1.00	1.00	1.00	0.95	1.00	1.00	1.00	1.00
100	0.96	1.00	1.00	1.00	1.00	1.00	1.00	1.00	1.00	1.00	0.95	1.00	1.00	1.00	1.00

Here m is chosen carefully as the number of clusters is influential in obtaining γ. Table 5.3 shows the values of γ for change in value of p and m on BATH database. Similar observations are made for CASIAV3 database as shown in Table 5.4.

Bin miss rate for change in p is shown in Figure 5.8(c). The curves are plotted for different values of m. The accuracy of an identification system is usually measured in terms of bin miss rate. From the graph it is evident that as the number of clusters increases, the bin miss rate reduces. The theoretical value of PR (Figure 5.8(a)) is slightly different from the actual implementation as shown in Figure 5.8(b). The difference is due to variation in probe and gallery templates that leads to false rejections. The plot of γ is shown in Figure 5.8(d). The relationship between PR and BM is shown in Figure 5.8(e). Thus, in this research m is selected where γ obtained is maximum with reduced penetration rate and lowest bin miss rate. In brief, the value of m and p are chosen where the value of γ is maximum for highest probability of identification. It has been observed through experiments that the value of γ varies with the size of the database. The proposed system is rank-10 based identification system for BATH database. The value of $m = 9$ and $p = 5$ gives significantly high γ of 0.98 with considerably low PR of 0.03 for no bin miss. For CASIAV3 database, $pi = 0.96$ is achieved for rank-200. These value are selected at $m = 5$ and $p = 50$ which gives
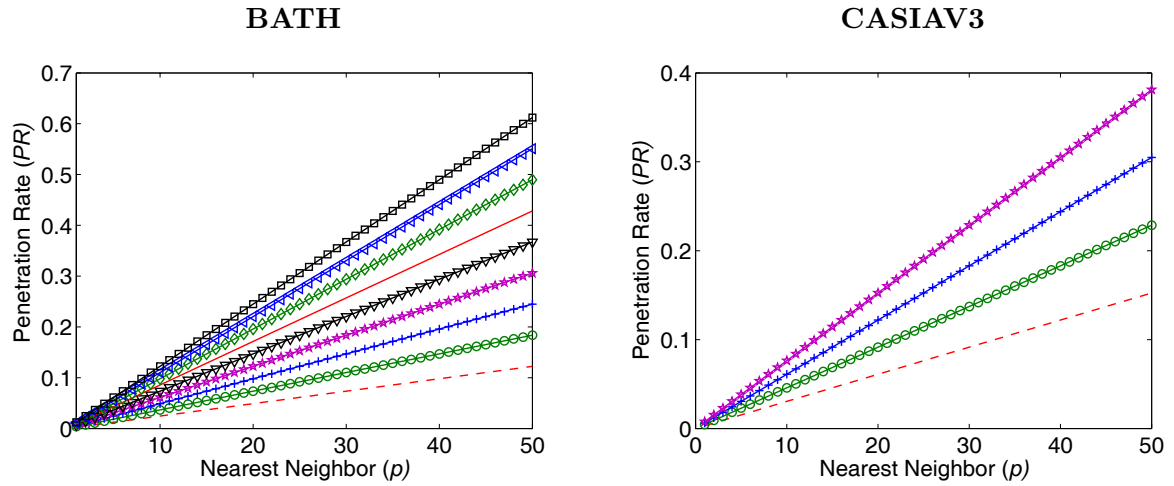
BATH   **CASIAV3**

(a) *PR* using equation (5.2)
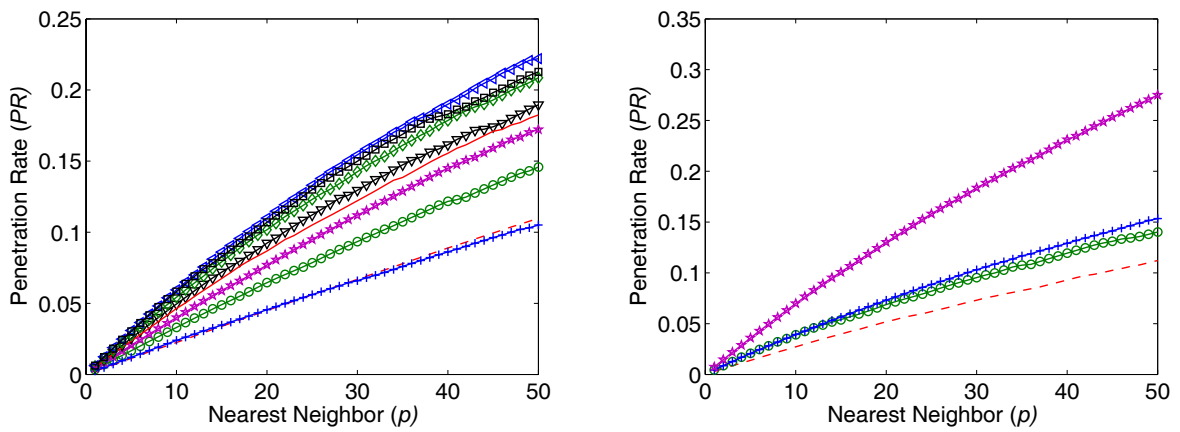
(b) *PR* through experiments

(c) *BM*

(d) γ

(e) PR vs. BM

- - -	m=2
—⊝—	m=3
—+—	m=4
—✳—	m=5
—▽—	m=6
——	m=7
—◇—	m=8
—◁—	m=9
—□—	m=10
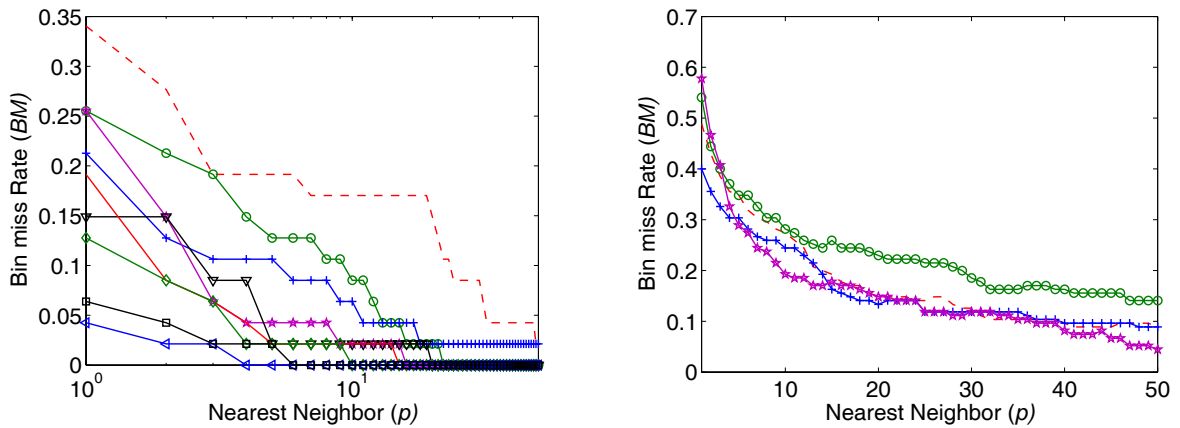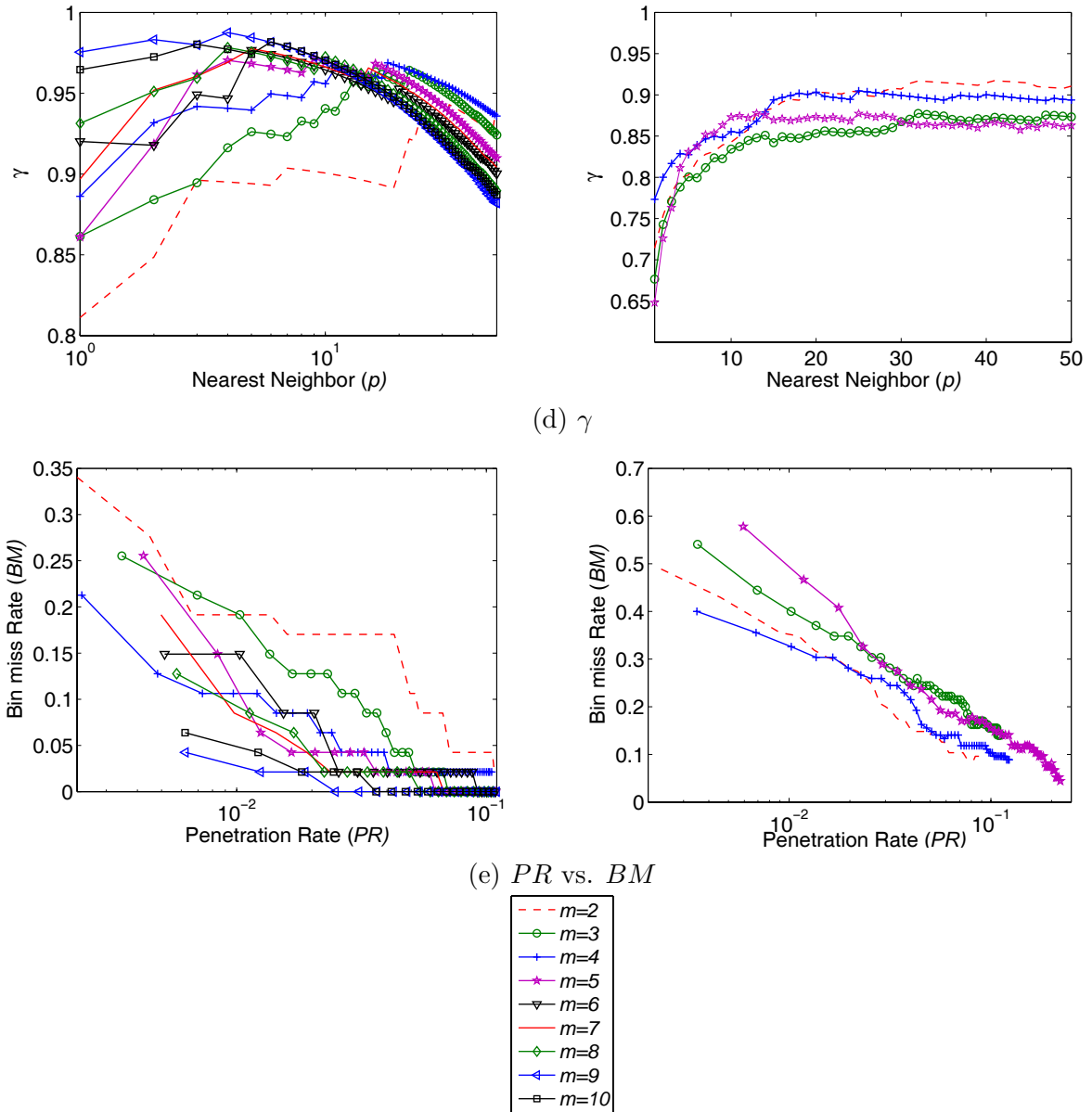
Figure 5.8: Performance measures for change in values of p and m using k-d tree based indexing.

90
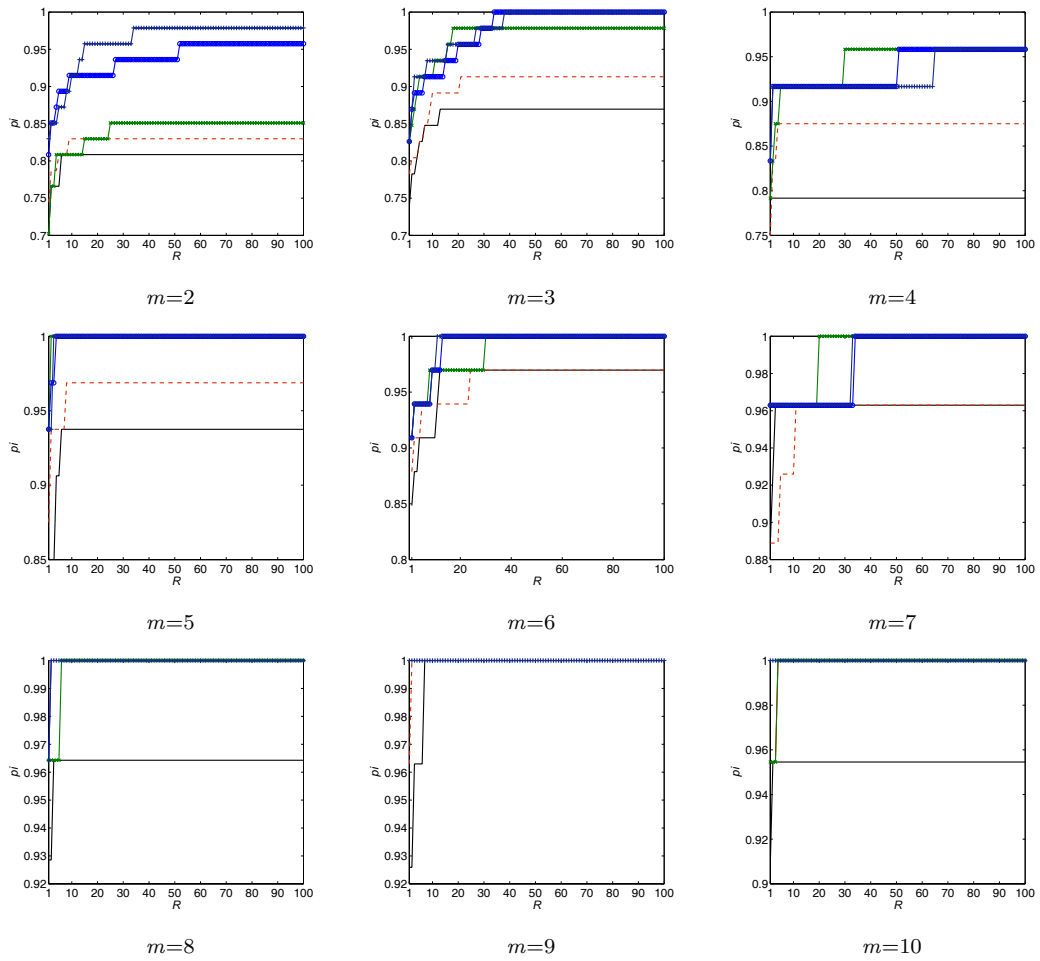
(a) **BATH**
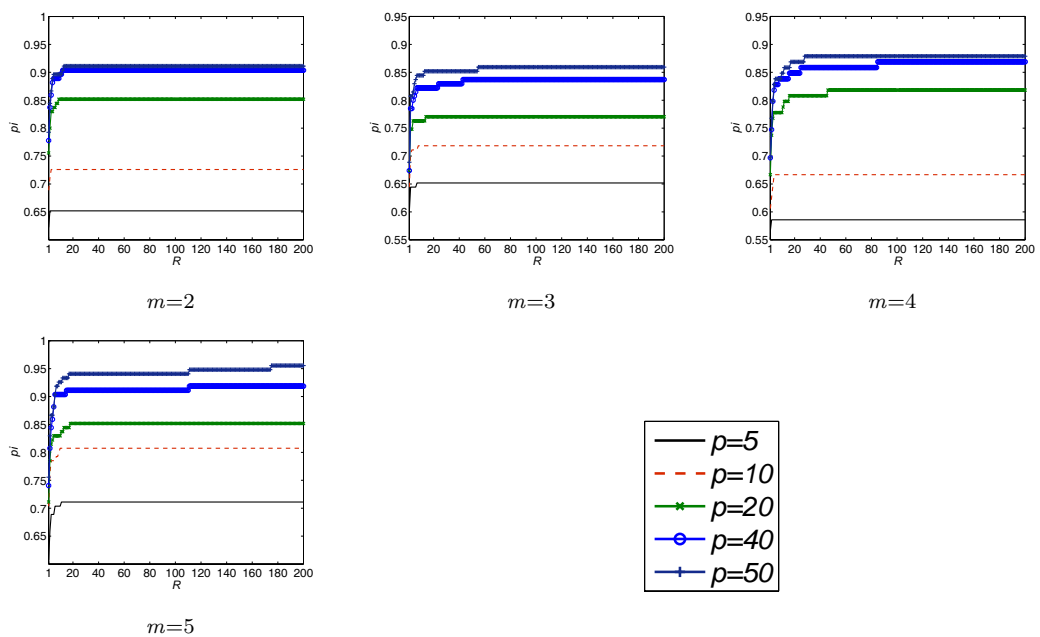
(b) **CASIAV3**

Figure 5.9: CMC curves of k-d tree based indexing for different clusters each with change in value of p.

Table 5.2: Showing pi for change in m, p, and R on CASIAV3 database using k-d tree.

$R \downarrow p \rightarrow$	$m = 2$					$m = 3$				
	5	**10**	**20**	**40**	**50**	**5**	**10**	**20**	**40**	**50**
1	0.62	0.69	0.76	0.78	0.79	0.60	0.64	0.67	0.67	0.69
2	0.65	0.71	0.80	0.84	0.84	0.64	0.70	0.75	0.79	0.81
5	0.65	0.73	0.84	0.89	0.90	0.64	0.71	0.76	0.81	0.83
10	0.65	0.73	0.85	0.90	0.90	0.65	0.72	0.76	0.82	0.84
20	0.65	0.73	0.85	0.90	0.91	0.65	0.72	0.77	0.82	0.85
30	0.65	0.73	0.85	0.90	0.91	0.65	0.72	0.77	0.83	0.85
50	0.65	0.73	0.85	0.90	0.91	0.65	0.72	0.77	0.84	0.85
100	0.65	0.73	0.85	0.90	0.91	0.65	0.72	0.77	0.84	0.86
200	0.65	0.73	0.85	0.90	0.91	0.65	0.72	0.77	0.84	0.86
$R \downarrow p \rightarrow$	$m = 4$					$m = 5$				
	5	**10**	**20**	**40**	**50**	**5**	**10**	**20**	**40**	**50**
1	0.57	0.61	0.67	0.70	0.70	0.61	0.70	0.71	0.74	0.76
2	0.59	0.63	0.74	0.75	0.77	0.66	0.76	0.79	0.81	0.83
5	0.59	0.67	0.78	0.83	0.84	0.69	0.79	0.83	0.88	0.88
10	0.59	0.67	0.78	0.84	0.85	0.70	0.81	0.83	0.90	0.93
20	0.59	0.67	0.81	0.85	0.87	0.71	0.81	0.85	0.91	0.94
30	0.59	0.67	0.81	0.86	0.88	0.71	0.81	0.85	0.91	0.94
50	0.59	0.67	0.82	0.86	0.88	0.71	0.81	0.85	0.91	0.94
100	0.59	0.67	0.82	0.87	0.88	0.71	0.81	0.85	0.91	0.94
200	0.59	0.67	0.82	0.87	0.88	0.71	0.81	0.85	0.92	**0.96**

$\gamma = 0.83$ for $PR = 0.28$ and $BM = 0.04$. From the experimental analysis it is found that γ cannot be taken as a conclusive performance measure but is considered as a good compromise between accuracy and time.

5.3   K-d-b Tree

It has been observed that the proposed k-d tree based indexing achieves good performance for iris. However, k-d tree by design suffers from the following two issues:

i. The conventional approach for k-d tree construction finds the median element from the features. This approach is static and requires re-construction of the tree on encountering a new batch of data during enrollment. Biometrics applications are continuously confronted with new data and re-constructing the tree for each new enrollment is not acceptable.

ii. k-d tree based indexing does not take paging of secondary memory into consideration. The time required to read the records from the disk far exceeds the time required to compare the records once available, after searching k-d tree.

Table 5.3: γ, PR, BM for change in m and p on BATH database using k-d tree.

$m \rightarrow$	**2**			**3**			**4**		
$p \downarrow$	γ	**PR**	**BM**	γ	**PR**	**BM**	γ	**PR**	**BM**
5	0.89	0.01	0.19	0.93	0.02	0.13	0.94	0.01	0.11
10	0.90	0.02	0.17	0.94	0.03	0.09	0.96	0.02	0.06
20	0.90	0.04	0.15	0.96	0.06	0.02	0.97	0.05	0.02
40	0.93	0.09	0.04	0.94	0.12	0.00	0.95	0.09	0.02
50	0.93	0.11	0.02	0.92	0.15	0.00	0.94	0.11	0.02
$m \rightarrow$	**5**			**6**			**7**		
$p \downarrow$	γ	**PR**	**BM**	γ	**PR**	**BM**	γ	**PR**	**BM**
5	0.97	0.02	0.04	0.98	0.03	0.02	0.98	0.02	0.02
10	0.97	0.04	0.02	0.96	0.05	0.02	0.97	0.05	0.02
20	0.96	0.08	0.00	0.95	0.09	0.00	0.96	0.09	0.00
40	0.92	0.14	0.00	0.92	0.16	0.00	0.92	0.16	0.00
50	0.91	0.17	0.00	0.90	0.19	0.00	0.90	0.18	0.00
$m \rightarrow$	**8**			**9**			**10**		
$p \downarrow$	γ	**PR**	**BM**	γ	**PR**	**BM**	γ	**PR**	**BM**
5	0.98	0.03	0.02	**0.98**	**0.03**	**0.00**	0.97	0.03	0.02
10	0.97	0.05	0.00	0.97	0.06	0.00	0.97	0.06	0.00
20	0.95	0.10	0.00	0.94	0.11	0.00	0.95	0.11	0.00
40	0.91	0.18	0.00	0.90	0.19	0.00	0.90	0.18	0.00
50	0.89	0.21	0.00	0.88	0.22	0.00	0.89	0.21	0.00

Table 5.4: γ, PR, BM for change in m and p on CASIAV3 database using k-d tree.

$m \rightarrow$	**2**			**3**		
$p \downarrow$	γ	**PR**	**BM**	γ	**PR**	**BM**
5	0.80	0.01	0.35	0.80	0.02	0.35
10	0.84	0.03	0.27	0.83	0.04	0.28
20	0.90	0.05	0.15	0.85	0.07	0.23
40	0.91	0.09	0.10	0.86	0.12	0.16
50	0.90	0.11	0.09	0.86	0.14	0.14
$m \rightarrow$	**4**			**5**		
$p \downarrow$	γ	**PR**	**BM**	γ	**PR**	**BM**
5	0.83	0.02	0.30	0.83	0.04	0.29
10	0.85	0.04	0.24	0.87	0.07	0.19
20	0.90	0.07	0.13	0.86	0.13	0.15
40	0.89	0.13	0.10	0.84	0.23	0.08
50	0.88	0.15	0.09	**0.83**	**0.28**	**0.04**

Due to multi-dimensional structure of nodes, balancing k-d trees needs precaution. Thus, a variant of k-d tree is applied for iris database indexing to overcome the aforementioned issues. In this thesis, a dynamic data structure coined k-d-b tree [149] combines the multi-dimensional capability of k-d tree with organisation efficiency of B-trees. The insertion of nodes is dynamic and avoids the tree to be reconstructed. The k-d-b tree is height balanced data structure and takes paging of secondary memory into consideration which improves disk access time. This is particularly due to high fanouts (children) for each node which reduces number of input-output operations required for searching.

5.3.1   Structure of k-d-b tree

This approach partitions the search space that consist of k-dimensional **point**(s) represented as $(k_0, k_1, \ldots, k_{k-1})$ to be an element of $domain_0 \times domain_1 \times \ldots domain_{k-1}$ into mutually exclusive **regions** satisfying

$$min_i \leq k_i < max_i, \quad 0 \leq i \leq k - 1 \tag{5.3}$$

where min_i and max_i are the maximum and minimum values of all the elements in the region along *ith* dimension. The k-d-b tree consist of two types of pages

- **Region page**: is the collection of regions and each region is represented by storing (min_i, max_i)

- **Point page**: is the collection of points represented by (k, irisID)

There are few properties that defines k-d-b tree. The region pages cannot contain null pointer which implies that point pages are the leaf nodes of the tree. All the leaf nodes are at the same level and contains pointer to the iris identifiers in the database. The union of two disjoint regions in a region page makes a region. The structure of 2-D k-d-b tree is shown in Figure 5.10 with point and region pages.

5.3.2   Indexing

For indexing iris database, the cluster centers are used to construct k-d-b trees. Similar to k-d tree, in this approach, the *yth* cluster center is used to develop the corresponding k-d-b tree. To perform insertion into k-d-b tree if root node of tree does not exist, then a point page is created and the keypoint center with corresponding iris ID is inserted in the point page. If root node exists, then the tree is traversed to reach the point page for inserting (point, irisID) pair. If the page overflows then splitting is performed by
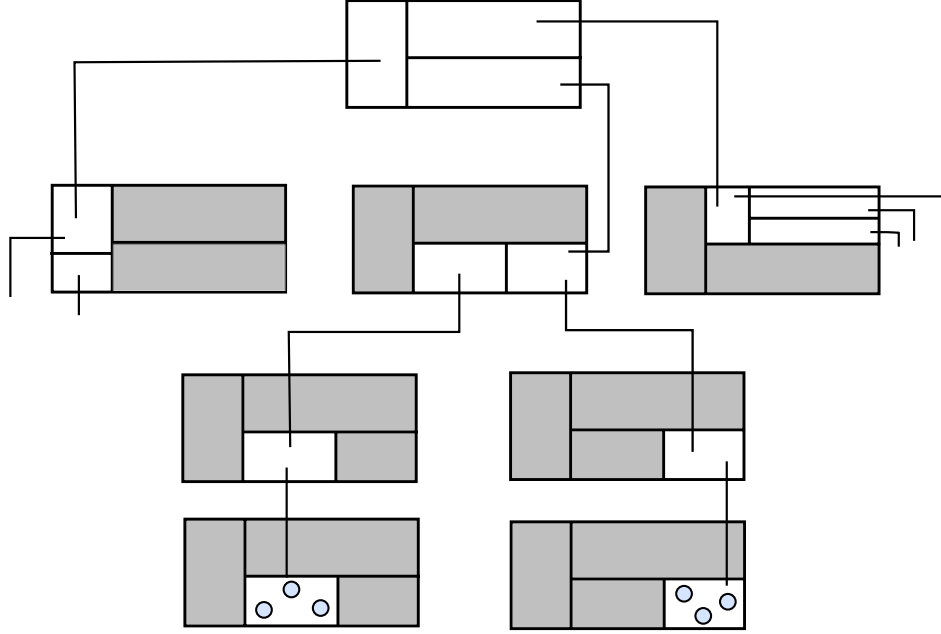
Figure 5.10: Structure of k-d-b tree ($k = 2$). The shaded regions are not included in region pages and point pages are leaf nodes of the tree.

finding a median (k_i) of all the elements in the point page along *ith* dimension. Splitting helps in balancing the k-d-b tree structure. This generates left and right children of the point page. A point y lies on left of k_i if $y_i < k_i$ and otherwise on the right. A new region page is created and marked as root node with left and right children assigned. Similarly, if the region page overflows then the splitting is done along k_i to generate the left and right regions of the page. Let the region page be defined as $I_0 \times I_1 \times \ldots I_{k-1}$, if $k_i \notin I_i$ the region remains unchanged by splitting otherwise let $I_i = [min_i \ max_i)$ and splitting generates two regions

$$
\begin{array}{ll}
\text{left region} & I_0 \times \ldots \times [min_i \ k_i) \times \ldots \times I_{k-1} \\
\text{right region} & I_0 \times \ldots \times [k_i \ max_i) \times \ldots \times I_{k-1}
\end{array}
\tag{5.4}
$$

To find the position of regions for $k_i \notin I_i$ the following scheme is used

$$
\text{region} =
\begin{cases}
k_i < min_i & \text{left} \\
k_i \geq max_i & \text{right}
\end{cases}
\tag{5.5}
$$

If the region lies to the left of k_i add (region, page id) to the left and otherwise to the right. The representation of splitting for region and point pages is shown in Figure 5.11. If splitting is done on root page then a new region page is created with the regions ($domain_0 \times \ldots \times [min_i \ k_i) \times \ldots \times domain_{k-1}$, left id) and ($domain_0 \times \ldots \times [k_i \ max_i) \times \ldots \times domain_{k-1}$, right id). For splitting page other than root, replace in parent of page

to be split (left region, left id) and (right region, right id). If this causes the parent page to overflow then the same process is iterated. The description of steps involved in insertion are given in Algorithm 12. The same process is repeated for m k-d-b trees representing m cluster centers. This approach is *dynamic* and avoids re-indexing the entire database on insertion of a new record. The proposed indexing structure is *balanced* by design unlike k-d tree and considers paging. Thus, the major problems specific to k-d tree based indexing approach are mitigated using k-d-b tree.

Algorithm 12: k-d-b_Insert

Input: point: *yth* cluster center from an iris, irisID: Name of the iris image to be indexed

Output: *root*: Pointer to the root node

1 **if** $root = \varnothing$ **then**
2   insert (point, irisID) in new point page
3   **return**
4 **end**
5 Do range search to reach the point page
6 **if** *point is already in the point page* **then**
7   **return** "duplicate record"
8 **end**
9 Add (point, irisID) to point page
10 **if** *page does not overflow* **then**
11   **return**
12 **else**
13   page = point page
14   k_i = median element along *ith* dimension
15   split the page along k_i
16   **if** *page = root* **then**
17   **Goto** 27
18   **else**
19   page = parent of the page
20   Replace its child by left and right pages obtained after splitting
21   **if** *page overflows* **then**
22   **Goto** 14
23   **else**
24   **return**
25   **end**
26   **end**
27   Create a new region page with left and right region and set it as *root*
28 **end**
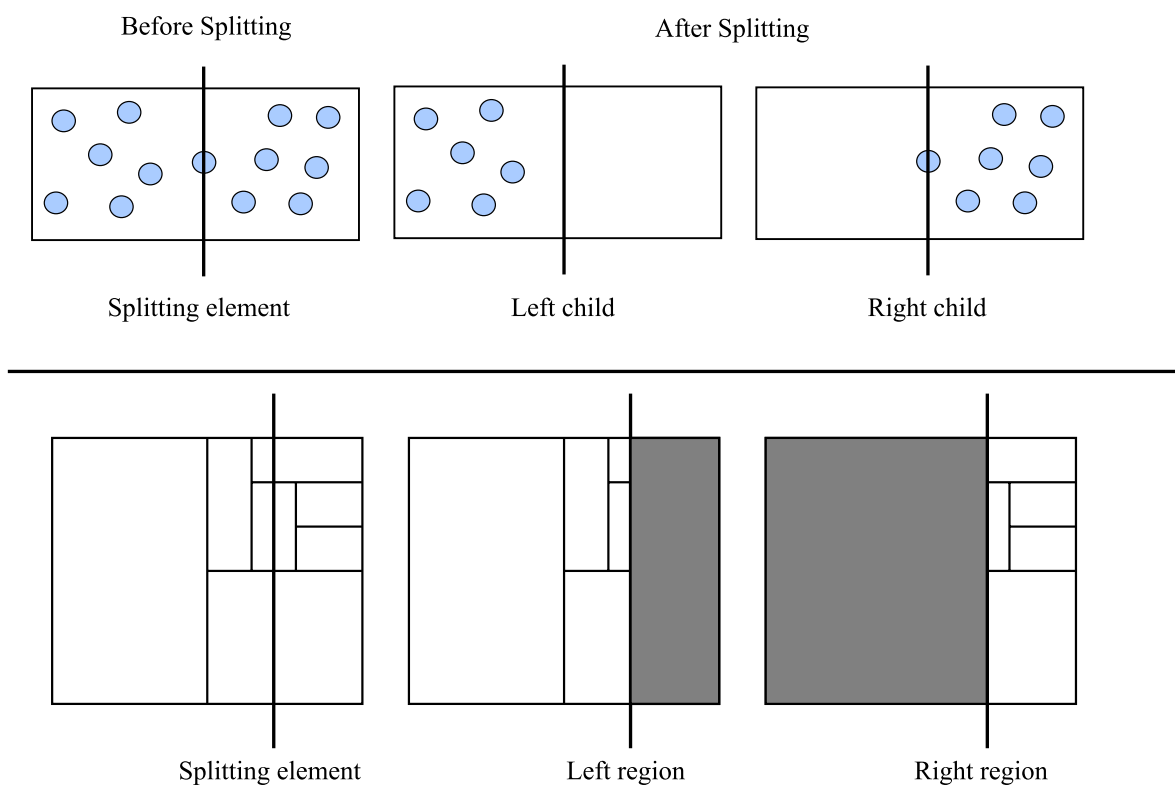
Figure 5.11: Splitting of point and region pages using k-d-b tree.

5.3.3 Range Query Retrieval

For retrieving gallery iris images corresponding to probe, range search is used [150]. The intersection of probe cluster center is found for each region on the page and those regions whose intersection with the probe are non-null are considered further to reach the point page(s). The image identifiers on the point page, referenced by query are retrieved (denoted as *List*). The range search procedure is given in Algorithm 13. This operation is repeated for m k-d-b trees and the identifiers retrieved are combined using set union operation to generate the candidate list. Finally, top S matches are obtained by individually comparing the probe feature descriptor with candidate irises.

5.3.4 Experimental Results

In this section, the performance of k-d-b tree is evaluated experimentally on BATH and CASIAV3 databases.

Design of Experiments

In this section, the results are obtained for k-d-b tree based indexing using BATH and CASIAV3 databases. Figure 5.12(a) shows CMC curves for change in number of

---

Algorithm 13: Range_Search

Input: Q: *yth* cluster center from probe iris, *page*: Pointer to root of *yth* k-d-b tree

Output: *List*: List of gallery *ids* retrieved

1 **if** *page = NULL* **then**
2   return
3 **end**
4 **if** *page = point page* **then**
5   **foreach** *(point, irisID) in page* **do**
6   *List* = [*List*, irisID]
7   **end**
8 **else**
9   **foreach** *region* $\in$ *page* **do**
10   I = {region | $Q \cap$ region $\neq \varnothing$}
11   **end**
12   **foreach** *child* $\in I$ **do**
13   *page* = I $\rightarrow$ child
14   **Range_Search**(Q, *page*)
15   **end**
16 **end**

---

clusters (m). The value of m is varied from 2 to 4 as BM becomes 0 following $m = 3$ for BATH database. Table 5.5 shows the values of pi for change in number of clusters at different ranks. Precisely, the value of pi becomes 1.00 at rank-29 for $m = 4$ using k-d-b tree. The pi of all ranks is not shown in the table due to space constraints. Similar observations are made for CASIAV3 database. The CMC curves for k-d-b tree on CASIAV3 database are shown in Figure 5.12(b). Here the value of m is varied from 2 to 5. From the curves it is found that the proposed tree based indexing approaches fail to achieve $pi = 1$ for CASIAV3 database. Table 5.5 shows identification probabilities for change in ranks. The rank-k identification improves over k-d tree based indexing for CASIAV3 database. However, there still remains the scope to further improve the probability of identification. The number of parameters, to tune during retrieval, are reduced using k-d-b tree based indexing in contrast to k-d tree. The range search approach is non-parametric and hence preferred over KNN retrieval.

5.4   R-tree

The k-d-b tree approach discussed earlier is designed to work with point data. This is not particularly suitable for many real time applications for instance biometrics where probe features may change due to transformations, illumination, and occlusion.

(a) **BATH**   (b) **CASIAV3**
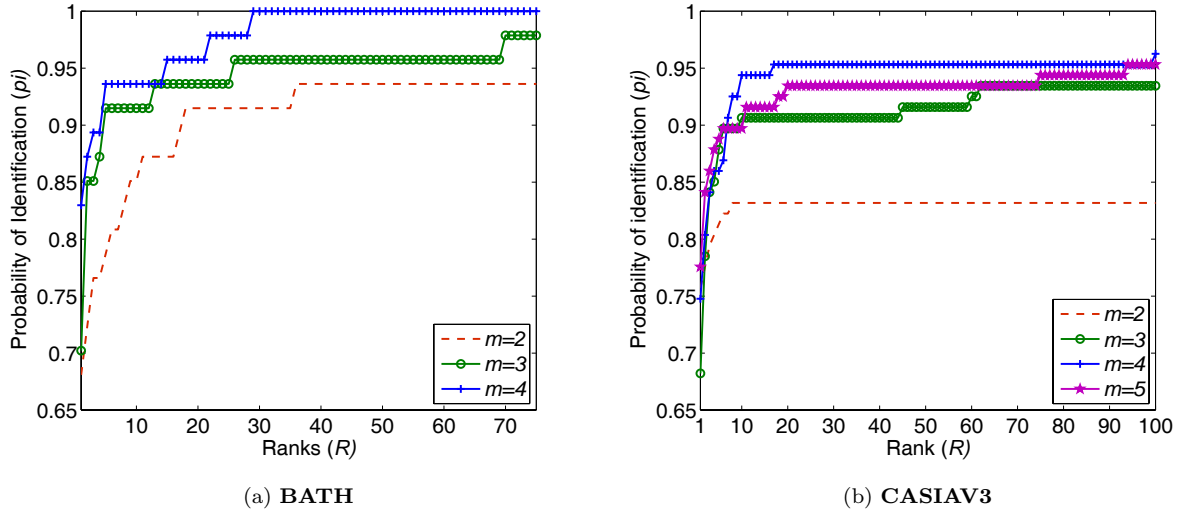
Figure 5.12: CMC curves for k-d-b tree with change in number of clusters.

Table 5.5: Probability of identification for k-d-b tree based indexing.

$R \downarrow m \rightarrow$	BATH			CASIAV3			
	2	3	4	2	3	4	5
1	0.68	0.70	0.83	0.76	0.68	0.75	0.78
2	0.72	0.85	0.87	0.78	0.79	0.80	0.84
5	0.78	0.92	0.94	0.81	0.88	0.86	0.89
10	0.85	0.92	0.94	0.83	0.91	0.95	0.90
20	0.91	0.94	0.96	0.83	0.91	0.95	0.94
50	0.94	0.96	**1.00**	0.83	0.92	0.95	0.94
100	0.94	0.98	1.00	0.83	0.94	**0.96**	0.95

In biometrics, the search is approximate and bears close resemblance to gallery features rather than exact match. Hence, point based approaches may not generate appropriate search results for biometric databases. In this thesis, an efficient spatial data structure called R-tree [151] is used for indexing biometrics databases. The tree structure is dynamic, height balanced, and considers paged data from the secondary memory. R-tree by design handles data range rather than considering exact point values. For indexing, R-tree is applied to enclose templates sharing similar properties by a rectangle. The retrieval errors are relatively reduced compared to other multi-dimensional trees. The proposed retrieval approach is based on hybrid coarse-to-fine strategy. At the coarse level, the identities are retrieved using range search to form the candidate list. The motivation behind using range search is attributable to better performance with no parameters to tune during searching. At the fine level, each identity in the candidate list is matched with the probe iris using global features based on 1-D Log-Gabor wavelet [112]. The matching scores of the

candidate individuals are weighted to rank the identities. Although, local features extracted from an image are invariant to various possible transformations but global features are still required for better class discrimination. Integrating local and global features generates an efficient indexing approach particularly suitable for content based image retrieval [152].

5.4.1 Structure of R-tree

R-trees are height balanced data structures for multi-dimensional indexing. The structure of R-tree is similar to B-trees and is used for hierarchical indexing of d-dimensional points represented as d-dimensional Minimum Bounding Rectangles (MBR). This approach is dynamic and does not require periodic re-organisation of the entire database on insertion. The maximum number of entries for each node is denoted by F and the minimum number is given by $f \leq \frac{F}{2}$. R-tree of order (f, F) satisfies the following properties:

- The number of entries in each node, except the root, ranges from $[f, F]$.

- Each entry in the leaf node is represented as (mbr, id), where mbr is d-dimensional rectangle that spatially surrounds the entry and id is the identifier of the multi-dimensional point.

- Each entry in the intermediate nodes is of the form $(mbr, child)$. Here $child$ is the pointer to the child node and mbr is the smallest rectangle that spatially contains mbr of the child node.

- The root node contains at least two children unless it is a leaf.

Each mbr is d-dimensional rectangle where each dimension is represented in the form of range given by $[a, b]$. This range specifies the extent of a point along the particular dimension [151]. For each node R, $R.mbr$ denotes the MBR of that node and $R.child$ is the pointer to the child node. In case of leaf $R.id$ is the object identifier.

5.4.2 MBR Generation

For R-tree construction, each point is represented by a range denoted as $[a, b]$ that defines a rectangle (known as MBR) enclosing the point. The input to R-tree is y^{th} cluster center of an image which is mapped to set of range values. To generate the set of ranges, each cluster center (C_{xy}) is represented by set of keys arranged in non-decreasing
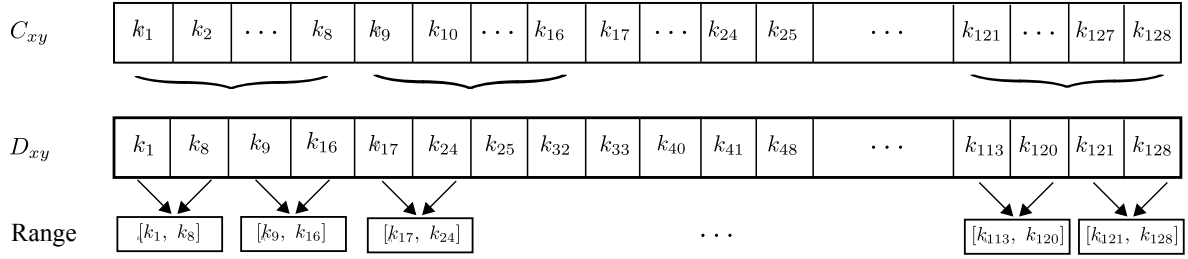
Figure 5.13: An example showing generation of ranges, for $\alpha = 7$ that generates $\eta = 32$ ranges using 128 dimensional SIFT features.

order and the values are selected at an increment of α. The predefined constant α controls the number of values selected (η) as given by:

$$\eta = 2 \left\lfloor \frac{k}{(\alpha + 1)} \right\rfloor \tag{5.6}$$

where k is the dimensionality of each cluster center (128 in case of SIFT). These selected values are stored in a vector (D_{xy}). Each non-overlapping range corresponding to C_{xy} is generated by selecting two consecutive elements of D_{xy}. This computes total of $\left\lfloor \frac{\eta}{2} \right\rfloor$ number of ranges. This process is iterated for m cluster centers each having 128 dimensional data. An example for generation of ranges is shown in Figure 5.13.

5.4.3   Indexing

Insertion into R-tree is similar to B trees in which new entries are inserted at the leaves. Nodes that overflow are split which propagates upward [151]. For indexing iris (I), each cluster center is used to generate range (D_{xy}) and the consecutive elements are selected to form MBR for I. The entry stored at the leaf node is of the form ($I.mbr, I.id$) where $I.mbr$ and $I.id$ are the MBR and iris identifier of I respectively. For non-leaf nodes, $I.id$ is replaced by $I.child$ which stores the pointer to the child node. The tree is traversed to reach an appropriate leaf node (R) whose MBR is expanded minimum to accommodate $I.mbr$. The new entry is inserted into R and MBR of all the nodes in path from root to R are updated. If R is found to be full, the split operation is performed to make room for I. To perform splitting, select two seeds e_i and e_j from all entries that belongs to R (including I). Form a rectangle (J) that encloses e_i and e_j. Compute the distance (d)

$$d = \mathbf{area}(J) - \mathbf{area}(e_i) - \mathbf{area}(e_j) \tag{5.7}$$

where **area** is the function to find the spatial extent of MBR. Choose e_i and e_j that generates maximum value of d. Create two nodes R_i and R_j using e_i and e_j as entries.

Allocate remaining members of R to R_i or R_j depending on minimum area enlargement of their respective MBRs. If R is a root node then create a new node w with R_i and R_j as its children; set w as root. If R is an intermediate node, then w points to parent of R and child pointers of w are updated to accommodate R_i and R_j. The MBR of all the nodes in path from root to w are updated. If w overflows then the splitting operation is performed again. The split operation is iterated until the order of each node in the tree is maintained. `Insert_Rtree` (Algorithm 14) is called to insert an element into R-tree which in turn calls `split_node` (Algorithm 15), if the node overflows on insertion. The insertion process is repeated for m cluster centers that generates m such R-trees.

Algorithm 14: Insert_Rtree

Input: R: Tree node, I: Iris to be inserted

1 **if** R is leaf node **then**
2   **if** $|R| < F$ **then**
3   insert I into R
4   Update all mbr in path from $root$ to R to cover $I.mbr$
5   **return**
6   **else**
7          $P \leftarrow$ **split_node**(R)
8   **Insert_Rtree**(P, I)
9   **end**
10 **else**
11      $R \leftarrow R.child$ // child with minimum increase in $R.mbr$ to include $I.mbr$
12   **Insert_Rtree**(R, I)
13 **end**

5.4.4 Hybrid Coarse-to-fine Retrieval Approach

A coarse-to-fine retrieval approach is proposed that unifies local as well as global features. At the coarse level, range search using local features generates candidate comprehensive list. At the refined level, each element of candidate comprehensive list is matched with the probe iris using global features. The elements of the candidate list are ranked using weighted scores. The detailed description of steps involved in proposed searching approach are given in sequel.

Candidate List Retrieval

The features extracted from probe iris image are clustered into m groups. These cluster centers are used to traverse the corresponding R-tree. For m cluster centers, m such

---

Algorithm 15: split_node

   Input: R: Tree node
   Output: w: Updated node after splitting

1 foreach *pair of elements e_i and e_j in node R* **do**
2   Construct J that encloses e_i and e_j `// MBR including` e_i `and` e_j
3 $d_{ij} = \mathbf{area}(J) - \mathbf{area}(e_i) - \mathbf{area}(e_j)$ `// Compute distance`
4 end
5 Select seeds e_i and e_j for maximum value of d
6 Create nodes R_i and R_j using e_i and e_j
7 Assign remaining elements of R to R_i or R_j with minimum increase in their *mbr*
8 if *R is root* **then**
9   create new root node (w) with R_i and R_j as children
10   **return**
11 else
12 $w \leftarrow$ parent of R
13   Update w with R_i and R_j as children
14   Update *mbr* of all nodes in path from root to w to accommodate R_i and R_j
15   **if** *$|w| > F$* **then**
16   split_node(w)
17   **end**
18 end

---

trees are traversed and retrieval is performed at coarse level using range search [153] as explained in Algorithm 13. The retrieved identities from each tree are combined into a comprehensive candidate list (L) as given by

$$L = [l_1 \cup l_2 \cup \ldots l_m] \tag{5.8}$$

where l_y is the candidate list generated from the *yth* tree for $1 \leq y \leq m$.

Weighted Rank based Top Matches

At the fine level, the candidate list elements are weighted to improve the identification accuracy. For generating scores, a sophisticated matcher is required that is specifically designed for iris. The choice of matcher is crucial as the retrieved irises possesses close similarity to the probe iris with subtle discrimination. In the proposed approach, global features are used to extract significant texture details from the iris whereas not compromising the local significance during index generation. Global features are particularly suitable for scenarios when the complete image describes potential features that can be used for authentication. For global feature extraction, 1D Log-Gabor wavelets [112] are used. The iris image corresponding to the retrieved iris identifier is

used to extract global features. These features are phase quantised and matched using Hamming distance. Sequentially comparing the probe (q) with each element (x) of L, generates a distance score (β_x). In order to further boost the performance, weights are assigned to each identifier (id) in the list. The frequency of occurrence of each identifier in the candidate list is obtained as,

$$\omega_{id} = \frac{\psi_{id}}{|L|} \tag{5.9}$$

where ψ_{id} represents frequency of occurrence of each id in the comprehensive list (L), $|\cdot|$ denotes the cardinality of the set, and ω_{id} is the corresponding value of weight. The weighted score for iris (τ_x) is obtained by

$$\tau_x = \omega_{id}(1 - \beta_x) \tag{5.10}$$

where $|id| \leq |L|$ as each id may occur more than once in L. The gallery iris most similar to probe will have higher frequency of occurrence in comparison to other identifiers. The list where each identifier occurs only once is a non-weighted list. The weighted list is sorted in decreasing order and the top best matches are obtained.

5.4.5 Experimental Results

The unification of R-tree for indexing with hybrid retrieval approach is subsequently referred as *hybrid* approach whereas R-tree based indexing uses conventional range search for retrieval. Hybrid approach is compared with proposed multi-dimensional tree based approaches and geometric hashing approach [89]. The experimental results of various local feature based indexing approaches are discussed in this section.

Design of Experiments

Two sets of experiments are conducted to study the efficiency of various indexing approaches. In Experiment 1, the hybrid approach is compared with proposed multi-dimensional tree based indexing approaches. In Experiment 2, the performance of tree based indexing approaches are compared to other local feature based indexes. The description of these experiments are given as follows:

Experiment 1: Multi-dimensional Trees

In this experiment, the performance of various multi-dimensional tree based indexing approaches are compared. The results are obtained for change in number of clusters.

Table 5.6: Showing identification performance of various multi-dimensional tree based indexing approaches on BATH database.

m	PR k-d	PR k-d-b	PR R-tree	BM k-d	BM k-d-b	BM R-tree	γ k-d	γ k-d-b	γ R-tree
2	0.01	0.03	0.005	0.19	0.06	0.15	0.90	0.95	0.92
3	0.02	0.04	0.006	0.13	0.00	0.13	0.92	0.98	0.93
4	0.01	0.05	0.007	0.11	0.00	0.02	0.94	0.97	0.99
5	0.02	-	0.009	0.04	-	0.00	0.97	-	1.00
6	0.03	-	0.010	0.02	-	0.00	0.98	-	1.00
7	0.02	-	0.011	0.02	-	0.00	0.98	-	1.00
8	0.03	-	0.012	0.02	-	0.00	0.98	-	0.99
9	0.03	-	0.012	0.00	-	0.00	0.99	-	0.99
10	0.03	-	0.013	0.02	-	0.00	0.98	-	0.99

The optimum cluster is chosen for minimum bin miss rate at relatively low penetration rate with maximum probability of identification.

- Table 5.6 shows the values of PR, BM, and γ for change in number of clusters using various multi-dimensional trees on BATH database. Here minimum BM is obtained for the selected clusters i.e., $m = \{9\}$, $m = \{3, 4\}$ and $m = \{5, 6, 7, 8, 9, 10\}$ for k-d tree, k-d-b tree, and R-tree approach[1] respectively. The optimum cluster is chosen from the selected ones with the highest probability of identification. Table 5.7 shows pi for change in number of clusters on BATH database[2]. For k-d tree, $pi = 1$ is obtained at $m = 9$. Thus, $m = 9$ is the optimum choice of cluster which gives considerably low PR of 0.03 and maximum γ of 0.985. In case of conflicting cases, where more than one selected clusters are chosen as in case of hybrid approach ($m = [5, \ldots, 10]$), pi can be taken as a conclusive measure for finding the optimum cluster.

- If we obtain maximum pi for more than one cluster then a new parameter rank (R) is introduced to generate the filtered list. For instance, Table 5.7 shows $pi = 1$ for all $m \geq 5$ using the hybrid approach. The optimum cluster is ascertained which achieves $pi = 1$ for minimum rank. In hybrid approach, $m = \{7, 9, 10\}$ generates $pi = 1$ for rank-1 in contrast to $pi = 1$ at rank-50 for $m = \{5, 6, 8\}$ as shown in Figure 5.15. However, still the conflict persists regarding the choice of an optimum cluster from the filtered list.

- Finally, from the list of filtered clusters ($m = \{7, 9, 10\}$) the one with minimum

---

[1]The hybrid approach at coarse level uses range search of R-tree so the indexing results of hybrid approach are not reported separately.

[2]R-tree indexing is tested using range search as well as hybrid search. The retrieval results are reported for both the approaches.

PR is considered as the optimum cluster. For hybrid approach, minimum $PR =$ 0.011 is obtained at $m = 7$.

Table 5.7: Probability of identification (pi) of multi-dimensional tree based searching approaches on BATH database.

k-d tree									
$R \downarrow m \rightarrow$	2	3	4	5	6	7	8	9	10
1	0.70	0.74	0.79	0.81	0.85	0.89	0.93	0.93	0.91
2	0.77	0.78	0.79	0.84	0.88	0.93	0.93	0.93	0.95
5	0.77	0.83	0.79	0.91	0.91	0.96	0.96	0.96	0.95
10	0.81	0.85	0.79	0.94	0.97	0.96	0.96	**1.00**	0.95
50	0.81	0.87	0.79	0.94	0.97	0.96	0.96	1.00	0.95
k-d-b tree									
$R \downarrow m \rightarrow$	2	3	4	5	6	7	8	9	10
1	0.68	0.70	0.83	-	-	-	-	-	-
2	0.72	0.85	0.87	-	-	-	-	-	-
5	0.78	0.92	0.94	-	-	-	-	-	-
10	0.85	0.92	0.94	-	-	-	-	-	-
50	0.94	0.96	**1.00**	-	-	-	-	-	-
R-tree									
$R \downarrow m \rightarrow$	2	3	4	5	6	7	8	9	10
1	0.72	0.66	0.85	0.79	0.85	0.87	0.83	0.85	0.89
2	0.77	0.68	0.87	0.83	0.91	0.87	0.87	0.89	0.94
5	0.77	0.77	0.87	0.85	0.91	0.91	0.89	0.94	0.94
10	0.77	0.77	0.87	0.87	0.91	0.91	0.89	0.96	0.96
50	0.85	0.87	0.96	0.96	0.96	**1.00**	0.91	0.96	0.98
Hybrid									
$R \downarrow m \rightarrow$	2	3	4	5	6	7	8	9	10
1	0.85	0.87	0.94	0.96	0.96	**1.00**	0.98	1.00	1.00
2	0.85	0.87	0.94	0.96	0.96	1.00	0.98	1.00	1.00
5	0.85	0.87	0.94	0.96	0.98	1.00	0.98	1.00	1.00
10	0.85	0.87	0.96	0.98	0.98	1.00	0.98	1.00	1.00
50	0.85	0.87	0.96	1.00	1.00	1.00	1.00	1.00	1.00

- Comparing various tree based indexing approaches, k-d-b tree generates minimum BM values for the initial choice of clusters (Figure 5.14) but PR needs further improvement. The PR of the R-tree approach is relatively low and combined with BM generates higher value of γ.

- The choice of clusters converge until $\gamma_m \geq \gamma_{m-1}$, for $m > 2$. For certain cases, though $\gamma_m < \gamma_{m-1}$ but the experiment is further taken if $BM_m \leq BM_{m-1}$ for $BM_m > 0$. However, even for $BM_m = 0$ the iterations do not converge if γ_m improves, which signifies that PR is further getting reduced.
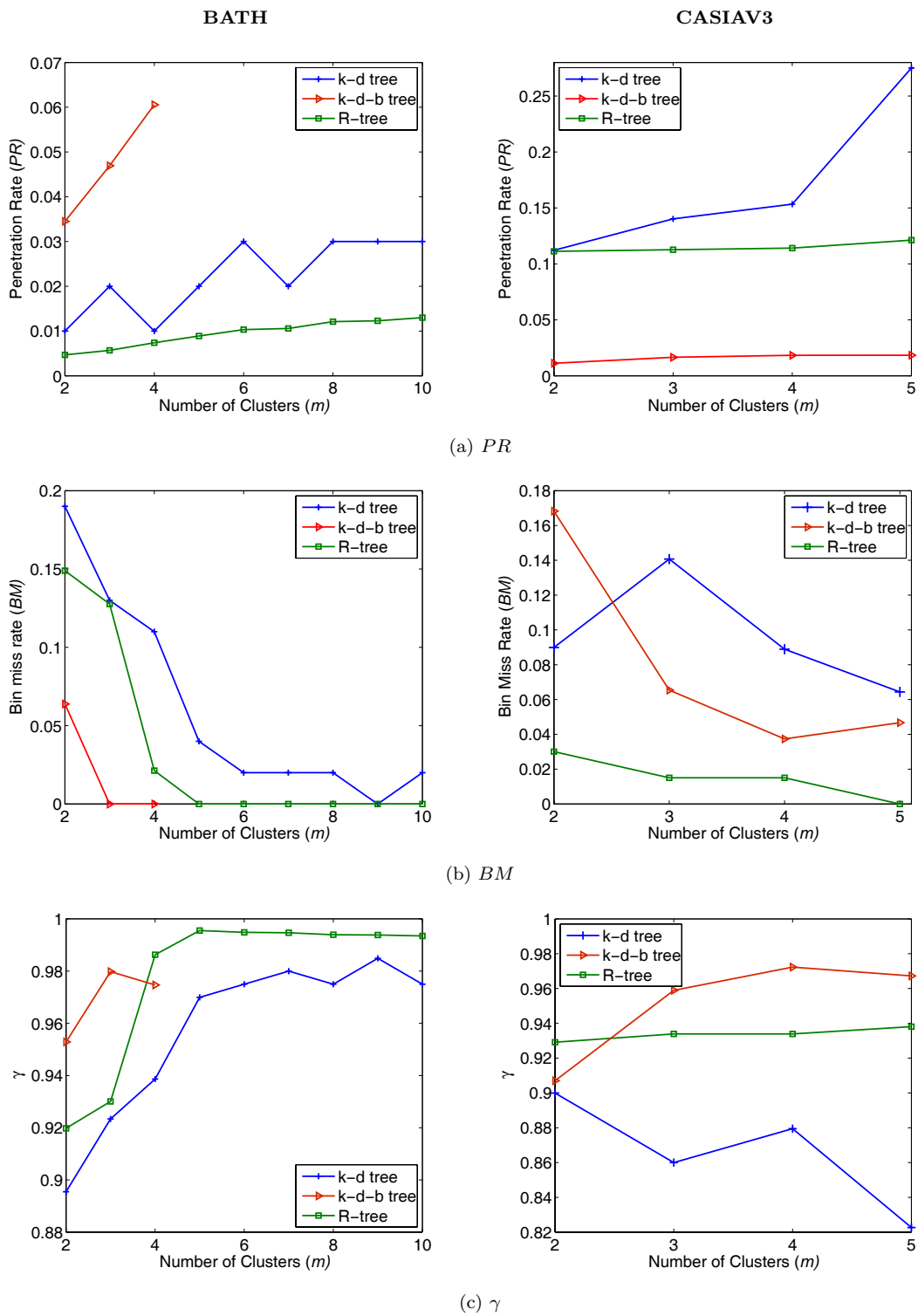
(a) *PR*

(b) *BM*

(c) *γ*

Figure 5.14: Performance measures for change in number of clusters using multi-dimensional tree based indexing approaches.

- The identification accuracy of an indexing approach is not solely dependent on BM. Though the candidate list contains an identity corresponding to the probe image but the reliability of genuine identity coming to the top is dependent on the performance of an underlying matcher. The value of pi becomes 1 for all indexing approaches on BATH database. However, the comparison between the approaches is the rank at which the value of pi becomes maximum. The k-d tree based indexing is rank-10 approach, k-d-b tree approach is rank-50, R-tree is rank-50, and the hybrid approach is rank-1 based identification system for BATH database.

- Table 5.8 shows performance of these indexing approaches on CASIAV3 database. The number of clusters ranges from $2 \leq m \leq 5$. The PR of the hybrid approach is high (for CASIAV3) compared to k-d-b tree but BM achieved is considerably low compared to k-d and k-d-b trees. The γ achieved using the hybrid approach reduces due to high PR. This clearly highlights that though γ achieved is low compared to k-d-b tree but hybrid approach achieves $BM = 0$, which is 0.05 in case of k-d-b tree. As stated earlier, γ cannot be taken as a conclusive measure rather a supportive evidence of the performance. This further substantiates the use of pi as shown Table 5.9 for the conflicting cases.

Table 5.8: Identification performance of various multi-dimensional tree based approaches on CASIAV3 database.

	PR			BM			γ		
m	k-d	k-d-b	R-tree	k-d	k-d-b	R-tree	k-d	k-d-b	R-tree
2	0.11	0.011	0.11	0.09	0.19	0.03	0.90	0.91	0.93
3	0.14	0.017	0.11	0.14	0.07	0.02	0.86	0.96	0.93
4	0.15	0.018	0.11	0.09	0.04	0.02	0.88	0.97	0.93
5	0.28	0.018	0.12	0.04	0.05	0.00	0.83	0.97	0.94

- CMC curves of R-tree based indexing approaches are shown in Figure 5.15. The k-d tree based approach is rank-200 system with maximum $pi = 0.96$ (please refer Table 5.9), k-d-b tree is rank-100 with $pi = 0.96$, R-tree approach gives $pi = 1$ for rank-30, and the hybrid approach gives $pi = 1$ for rank-5 which is lowest in comparison to other approaches.

- The most remarkable property of the hybrid approach is zero bin miss which is not achieved by other indexing approaches. Further, the proposed hybrid retrieval strategy when combined with R-tree improves the rank of identification by using

Table 5.9: Probability of identification of various multi-dimensional tree based searching approaches on CASIAV3 database

$R \downarrow m \rightarrow$	k-d tree				k-d-b tree			
	2	3	4	5	2	3	4	5
1	0.79	0.69	0.7	0.76	0.76	0.68	0.75	0.78
2	0.84	0.81	0.77	0.83	0.78	0.79	0.8	0.84
5	0.89	0.83	0.84	0.88	0.81	0.88	0.86	0.89
10	0.89	0.84	0.85	0.93	0.83	0.91	0.95	0.90
20	0.91	0.85	0.87	**0.94**	0.83	0.91	0.95	0.94
30	0.91	0.85	0.88	0.94	0.83	0.91	0.95	0.94
50	0.91	0.85	0.88	0.94	0.83	0.92	0.95	0.94
100	0.91	0.85	0.88	0.94	0.83	0.94	**0.96**	0.95

$R \downarrow m \rightarrow$	R-tree				Hybrid			
	2	3	4	5	2	3	4	5
1	0.75	0.78	0.74	0.77	0.96	0.97	0.96	0.98
2	0.81	0.85	0.83	0.85	0.96	0.97	0.97	0.99
5	0.87	0.9	0.9	0.91	0.97	0.98	0.98	**1.00**
10	0.93	0.95	0.93	0.96	0.97	0.98	0.98	1.00
20	0.94	0.96	0.96	0.99	0.97	0.98	0.98	1.00
30	0.96	0.98	0.98	**1.00**	0.97	0.98	0.98	1.00
50	0.96	0.98	0.98	1.00	0.97	0.98	0.98	1.00
100	0.96	0.98	0.98	1.00	0.97	0.98	0.98	1.00

an efficient matcher and weight. For brevity, the performance values obtained for optimal cluster are shown in Table 5.10.

Table 5.10: Performance results of proposed multi-dimensional tree based indexing approaches obtained for optimal choice of m.

Approaches	BATH						CASIAV3					
	m	BM	PR	γ	pi	R	m	BM	PR	γ	pi	R
k-d	9	0.00	0.03	0.99	1.00	10	5	0.04	0.28	0.83	0.96	200
k-d-b	4	0.00	0.05	0.97	1.00	50	4	0.04	0.018	0.97	0.96	100
R-tree	7	0.00	0.011	1.00	1.00	50	5	0.00	0.12	0.94	1.00	30
Hybrid	7	0.00	0.011	1.00	1.00	1	5	0.00	0.12	0.94	1.00	5

Experiment 2: Comparison with Local Feature based Indexing

The performance of various multi-dimensional tree based indexing approaches (discussed in Experiment 1) are compared with geometric hashing [89]. In this experiment, the results are also compared with exhaustive search to demonstrate the merits of indexing biometric databases. The results of tree based approaches are found at optimal cluster (m) as shown in Table 5.10. Comparative CMC curves of various local feature based approaches are shown in Figure 5.16. The ROC curves
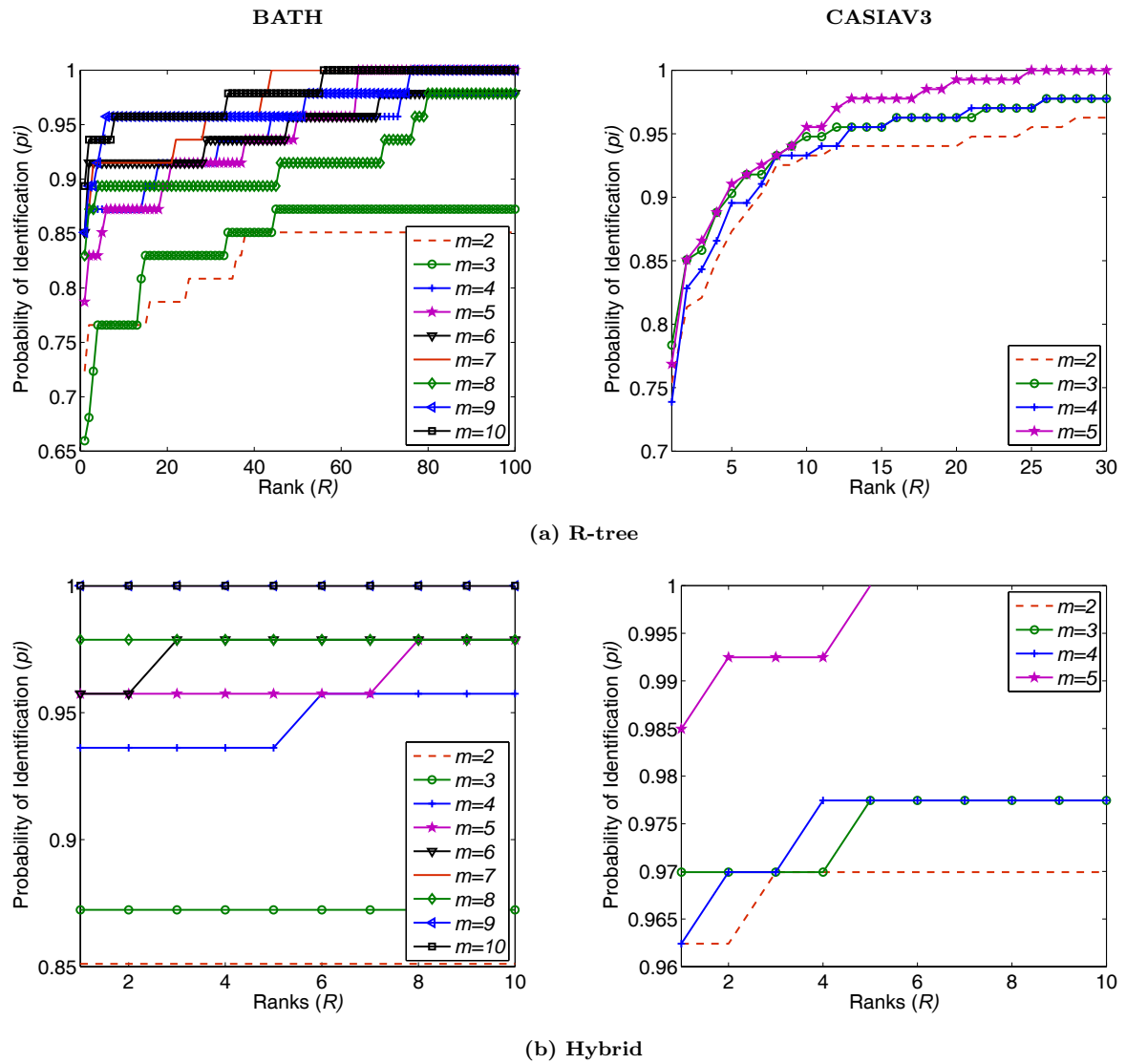
(a) R-tree

(b) Hybrid

Figure 5.15: Cumulative match characteristic curves of R-tree based searching approaches.

of various indexing approaches are shown in Figure 5.17. The accuracy of indexing approaches are found at 0.01% FMR as shown in Table 5.11. The rank based identification and recognition performance improves considerably using the hybrid indexing approach. The experiments are performed using Matlab on Intel i5 machine with 4GB RAM. Table 5.12 shows average retrieval time taken (in seconds) by various indexing approaches. From the results it is found that the hybrid approach achieves $pi = 1$ for low ranks. Though k-d tree performs retrieval in sufficiently less time but hybrid retrieval approach exhibits considerable improvement in accuracy. The penetration rate and hit rate (100-BM) are compared using other existing indexing approaches on CASIAV3 database (please refer Table 5.13). From results it is found that proposed k-d-b tree approach achieves PR of 1.8% which is significantly low compared to state-of-the-art indexing approaches. The hybrid approach achieves 100% hit rate for CASIAV3 database which is otherwise not achieved by other indexing approaches.

Table 5.11: Identification and recognition accuracy of various local feature based indexing approaches.

Correct Recognition Rate						
Approach→	**Exhaustive**	**Geometric**	**k-d**	**k-d-b**	**R-tree**	**Hybrid**
Database↓		**hashing**				
BATH	0.32	0.45	0.93	0.83	0.87	1.00
CASIAV3	0.58	0.82	0.76	0.75	0.77	0.99
GAR at 0.01% FMR						
Approach→	**Exhaustive**	**Geometric**	**k-d**	**k-d-b**	**R-tree**	**Hybrid**
Database↓		**hashing**				
BATH	2.70	0.37	31.62[3]	25.82	40.03	77.61
CASIAV3	19.84	21.76	23.66	20.12	49.72	85.43

[3]The value of GAR is obtained at 0.05% FMR on BATH database for k-d tree based indexing. ROC for k-d tree does not have representative values below 0.05% FMR.

Table 5.12: Average identification time (in seconds) taken by various local feature based indexing approaches. The identification time reported in this table is the consolidated time required to perform single retrieval and determine the rank of an individual.

Approach→	**Exhaustive**	**Geometric**	**k-d**	**k-d-b**	**R-tree**	**Hybrid**
Database↓		**hashing**				
BATH	03.55	01.14	0.47	1.01	1.12	0.52
CASIAV3	19.44	09.22	0.32	1.04	2.25	1.09

(a) **BATH**

(b) **CASIAV3**
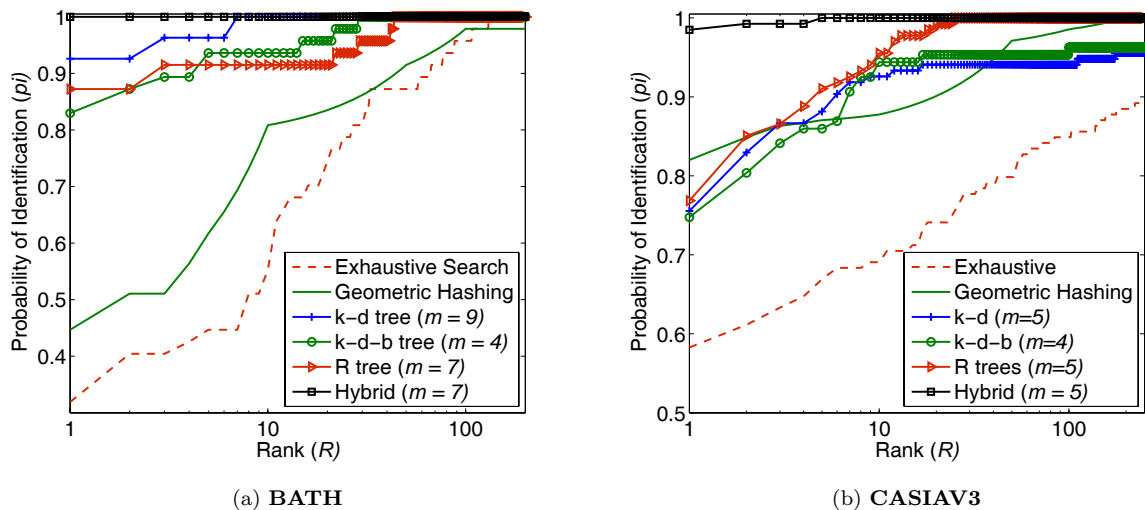
Figure 5.16: Cumulative match characteristic curves of different local feature based indexing approaches.

(a) **BATH**
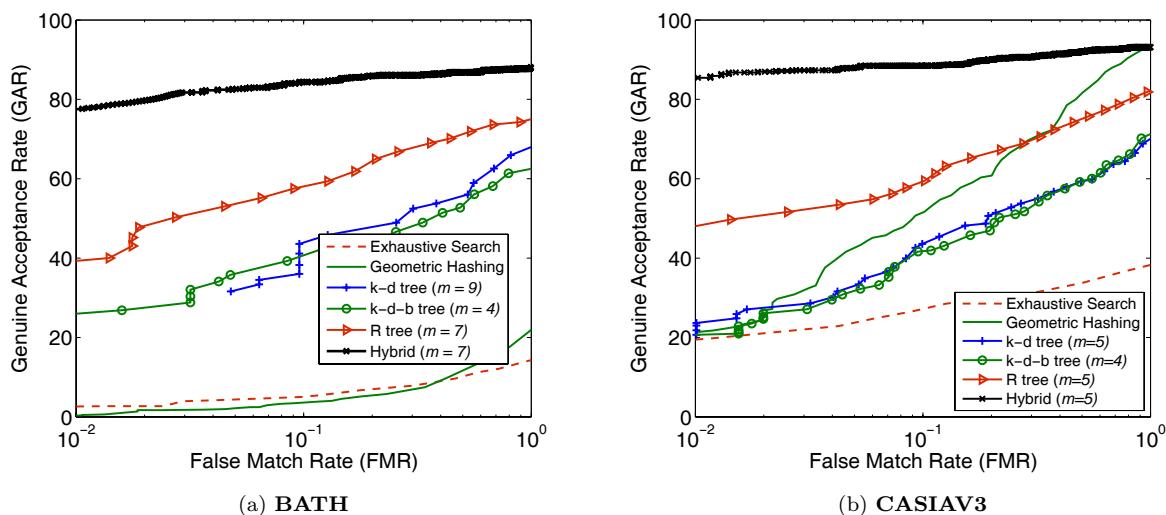
(b) **CASIAV3**

Figure 5.17: Receiver operating characteristic curves of different local feature based indexing approaches.

Table 5.13: Comparison of different indexing approaches on CASIAV3 database (in %). PR denotes penetration rate and HR denotes hit rate.

Year	Author	PR	HR
2008	Mukherjee [74]	30	84
2010	Mehrotra [89]	24	76
2012	Dey [80]	14	91
2013	k-d tree	28	96
2013	k-d-b tree	**1.8**	96
2013	R-tree	12	**100**

5.5   Summary

This chapter proposes various multi-dimensional tree based indexing approaches using local features. The application of k-d tree for biometrics is found to be encouraging but k-d tree is not scalable to new enrollments and the index structure often becomes skewed. These issues are addressed using k-d-b tree that improves the identification performance. However, the proposed indexing approaches still leaves scope for improvement of identification accuracy. R-tree is applied for indexing biometrics databases to further improve the probability of identification. For retrieval, a hybrid coarse-to-fine searching strategy is proposed. The performance of multi-dimensional trees and some state-of-the-art indexing approaches are compared in identification and recognition scenarios. During identification, hybrid approach achieves $pi = 1$ for initial ranks compared to existing indexing approaches. Further, the recognition accuracy of hybrid approach, also outperforms existing indexing approaches. Empirically, the average time taken by hybrid approach to perform single probe search is more than k-d tree which is due to an additional overhead required by the proposed retrieval approach to perform weighted matching. It is experimentally shown that the unique combination of local and global features for retrieval considerably improves the identification performance.

Chapter 6

Effect of Aging on Iris Performance

Human growth or aging from newborn to toddler to adult to elderly is a natural phenomenon. This process leads to changes in different characteristics such as height, weight, face, gait, and voice. Several of these characteristics are being used as biometric identifiers. In literature, it is well established that over a long period of time, some biometric modalities such as face and voice can change, thereby reducing the recognition performance. On the other hand, iris is considered to be one of the most accurate and stable biometric modalities [3].

The objective of this thesis is to improve the performance of iris recognition systems under practical scenarios. Aging is one such factor that can degrade performance over the period of time. Existing literature supports that the performance of iris degrades over time due to aging [107, 108, 109, 110, 111, 116]. However, recent NIST report suggests that iris patterns are stable and do not change due to aging [120]. The researchers do not have a consensus on the effect of aging in iris. The motivation of this study is to use the existing publicly available iris aging databases to understand iris aging and reasons for degradation in performance. In the experiments, it is observed that increase in false rejection is due to poor acquisition, presence of occlusion, noise/blur, and not due to aging. The quality values of the falsely rejected gallery-probe pairs further substantiate the fact that the quality of rejected iris images taken from two different sessions are different in comparison to the genuinely accepted pairs. This chapter is organised as follows—Section 6.1 discusses the databases and algorithms used to study aging. In Section 6.2, three different experiments are performed to find the reason for degradation in performance over time. The key observations and summary are given in Section 6.3.

6.1   Materials and Methods

This research re-investigates the challenge of iris aging [107, 108, 109, 110, 111, 116]. The databases and algorithms used in this research are briefly explained below.

6.1.1   Databases Used

Two publicly available iris aging databases are used to investigate the effect of aging on iris with the time lapse of two years and four years[1].

1. **ND-Iris-Template-Aging-2008-2010 Database**:   The images in the ND-Iris-Template-Aging-2008-2010 database [111] are acquired using the LG 4000 iris sensor during spring 2008, spring 2009, and spring 2010. This allows to conduct two different one year template aging studies, i.e., for the year 2008-2009 and 2009-2010, and one two year template aging study for 2008-2010. The number of subjects for the study are 88, 157, and 40 for 2008–2009, 2009–2010, and 2008–2010 sessions respectively.

2. **ND-TimeLapseIris-2012 Database**: The ND-TimeLapseIris-2012 database [113] contains images acquired with the LG2200 iris camera located in the same studio throughout all the acquisitions. A total of 6797 images are collected from 23 subjects (46 irises) in between 2004 to 2008. The age of these subjects ranges from 22 to 56 years where 16 subjects are male and 7 are female.

6.1.2   Commercial Matcher

Iris recognition is performed using the commercial VeriEye SDK [17], that has shown good performance in the state-of-art evaluations by NIST [154]. VeriEye contains advanced segmentation, enrollment, and matching routines[2]. For segmentation, VeriEye uses active shape models that accurately detect contours of the irises which are not perfect circles. The enrollment and matching routines are fast and yield very high matching performance/accuracy.

6.1.3   Experimental Protocol

The experimental protocol used to perform the experiments are explained below for each database.

---

[1]BATH and CASIAV3 databases do not possess temporal information and hence cannot be used to perform aging study.

[2]For evaluation, the commercial matcher which has shown to yield accurate results is chosen such that degradation in performance over time should not arise due to weakness of the algorithm.

1. ND-Iris-Template-Aging-2008-2010: The protocol followed for this database is same as provided by Fenker and Bowyer [111]. All the possible genuine comparisons are provided as part of the protocol. In the experiments, *short* refers to images captured within the same year whereas *long* refers to comparisons across years. The cross session irises for this particular study refers to the images captured over a time lapse of one or two years.

2. ND-TimeLapseIris-2012: The protocol followed in this study consists of two sets of image pairs [113]. The *short* time lapse set consists of image pairs with no more than 120 days of time lapse between them. The *long* time lapse set consists of image pairs with more than 1200 days of time lapse. An image instance can participate in multiple short and long time lapse pairs. Each image instance has several associated attributes such as date of acquisition, unit, color, glasses, and contact lens. For a genuine comparison, the units of two iris images must match along with the time lapse mentioned above. However, in the experiments, some false acceptance cases with exceptionally high scores (almost close to genuine acceptance) were observed. On carefully analysing these images, we observed that there are ground truth errors in the database due to incorrect ID labels. These incorrectly labeled instances belong to ids: `04870d1810` and `04888d395`. The cases associated with these incorrectly labeled ids were not considered in this study.

6.2 Results

If the performance degradation is caused due to aging, then this should hold true for all genuine comparisons pertaining to an individual across different sessions. Therefore, three sets of experiments are performed to closely study the cause of rejections that happen over time. The detailed description and analysis of each experiment are given below.

6.2.1 Experiment 1: Performance Evaluation

The first experiment is performed to compute iris matching accuracy for both short and long time lapses. Genuine and impostor scores are obtained using the VeriEye SDK on the protocols explained in Section 6.1.3. Table 6.1 shows the GAR at 0.001% FMR for both long and short time lapses on the ND-Iris-Template-Aging-2008-2010 and ND-TimeLapseIris-2012 databases. The results show that we are able to reproduce the accuracies reported by the researchers [111, 113]. The distribution of genuine and

impostor scores are shown in Figure 6.1. There is no evident shift in the impostor scores whereas the genuine scores show a shift towards the impostor scores for the long time lapse. Further, ROC curves in Figure 6.2 show a slight variation between long and short time lapses. The performance with the long time lapse is slightly lower than the short time lapse. McNemar test [155] shows that at 95% confidence interval, these results are statistically significant. This experiment shows that there is a reduction in the verification results in the long time lapse. However, the cause of shift in distributions or decrement in genuine accept rate cannot merely be attributed to aging. Therefore, the next experiments focus on determining the cause for performance reduction.

Table 6.1: Verification results for Experiments 1 and 2 on the two databases using VeriEye [17]. The GAR is computed at 0.001% FMR.

Database	Time lapse	Experiment 1	Experiment 2	
		GAR (%)	Genuine Accepts	False Rejects
ND-Iris-Template-Aging-2008-2010	2008-2009 (Short)	99.96	5434	0
	2008-2009 (Long)	99.88	14202	17
	2009-2010 (Short)	99.90	6720	4
	2009-2010 (Long)	99.88	15230	28
	2008-2010 (Short)	100.00	5434	0
	2008-2010 (Long)	99.90	13425	19
ND-TimeLapseIris-2012	Short	99.44	128690	815
	Long	99.08	128875	1280

6.2.2   Experiment 2: Common Subjects Over Time

It is our hypothesis that for a given subject, if aging exists and if the false rejections can be attributed to aging, then all the iris images of this subject with the same or more time lapse should be rejected. With this hypothesis, the false rejection cases are analysed to understand if the rejections are occurring due to aging or any other factor. In the ND-Iris-Template-Aging-2008-2010 database, the subjects that are common over multiple years are selected. There are 34 subjects common to 2008, 2009, and 2010 sessions. These common subjects are chosen to carefully study the cases of rejection and investigate the corresponding cases which are otherwise accepted. Table 6.1 illustrates the total number of genuine comparisons pertaining to these 34 subjects along with the number of false rejects. Here, all the experiments are performed using a threshold that produces the FMR of 0% in order to solely concentrate on the cause of genuine rejections over a period of time. Similarly, the rejections at 0% FMR from the ND-TimeLapseIris-2012 database are also obtained (all 23 subjects are present in both short and long time lapses). The number of genuine matches and false rejections at 0% FMR are shown in Table 6.1. It is our hypothesis that for a given subject, if iris aging
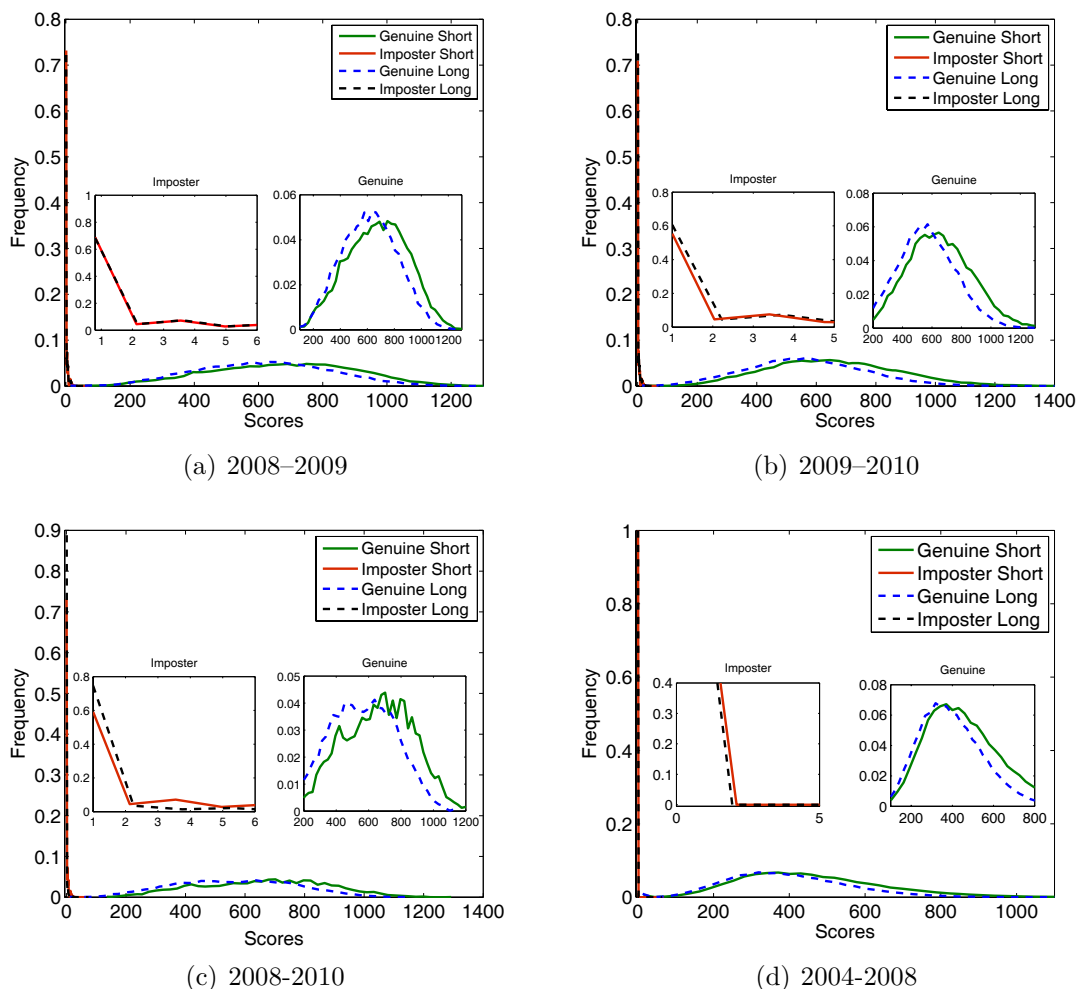
Figure 6.1: Histogram plots for Experiment 1 on (a), (b), and (c) ND-Iris-Template-Aging-2008-2010 database and (d) ND-TimeLapseIris-2012 database.

exists and if the false rejections can be attributed to iris aging, then all the images of this subject with the same or more time lapse should be rejected. Some observations from this experiment are:

- Figure 6.3 illustrates sample cases of false rejection on the ND-Iris-Template-Aging-2008-2010 database. It is interesting to note that for time lapse 2008-2009 (Long), all the false rejections are caused due to a single probe instance (`spring_2009/05379d624`)[3] which is actually blurred. The same instance when compared with other irises in 2009, for short comparison, also leads to rejections. For 2009-2010 (Long), 28 false rejections are observed, which

---

[3]Each image instance in the ND-Iris-Template-Aging-2008-2010 is labelled as session_year/instance_id where instance_id contains the subject id as the first five characters followed by the iris instance number.

(a) 2008–2009

(b) 2009–2010

(c) 2008-2010

(d) 2004-2008
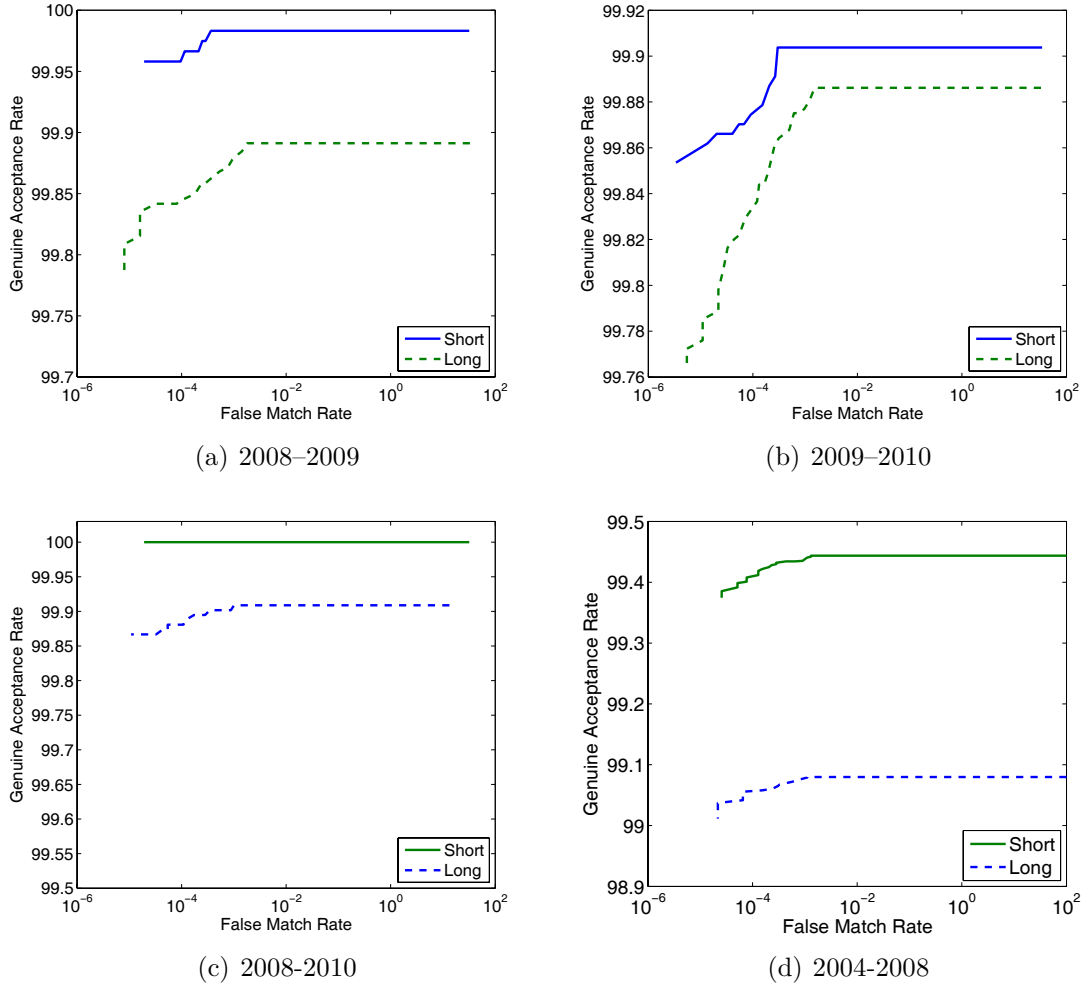
Figure 6.2: ROC curves for Experiment 1 on the (a), (b), (c) ND-Iris-Template-Aging-2008-2010 database and (d) ND-TimeLapseIris-2012 database.

is the maximum in any year. These cases are also studied in detail and after careful investigation, it is found that all the rejections are either due to blurring, occlusion, off-angle, or pupil dilation.

- For two year time lapse, i.e., 2008-2010 (Long), there are 19 false rejections. It is observed that these rejections are also due to noisy gallery or noisy probe instances. Similarly, as shown in Table 6.1, there are 1280 cases of false rejection for the long time lapse in the ND-TimeLapseIris-2012 database. This number is actually very small compared to the total number of genuine matches, i.e., 128,875. Here also, it is observed that the cases are rejected primarily due to variations in quality (quality aspect is discussed as part of Experiment 3).

- Figures 6.4 and 6.5 show cases from the gallery image captured in one session

119

Gallery   **Probe**

spring_2008/05379d214   spring_2009/05379d624
Blurred probe image.

spring_2009/05455d488   spring_2010/05455d984
Gallery occluded

spring_2008/04261d1029   spring_2010/04261d1572
Rotated probe and subject wearing contact lens

spring_2008/05432d139   spring_2010/05432d886
Pupil dilation in gallery
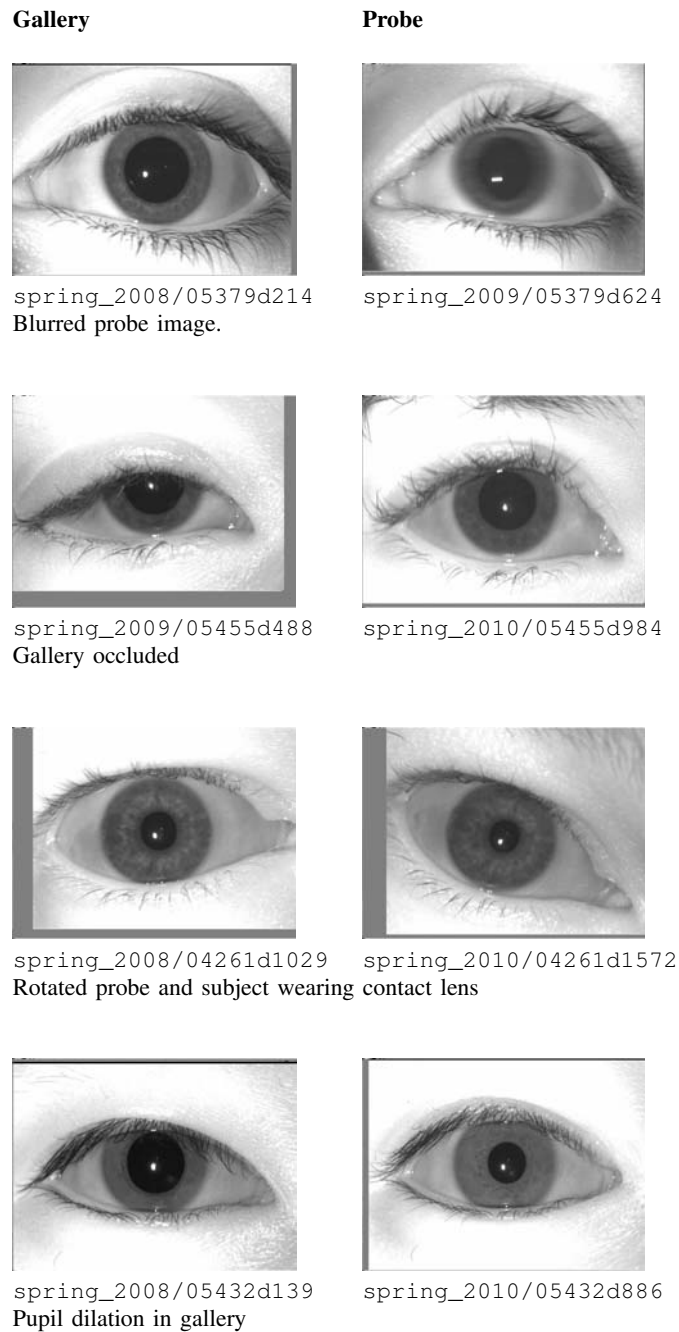
Figure 6.3: Cases of false non-match for variation in time on the ND-Iris-Template-Aging-2008-2010 database. Here, the gallery and probe instances are taken from cross sessions and the possible cause of rejection is mentioned as a remark. The image labels are provided for reproducibility.

and probe images captured in session from another year. It is observed that some probe images of the subject match whereas others from the same session and same subject do not match. Thus, it can be inferred that aging is not the cause

of false rejections and there are other covariates/challenges involved.

- The test of proportions at 95% confidence interval, where proportions $\left(\frac{\textbf{False Rejects}}{\textbf{Genuine Matches}}\right)$ are calculated between one year, two year, and four year differences also show that the proportions are statistically *non-significant*.

6.2.3 Experiment 3: Analysing Quality of Rejected Iris Pairs

From Experiment 2, it can be inferred that the performance reduction on the ND-Iris-Template-Aging-2008-2010 and ND-TimeLapseIris-2012 databases is not due to iris template aging. Therefore, to determine the actual cause of degradation, the image quality of the gallery and probe pairs are obtained. The quality of iris images is assessed using the quality assessment algorithm proposed by Kalka *et al.* [156]. It computes quality metrics such as blur, rotation, off-angle, and occlusion to determine a single composite quality score. The quality values of the gallery and probe images are obtained for the falsely rejected and the corresponding genuinely accepted pairs of these subjects over the long time lapse. Let q be the quality of an input iris image. For a gallery and probe iris image pair i, the absolute difference, c_i, is calculated as $c_i = |q_{gallery-i} - q_{probe-i}|$. This absolute difference is calculated for all the selected genuine accept and false reject cases and $\forall i, \quad \tilde{q} = median\{c_1, c_2, \cdots, c_i\}$ is obtained. Table 6.2 illustrates the median quality differences for the examined datasets. It can be observed that $\tilde{q}$ for falsely rejected pairs is higher than genuinely accepted iris pairs. This observation suggests that the pairs are falsely rejected because of the increased difference in the quality of the gallery and probe image pairs.

The results of these three experiments put together suggest that the false rejections on the two iris databases are due to occlusion, rotation, blurring, illumination and pupil dilation or constriction and not because of iris template aging.

Table 6.2: Difference between the quality scores of the gallery and probe pairs ($\tilde{q}$) for Experiment 3.

Database	Time lapse	Quality Difference (Median)	
		Genuine Accepts	False Rejects
ND-Iris-Template-Aging-2008-2010	2008-2009 (Long)	0.17	0.46
	2009-2010 (Long)	0.26	0.36
	2008-2010 (Long)	0.14	0.27
ND-TimeLapseIris-2012	Long	0.12	0.16

Gallery	Rejected Probe	Accepted Probe

spring_2008/05379d194   spring_2009/05379d624   spring_2009/05379d567

Iris image from 2008 session when compared to a blurred iris image of the same person from 2009 session leads to false rejection whereas the same iris when compared to a good quality iris image from 2009 session leads to genuine acceptance.

spring_2010/05379d1002   spring_2009/05379d624   spring_2009/05379d712

Iris images captured in 2009 and 2010 sessions. Rejected probe image is blurred.

spring_2008/04261d1029   spring_2010/04261d1572   spring_2010/04261d1540

Iris images compared across 2008 and 2010 sessions where probe image from rejected case showcases larger head tilt relative to the accepted probe.

spring_2010/04261d1571   spring_2008/04261d1014   spring_2008/04261d1016

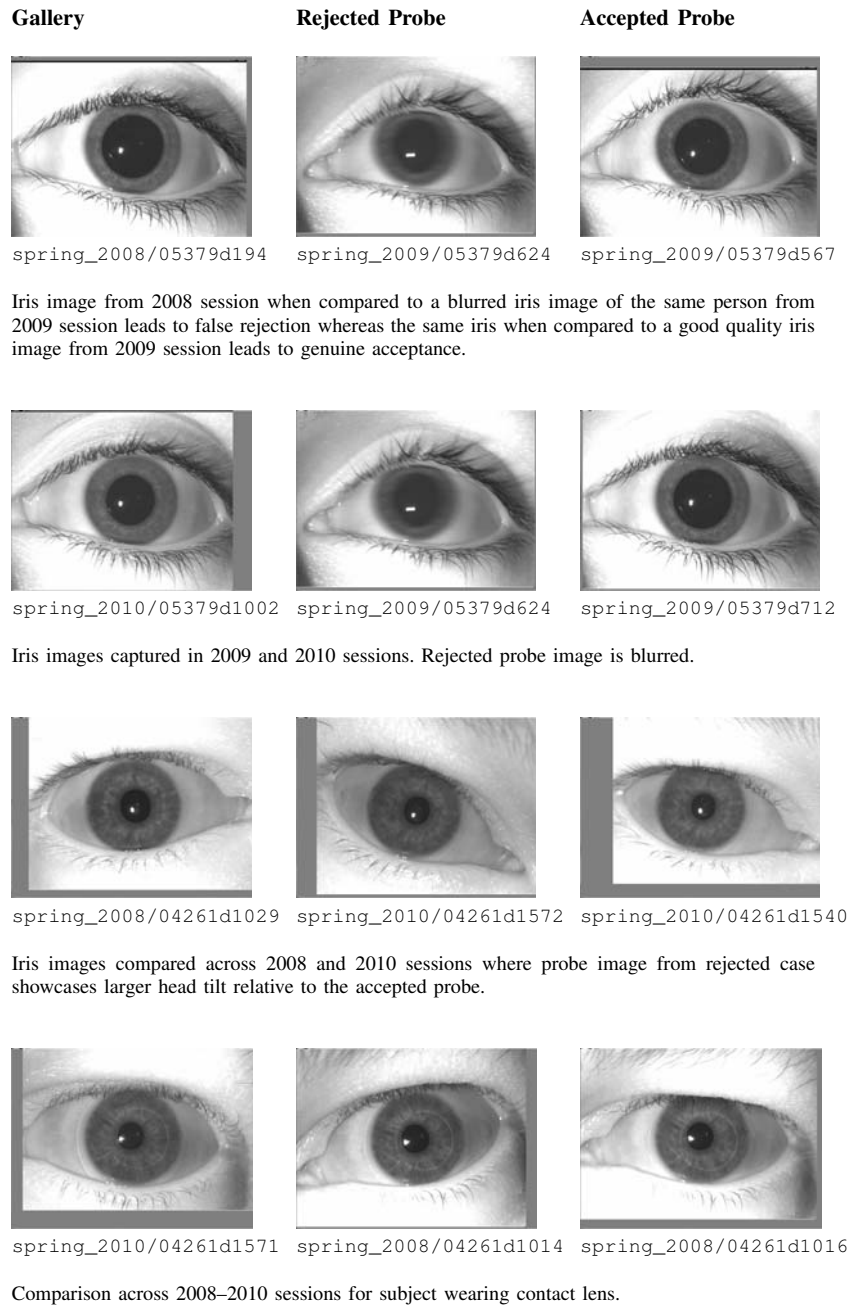Comparison across 2008–2010 sessions for subject wearing contact lens.

Figure 6.4: Illustrating cross session iris comparisons for the ND-Iris-Template-Aging-2008-2010 database. The gallery instance (1st column) is compared to probe images (columns 2 and 3) that belong to the same session. While one probe is rejected, the other probe image for the same session is accepted. The cause of rejection is stated as remark below the images. These examples illustrate that aging is not the key factor in performance degradation on this database rather other factors affected the recognisability.
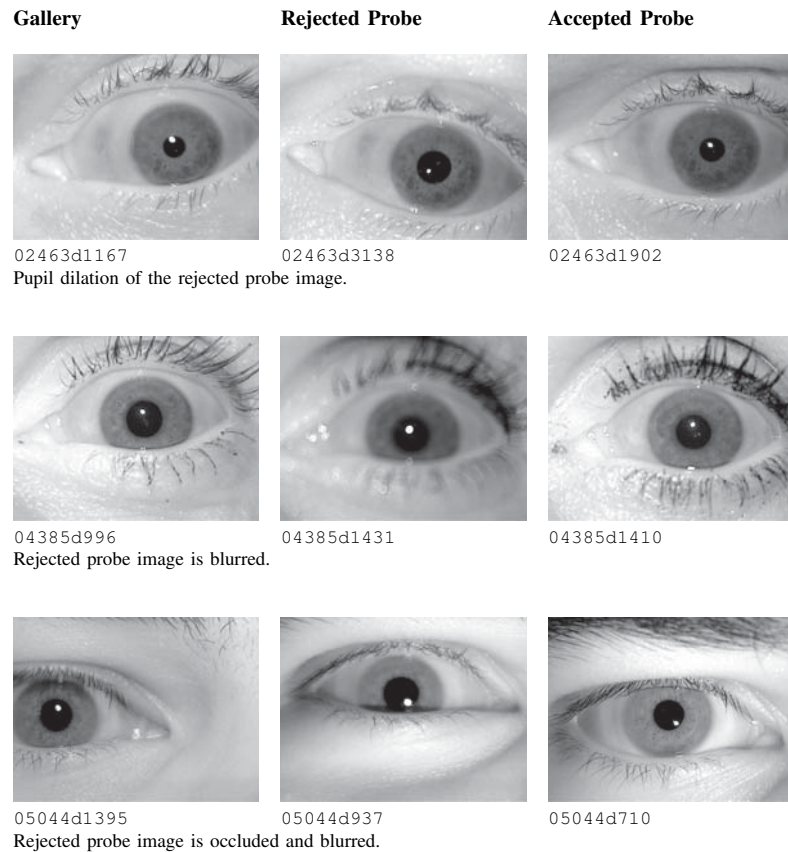
Gallery   **Rejected Probe**   **Accepted Probe**

02463d1167   02463d3138   02463d1902

Pupil dilation of the rejected probe image.

04385d996   04385d1431   04385d1410

Rejected probe image is blurred.

05044d1395   05044d937   05044d710

Rejected probe image is occluded and blurred.

Figure 6.5: Cross session iris comparisons for the ND-TimeLapseIris-2012 database. The accepted and rejected probes belong to the same session.

6.3   Summary

Recent results initiated the discussion on whether aging affects iris templates or not. Several researchers used the ND iris template aging databases to establish the *iris aging* effect. Contrary to the existing results, it is found that the reduced performance of iris recognition may not be caused by aging but due to noise and differences in the quality of gallery and probe pairs. Some key observations are:

- Though, for long time lapse, genuine score distributions demonstrate a shift towards the impostor score distributions, empirical investigation suggests that the rejections are caused by improper capture that leads to occlusion, rotation, blurring, illumination, and pupil dilation or constriction in iris images.

- The analysis also suggests that had aging been the cause of rejections then this should uniformly affect the performance. However, only few samples with time difference are rejected and other samples of the same subject with similar time difference are accepted.

Chapter 7

Conclusions

A generic iris recognition system delineates iris from the acquired image, characterises iris patterns using features and exhaustively search the database to claim the identity of an individual. In this thesis, the propositions are made to develop feature extraction, match score level fusion, and indexing approaches for iris biometrics. The experiments are performed using publicly available BATH and CASIAV3 iris databases. Further, an investigation has been made to study the effect of aging on the performance of iris biometric system.

The input iris image is segmented to generate sector based annular iris image. In Chapter 3, a feature descriptor (F-SIFT) is developed that combines the merits of Fourier transform with SIFT. Fourier transform has the property of characterising the repetitive patterns such as texture and SIFT possesses invariance to various possible transformations, occlusion, and illumination. The unique combination of Fourier and SIFT improves the recognition performance. From the experimental results, it is found that on CASIAV3 database, F-SIFT performs better compared to other keypoint descriptors like SIFT and SURF. The performance is comparable to SURF on BATH database. The results highlight the efficiency of customised SIFT descriptor designed for iris biometrics.

The matching scores from both the units of iris (left and right) are unified to improve the performance of existing iris recognition system. For fusion, a novel classifier is proposed in Chapter 4 that incorporates incremental and granular learning into RVM to develop Incremental Granular Relevance Vector Machine (iGRVM). This classifier is scalable, faster and can be trained with unbalanced large training samples. A case study is performed for multi-biometric score classification using standard match score databases. Results suggest that the proposed variant performs better than the original RVM classifier and comparable to existing classifiers such as LR and SVM. iGRVM significantly reduces the testing time compared to SVM.

The results of proposed *i*GRVM are found to be encouraging, which motivates its application for fusion. The scores from multiple units of iris are taken as *d*-dimensional vectors, which are classified using the proposed *i*GRVM. The performance improves over single unit iris recognition. Another proposition is to design a fusion framework where the match scores from individual units of iris are passed as an input to the corresponding *i*GRVM classifier and the posterior probabilities are combined using weighted sum rule. The fusion approach further boosts the performance over classification of scores.

During identification, the search space of large biometric databases can be reduced through indexing. In Chapter 5 various local feature based indexing approaches are proposed using multi-dimensional trees. Local features are extracted directly from the annular iris image using SIFT. The keypoints sharing similar descriptor property are clustered, and the cluster centers are used to generate corresponding k-d trees. The probe iris image is searched using KNN. Though k-d tree improves searching time, but insertion into the tree is not dynamic. This is not suitable as biometric databases are continuously updated to new enrollments. These issues are resolved by applying another data structure known as k-d-b tree, which is scalable and height balanced. The k-d-b tree reduces the search space to 5% and 1.8% on BATH and CASIAV3 databases respectively.

The application of R-tree generates an indexing approach with no bin miss. To further improve the rank of identification for R-tree indexing, a hybrid coarse-to-fine searching strategy is proposed. The hybrid approach performs retrieval using range search followed by weighted matching of global features. The unification of R-tree and hybrid retrieval achieves CRR of 100% and 99% for BATH and CASIAV3 databases respectively. The time required to claim identification is comparable to proposed k-d tree based indexing.

Recently, some research investigations are done towards the effect of aging on iris recognition performance [16, 110]. Motivated by these studies, an effort has been made to find if aging effects the iris pattern over the period of time. Chapter 6 shows an empirical study on ND Iris Template Aging databases acquired over the time lapse of four years. The false rejections are found by fixing the false acceptances at 0%. The rejection cases are studied individually to find if degradation in performance is due to aging or some other covariates are involved. Further, the difference in quality is found between the gallery and rejected probe iris images. Quality results showcase that the rejections are mainly because of noisy gallery or probe iris instances. It has been observed that the performance of iris recognition is not affected due to aging. If aging causes rejection over time, then this should uniformly affect all the comparisons,

which is not found to be true.

Scope for Future Work

The work described in this thesis unwraps some interesting research directions. During feature extraction, the performance of proposed F-SIFT approach can be enhanced by combining spatial and frequency information to generate the descriptor. The performance of F-SIFT is encouraging during the recognition mode. The application of F-SIFT for fusion and indexing is not explored in this thesis and can be considered for future study. The proposed indexing approaches are implemented in serial architecture. The retrieval time can be further reduced by searching the multi-dimensional trees in parallel.

Iris template aging is an important research problem which requires a longitudinal study; similar to face biometrics where 2-60 years time lapse are studied. To conduct a proper study, a controlled iris database is required over a period of several years in which the images should not be affected by other factors/covariates of iris recognition.

Bibliography

[1] A. Jain, P. Flynn, and A. A. Ross, *Handbook of Biometrics.* Springer-Verlag New York, Inc., 2007.

[2] J. L. Wayman, A. K. Jain, D. Maltoni, and D. Maio, *Biometric Systems: Technology, Design and Performance Evaluation.* Secaucus, NJ, USA: Springer-Verlag New York, Inc., 2004.

[3] J. Daugman, "The Importance of Being Random: Statistical Principles of Iris Recognition," *Pattern Recognition*, vol. 36, no. 2, pp. 279–291, 2003.

[4] S. Z. Li and A. K. Jain, Eds., *Encyclopedia of Biometrics.* Springer US, 2009.

[5] Unique Identification Authority of India, Available: http://uidai.gov.in/.

[6] M. Burge and K. Bowyer, *Handbook of Iris Recognition.* Springer Publishing Company, 2013.

[7] Iris Anatomy, Available: http://www.princeton.edu/~achaney/tmve/wiki100k/docs/Iris_(anatomy).html.

[8] Eye Images, Available: http://www.behance.net/gallery/Your-beautiful-eyes/428809.

[9] A. K. Jain and D. Maltoni, *Handbook of Fingerprint Recognition.* Secaucus, NJ, USA: Springer-Verlag New York, Inc., 2003.

[10] J. Daugman, "High Confidence Visual Recognition of Persons By A Test of Statistical Independence," *IEEE Transactions on Pattern Analysis and Machine Intelligence*, vol. 15, no. 11, pp. 1148–1161, 1993.

[11] J. L. Wayman, "Error Rate Equations for The General Biometric System," *IEEE Robotics and Automation Magazine*, vol. 6, no. 1, pp. 35–48, 1999.

[12] R. Gadde, D. Adjeroh, and A. Ross, "Indexing Iris Images Using the Burrows-Wheeler Transform," in *IEEE International Workshop on Information Forensics and Security*, 2010, pp. 1–6.

[13] H. Proenca and L. Alexandre, "Iris Recognition: An Analysis of the Aliasing Problem in the Iris Normalization Stage," in *International Conference on Computational Intelligence and Security*, vol. 2, 2006, pp. 1771–1774.

[14] Iris Recognition Immigration System (IRIS), Available: http://www.ukba.homeoffice.gov.uk/travellingtotheuk/Enteringtheuk/usingiris/.

[15] J. Daugman, "How Iris Recognition Works," *IEEE Transactions on Circuits and Systems for Video Technology*, vol. 14, no. 1, pp. 21–30, 2004.

[16] S. Fenker, E. Ortiz, and K. Bowyer, "Template Aging Phenomenon in Iris Recognition," *IEEE Access*, vol. 1, pp. 266–274, 2013.

[17] VeriEye SDK, Available: http://www.neurotechnology.com/verieye.html.

[18] United Arab Emirates Deployment of Iris Recognition, Available: http://www.cl.cam.ac.uk/~jgd1000/deployments.html.

[19] K. Miyazawa, K. Ito, T. Aoki, K. Kobayashi, and H. Nakajima, "An Effective Approach for Iris Recognition Using Phase-Based Image Matching," *IEEE Transactions on Pattern Analysis and Machine Intelligence*, vol. 30, no. 10, pp. 1741–1756, 2008.

[20] E. Krichen, S. Garcia-Salicetti, and B. Dorizzi, "A New Phase-Correlation-Based Iris Matching for Degraded Images," *IEEE Transactions on Systems, Man, and Cybernetics, Part B: Cybernetics*, vol. 39, no. 4, pp. 924–934, 2009.

[21] CASIA Database, Available: http://www.cbsr.ia.ac.cn/english/Databases.asp.

[22] National Institute of Standards and Technology. Iris Challenge Evaluation, Available: http://www.nist.gov/itl/iad/ig/ice.cfm.

[23] R. Wildes, "Iris Recognition: An Emerging Biometric Technology," *Proceedings of the IEEE*, vol. 85, no. 9, pp. 1348–1363, 1997.

[24] L. Ma, Y. Wang, and T. Tan, "Iris Recognition Based on Multichannel Gabor Filtering," in *Asian Conference on Computer Vision*, 2002, pp. 279–283.

[25] ——, "Iris Recognition Using Circular Symmetric Filters," in *International Conference on Pattern Recognition*, vol. 2, 2002, pp. 414–417.

[26] L. Ma, T. Tan, Y. Wang, and D. Zhang, "Personal Identification Based on Iris Texture Analysis," *IEEE Transactions on Pattern Analysis and Machine Intelligence*, vol. 25, no. 12, pp. 1519–1533, 2003.

[27] ——, "Efficient Iris Recognition by Characterizing Key Local Variations," *IEEE Transactions on Image Processing*, vol. 13, no. 6, pp. 739–750, 2004.

[28] Z. Sun and T. Tan, "Ordinal Measures for Iris Recognition," *IEEE Transactions on Pattern Analysis and Machine Intelligence*, vol. 31, no. 12, pp. 2211–2226, 2009.

[29] BATH University Database, Available: http://www.bath.ac.uk/elec-eng/research/sipg/irisweb.

[30] M. Zhang, Z. Sun, and T. Tan, "Perturbation-Enhanced Feature Correlation Filter for Robust Iris Recognition," *IET Biometrics*, vol. 1, no. 1, pp. 37–45, 2012.

[31] W. Boles and B. Boashash, "A Human Identification Technique Using Images of The Iris and Wavelet Transform," *IEEE Transactions on Signal Processing*, vol. 46, no. 4, pp. 1185–1188, 1998.

[32] C. Sanchez-Avila, R. Sanchez-Reillo, and D. De Martin-Roche, "Iris-Based Biometric Recognition Using Dyadic Wavelet Transform," *IEEE Aerospace and Electronic Systems Magazine*, vol. 17, no. 10, pp. 3–6, 2002.

[33] C. Sanchez-Avila and R. Sanchez-Reillo, "Two Different Approaches For Iris Recognition Using Gabor Filters and Multiscale Zero-Crossing Representation," *Pattern Recognition*, vol. 38, no. 2, pp. 231–240, 2005.

[34] D. M. Monro, S. Rakshit, and D. Zhang, "DCT-Based Iris Recognition," *IEEE Transactions on Pattern Analysis and Machine Intelligence*, vol. 29, no. 4, pp. 586–595, 2007.

[35] A. Ahamed and M. Bhuiyan, "Low Complexity Iris Recognition Using Curvelet Transform," in *International Conference on Informatics, Electronics Vision*, 2012, pp. 548–553.

[36] H. Proenca and L. A. Alexandre, "UBIRIS: A Noisy Iris Image Database," in *13th International Conference on Image Analysis and Processing*, 2005, pp. 970–977.

[37] M. Dobe and L. Machala, "Iris Database," Available: http://www.inf.upol.cz/iris/.

[38] C. Belcher and Y. Du, "Region-based SIFT Approach to Iris Recognition," *Optics and Lasers in Engineering*, vol. 47, no. 1, pp. 139–147, 2009.

[39] Multimodal Biometric Dataset Collection, BIOMDATA, Release 1, Available: http://www.citer.wvu.edu/multimodal_biometric_dataset_collection__biomdata_release1.

[40] H. Mehrotra, G. Badrinath, B. Majhi, and P. Gupta, "An Efficient Dual Stage Approach For Iris Feature Extraction Using Interest Point Pairing," in *IEEE Workshop on Computational Intelligence in Biometrics: Theory, Algorithms, and Applications*, 2009, pp. 59–62.

[41] H. Mehrotra, G. S. Badrinath, B. Majhi, and P. Gupta, "An Efficient Iris Recognition Using Local Feature Descriptor," in *IEEE International Conference on Image Processing*, 2009, pp. 1957–1960.

[42] Y. Du, C. Belcher, and Z. Zhou, "Scale Invariant Gabor Descriptor-Based Noncooperative Iris Recognition," *EURASIP Journal on Advances in Signal Processing*, vol. 2010, no. 1, p. 936512, 2010.

[43] M. Zhang, Z. Sun, and T. Tan, "Deformable DAISY Matcher for Robust Iris Recognition," in *IEEE International Conference on Image Processing*, 2011, pp. 3189–3192.

[44] S. Sun, S. Yang, and L. Zhao, "Noncooperative Bovine Iris Recognition via SIFT," *Neurocomputing*, vol. 120, pp. 310–317, 2013.

[45] D. G. Lowe, "Distinctive Image Features from Scale-Invariant Keypoints," *International Journal of Computer Vision*, vol. 60, no. 2, pp. 91–110, 2004.

[46] A. Ross and A. Jain, "Information Fusion in Biometrics," *Pattern Recognition Letters*, vol. 24, no. 13, pp. 2115–2125, 2003.

[47] K. Nandakumar, Y. Chen, S. Dass, and A. Jain, "Likelihood Ratio-Based Biometric Score Fusion," *IEEE Transactions on Pattern Analysis and Machine Intelligence*, vol. 30, no. 2, pp. 342–347, 2008.

[48] A. Jain, K. Nandakumar, and A. Ross, "Score Normalization in Multimodal Biometric Systems," *Pattern Recognition*, vol. 38, no. 12, pp. 2270–2285, 2005.

[49] R. Brunelli and D. Falavigna, "Person Identification Using Multiple Cues," *IEEE Transactions on Pattern Analysis and Machine Intelligence*, vol. 17, no. 10, pp. 955–966, 1995.

[50] K.-A. Toh, X. Jiang, and W.-Y. Yau, "Exploiting Global and Local Decisions for Multimodal Biometrics Verification," *IEEE Transactions on Signal Processing*, vol. 52, no. 10, pp. 3059–3072, 2004.

[51] J. Kittler, M. Hatef, R. Duin, and J. Matas, "On Combining Classifiers," *IEEE Transactions on Pattern Analysis and Machine Intelligence*, vol. 20, no. 3, pp. 226–239, 1998.

[52] A. Jain, S. Prabhakar, and S. Chen, "Combining Multiple Matchers For A High Security Fingerprint Verification System," *Pattern Recognition Letters*, vol. 20, no. 11-13, pp. 1371–1379, 1999.

[53] R. Snelick, U. Uludag, A. Mink, M. Indovina, and A. Jain, "Large-Scale Evaluation of Multimodal Biometric Authentication Using State-of-the-art Systems," *IEEE Transactions on Pattern Analysis and Machine Intelligence*, vol. 27, no. 3, pp. 450–455, 2005.

[54] National Institute of Standards and Technology, NIST Biometric Scores Set-Release 1, Available: http://www.itl.nist.gov/iad/894.03/biometricscores.

[55] The Color FERET Database, Available: http://www.nist.gov/itl/iad/ig/colorferet.cfm.

[56] S. Ben-Yacoub, Y. Abdeljaoued, and E. Mayoraz, "Fusion of Face and Speech Data For Person Identity Verification," *IEEE Transactions on Neural Networks*, vol. 10, no. 5, pp. 1065–1074, 1999.

[57] K. Messer, J. Matas, J. Kittler, J. Lttin, and G. Maitre, "XM2VTSDB: The Extended M2VTS Database," in *International Conference on Audio and Video-based Biometric Person Authentication*, 1999, pp. 72–77.

[58] B. Gutschoven and P. Verlinde, "Multi-modal Identity Verification Using Support Vector Machines (SVM)," in *International Conference on Information Fusion*, vol. 2, 2000, pp. 3–8.

[59] ACTS, "Multi-modal verification for tele-services and securiry applications", Available: www.uk.infowin.org.

[60] X. Lu, Y. Wang, and A. Jain, "Combining Classifiers for Face Recognition," in *International Conference on Multimedia and Expo*, vol. 3, 2003, pp. 13–16.

[61] The ORL Database of Faces, Available: http://www.cl.cam.ac.uk/research/dtg/attarchive/facedatabas

[62] The Yale Face Database, Available: http://cvc.yale.edu/projects/yalefaces/yalefaces.html.

[63] AR Face Database, Available: http://www2.ece.ohio-state.edu/~aleix/ARdatabase.html.

[64] M. Vatsa, R. Singh, and A. Noore, "Unification of Evidence-Theoretic Fusion Algorithms: A Case Study in Level-2 and Level-3 Fingerprint Features," *IEEE Transactions on Systems, Man, and Cybernetics, Part A: Systems and Humans*, vol. 39, no. 1, pp. 47–56, 2009.

[65] S. Prabhakar and A. Jain, "Decision-Level Fusion In Fingerprint Verification," *Pattern Recognition*, vol. 35, no. 4, pp. 861–874, 2002.

[66] N. Poh and S. Bengio, "Database, Protocols and Tools for Evaluating Score-level Fusion Algorithms in Biometric Authentication," *Pattern Recognition*, vol. 39, no. 2, pp. 223–233, 2006.

[67] M. Vatsa, R. Singh, A. Noore, and A. Ross, "On the dynamic selection of biometric fusion algorithms," *IEEE Transactions on Information Forensics and Security*, vol. 5, no. 3, pp. 470–479, 2010.

[68] Q. Tao and R. Veldhuis, "Robust Biometric Score Fusion by Naive Likelihood Ratio via Receiver Operating Characteristics," *IEEE Transactions on Information Forensics and Security*, vol. 8, no. 2, pp. 305–313, 2013.

[69] P. Phillips, P. Flynn, T. Scruggs, K. Bowyer, J. Chang, K. Hoffman, J. Marques, J. Min, and W. Worek, "Overview of The Face Recognition Grand Challenge," in *IEEE Computer Society Conference on Computer Vision and Pattern Recognition*, vol. 1, 2005, pp. 947–954.

[70] N. Ratha, K. Karu, S. Chen, and A. Jain, "A Real-time Matching System For Large Fingerprint Databases," *IEEE Transactions on Pattern Analysis and Machine Intelligence*, vol. 18, no. 8, pp. 799–813, 1996.

[71] A. Lumini, D. Maio, and D. Maltoni, "Continuous Versus Exclusive Classification For Fingerprint Retrieval," *Pattern Recognition Letters*, vol. 18, no. 10, pp. 1027–1034, 1997.

[72] A. Mhatre, S. Palla, S. Chikkerur, and V. Govindaraju, "Efficient Search and Retrieval in Biometric Databases," in *Society of Photo-Optical Instrumentation Engineers (SPIE) Conference Series*, vol. 5779, 2005, pp. 265–273.

[73] M. Liu, X. Jiang, and A. Kot, "Efficient Fingerprint Search Based on Database Clustering," *Pattern Recognition*, vol. 40, no. 6, pp. 1793–1803, 2007.

[74] R. Mukherjee and A. Ross, "Indexing Iris Images," in *International Conference on Pattern Recognition*, 2008, pp. 1–4.

[75] U. Jayaraman, S. Prakash, and P. Gupta, "Indexing Multimodal Biometric Databases Using Kd-Tree with Feature Level Fusion," in *International Conference on Information Systems Security*, 2008, pp. 221–234.

[76] H. Mehrotra, B. Srinivas, B. Majhi, and P. Gupta, "Indexing Iris Biometric Database Using Energy Histogram of DCT Subbands," in *International Conference on Contemporary Computing*, 2009, pp. 194–204.

[77] J. Fu, H. J. Caulfield, S.-M. Yoo, and V. Atluri, "Use of Artificial Color Filtering to Improve Iris Recognition and Searching," *Pattern Recognition Letters*, vol. 26, no. 14, pp. 2244–2251, 2005.

[78] N. Puhan and N. Sudha, "A Novel Iris Database Indexing Method Using the Iris Color," in *IEEE Conference on Industrial Electronics and Applications*, 2008, pp. 1886–1891.

[79] C. Rathgeb and A. Uhl, "Iris-Biometric Hash Generation for Biometric Database Indexing," in *International Conference on Pattern Recognition*, 2010, pp. 2848–2851.

[80] S. Dey and D. Samanta, "Iris Data Indexing Method Using Gabor Energy Features," *IEEE Transactions on Information Forensics and Security*, vol. 7, no. 4, pp. 1192–1203, 2012.

[81] C. Watson, "NIST Special Database 9: Mated Fingerprint Card Pairs," Advanced Systems Division, Image Recognition Group, National Institute for Standards and Technology, 1993.

[82] C. Watson and C. Wilson, "NIST Special Database 4: Fingerprint Database," U.S. National Institute for Standards and Technology, 1992.

[83] H. Feng, J. Daugman, and P. Zielinski, "A Fast Search Algorithm for A Large Fuzzy Database," *IEEE Transactions on Information Forensics and Security*, vol. 3, no. 2, pp. 203–212, 2008.

[84] Multimedia University, Available: http://pesona.mmu.edu.my/~ccteo/.

[85] R. S. Germain, A. Califano, and S. Colville, "Fingerprint Matching Using Transformation Parameter Clustering," *IEEE Computational Science & Engineering*, vol. 4, no. 4, pp. 42–49, October 1997.

[86] G. Bebis, T. Deaconu, and M. Georgiopoulos, "Fingerprint Identification Using Delaunay Triangulation," in *International Conference on Information Intelligence and Systems*, 1999, pp. 452–459.

[87] B. Bhanu and X. Tan, "Fingerprint Indexing Based on Novel Features of Minutiae Triplets," *IEEE Transactions on Pattern Analysis and Machine Intelligence*, vol. 25, no. 5, pp. 616–622, 2003.

[88] A. Mhatre, S. Chikkerur, and V. Govindaraju, "Indexing Biometric Databases Using Pyramid Technique," in *Audio and Video based Biometric Person Authentication*, 2005, pp. 841–849.

[89] H. Mehrotra, B. Majhi, and P. Gupta, "Robust Iris Indexing Scheme Using Geometric Hashing of SIFT Keypoints," *Journal of Network and Computer Applications*, vol. 33, no. 3, pp. 300–313, 2010.

[90] Biometric Research Lab, Indian Institute of Technology Kanpur, Available: http://www.cse.iitk.ac.in/users/biometrics/.

[91] R. Cappelli, M. Ferrara, and D. Maltoni, "Fingerprint Indexing Based on Minutia Cylinder-Code," *IEEE Transactions on Pattern Analysis and Machine Intelligence*, vol. 33, no. 5, pp. 1051–1057, 2011.

[92] C. Watson, "NIST Special Database 14: NIST Mated Fingerprint Card Pairs 2 (MFCP2)," Advanced Systems Division, Image Recognition Group, National Institute for Standards and Technology, 1993.

[93] Fingerprint Verification Competition (FVC) 2000, Available: http://bias.csr.unibo.it/fvc2000/databases.asp.

[94] Fingerprint Verification Competition (FVC) 2002, Available: http://bias.csr.unibo.it/fvc2002/databases.asp.

[95] U. Jayaraman, A. Gupta, S. Prakash, and P. Gupta, "An Enhanced Geometric Hashing," in *IEEE International Conference on Communications*, 2011, pp. 1–5.

[96] A. Gago-Alonso, J. Hernandez-Palancar, E. Rodriguez-Reina, and A. Munoz-Briseno, "Indexing and Retrieving in Fingerprint Databases Under Structural Distortions," *Expert Systems with Applications*, vol. 40, no. 8, pp. 2858–2871, 2013.

[97] A. Munoz-Briseno, A. Gago-Alonso, and J. Hernandez-Palancar, "Fingerprint Indexing With Bad Quality Areas," *Expert Systems with Applications*, vol. 40, no. 5, pp. 1839–1846, 2013.

[98] J. de Boer, A. M. Bazen, and S. H. Gerez, "Indexing Fingerprint Databases Based on Multiple Features," in *Annual Workshop on Circuits, Systems and Signal Processing*, 2001, pp. 300–306.

[99] R. Cappelli and M. Ferrara, "A Fingerprint Retrieval System Based on Level-1 and Level-2 Features," *Expert Systems with Applications*, vol. 39, no. 12, pp. 10 465–10 478, 2012.

[100] W. Li, J. You, and D. Zhang, "Texture-Based Palmprint Retrieval Using A Layered Search Scheme For Personal Identification," *IEEE Transactions on Multimedia*, vol. 7, no. 5, pp. 891–898, 2005.

[101] T. Maeda, M. Matsushita, and K. Sasakawa, "Characteristics of the Identification Algorithm Using aMatching Score Matrix," in *Biometric Authentication*, ser. Lecture Notes in Computer Science, D. Zhang and A. Jain, Eds. Springer Berlin Heidelberg, 2004, vol. 3072, pp. 330–336.

[102] P. Gupta, A. Sana, H. Mehrotra, and C. Hwang, "An Efficient Indexing Scheme For Binary Feature Based Biometric Database," in *Proceedings of SPIE 6539*, 2007.

[103] A. Gyaourova and A. Ross, "Index Codes for Multibiometric Pattern Retrieval," *IEEE Transactions on Information Forensics and Security*, vol. 7, no. 2, pp. 518–529, 2012.

[104] A. Paliwal, U. Jayaraman, and P. Gupta, "A Score Based Indexing Scheme for Palmprint Databases," in *IEEE International Conference on Image Processing*, 2010, pp. 2377–2380.

[105] The Hong Kong Polytechnic University (PolyU) Palmprint Database, Available: http://www4.comp.polyu.edu.hk/~biometrics/index.htm.

[106] J. Daugman, "New Methods in Iris Recognition," *IEEE Transactions on Systems, Man, and Cybernetics, Part B: Cybernetics*, vol. 37, no. 5, pp. 1167–1175, 2007.

[107] P. Tome-Gonzalez, F. Alonso-Fernandez, and J. Ortega-Garcia, "On the Effects of Time Variability in Iris Recognition," in *IEEE International Conference on Biometrics: Theory, Applications and Systems*, 2008, pp. 1–6.

[108] S. Baker, K. Bowyer, and P. Flynn, "Empirical Evidence for Correct Iris Match Score Degradation with Increased Time-Lapse Between Gallery and Probe Matches," in *International Conference on Advances in Biometrics*, 2009, pp. 1170–1179.

[109] S. Fenker and K. Bowyer, "Experimental Evidence of A Template Aging Effect In Iris Biometrics," in *IEEE Computer Society Workshop on Applications of Computer Vision*, 2011, pp. 232–239.

[110] D. Rankin, B. Scotney, P. Morrow, and B. Pierscionek, "Iris Recognition Failure Over Time: The Effects of Texture," *Pattern Recognition*, vol. 45, no. 1, pp. 145–150, 2012.

[111] S. Fenker and K. Bowyer, "Analysis of Template Aging in Iris Biometrics," in *IEEE Computer Society Conference on Computer Vision and Pattern Recognition Workshops*, 2012, pp. 45–51.

[112] L. Masek and P. Kovesi, "MATLAB Source Code For a Biometric Identification System Based on Iris Patterns," *The School of Computer Science and Software Engineering*, 2003.

[113] S. Baker, K. Bowyer, P. Flynn, and P. Phillips, "Template Aging in Iris Biometrics: Evidence of Increased False Reject Rate in ICE 2006," in *Handbook of Iris Recognition*, M. Burge and K. Bowyer, Eds. Springer, 2013, pp. 205–218.

[114] M. Fairhurst and M. Erbilek, "Analysis of Physical Ageing Effects in Iris Biometrics," *IET Computer Vision*, vol. 5, no. 6, pp. 358–366, 2011.

[115] Ageing Eyes Hinder Biometric Scans, Available: http://www.nature.com/news/ageing-eyes-hinder-biometric-scans-1.10722.

[116] E. Ellavarason and C. Rathgeb, "Template Ageing in Iris Biometrics: A Cross-Algorithm Investigation of the ND-Iris-Template-Ageing-2008-2010 Database,"

Biometrics and Internet-Security Research Group, Center for Advanced Security Research, Darmstadt, Germany, Tech. Rep. HDA-da/sec-2013-001, 2013.

[117] N. Sazonova, F. Hua, X. Liu, J. Remus, A. Ross, L. Hornak, and S. Schuckers, "A Study on Quality-Adjusted Impact of Time Lapse on Iris Recognition," in *Sensing Technologies for Global Health, Military Medicine, Disaster Response, and Environmental Monitoring II; and Biometric Technology for Human Identification IX*, 2012, pp. 83 711–83 719.

[118] A. Czajka, "Template Ageing in Iris Recognition," in *International Conference on Bio-inspired Systems and Signal Processing*, 2013.

[119] J. Daugman and C. Downing, "No Change Over Time is Shown in Rankin et al. Iris Recognition Failure Over Time: The Effects of Texture," *Pattern Recognition*, vol. 46, no. 2, pp. 609–610, 2013.

[120] IREX VI Temporal Stability of Iris Recognition Accuracy, Available: http://biometrics.nist.gov/cs_links/iris/irexVI/irex_report.pdf.

[121] H. Proenca and L. Alexandre, "Toward Noncooperative Iris Recognition: A Classification Approach Using Multiple Signatures," *IEEE Transactions on Pattern Analysis and Machine Intelligence*, vol. 29, no. 4, pp. 607–612, 2007.

[122] H. Bay, A. Ess, T. Tuytelaars, and L. Van Gool, "Speeded-Up Robust Features (SURF)," *Computer Vision and Image Understanding*, vol. 110, no. 3, pp. 346–359, 2008.

[123] H. Mehrotra, "Iris Identification Using Keypoint Descriptors and Geometric Hashing," Master's thesis, National Institute of Technology Rourkela, 2010.

[124] G. Xu, Z. Zhang, and Y. Ma, "Automatic Iris Segmentation Based on Local Areas," in *International Conference on Pattern Recognition*, vol. 4, 2006, pp. 505–508.

[125] S. Bakshi, H. Mehrotra, and B. Majhi, "Real-time Iris Segmentation Based on Image Morphology," in *International Conference on Communication, Computing & Security*. ACM, 2011, pp. 335–338.

[126] Q. Tian, Q. Pan, Y. Cheng, and Q. Gao, "Fast Algorithm and Application of Hough Transform in Iris Segmentation," in *International Conference on Machine Learning and Cybernetics*, vol. 7, 2004, pp. 3977–3980.

[127] B. Lipinski, "Iris Recognition: Detecting The Pupil," in *Connexions Web site. http://cnx.org/content/m12487/1.4/*, 2004.

[128] J. Weszka, C. Dyer, and A. Rosenfeld, "A Comparative Study of Texture Measures for Terrain Classification," *IEEE Transactions on Systems, Man and Cybernetics*, vol. 6, no. 4, pp. 269–285, 1976.

[129] K. Ito, H. Nakajima, K. Kobayashi, T. Aoki, and T. Higuchi, "A Fingerprint Matching Algorithm Using Phase-Only Correlation," *IEICE Transactions Fundamentals*, vol. 87-A, no. 3, pp. 682–691, 2004.

[130] R. Singh, M. Vatsa, A. Ross, and A. Noore, "Biometric Classifier Update Using Online Learning: A Case Study in Near Infrared Face Verification," *Image and Vision Computing*, vol. 28, no. 7, pp. 1098–1105, 2010.

[131] US-VISIT, Available: http://www.dhs.gov/us-visit-office.

[132] V. Vapnik, *The Nature of Statistical Learning Theory.* USA: Springer-Verlag New York, Inc., 1995.

[133] M. Tipping, "Sparse Bayesian Learning and The Relevance Vector Machine," *Journal of Machine Learning Research*, vol. 1, pp. 211–244, 2001.

[134] J. C. MacKay, "The Evidence Framework Applied to Classification Networks," *Neural Computation*, vol. 4, no. 5, pp. 720–736, 1992.

[135] N. A. Syed, S. Huan, L. Kah, and K. Sung, "Incremental Learning with Support Vector Machines," in *Workshop on Support Vector Machines at the International Joint Conference on Artificial Intelligence*, 1999.

[136] T. Lin, "Data Mining and Machine Oriented Modeling: A Granular Computing Approach," *Applied Intelligence*, vol. 13, no. 2, pp. 113–124, 2000.

[137] M. Tipping and A. Faul, "Fast Marginal Likelihood Maximisation for Sparse Bayesian Models," in *International Workshop on Artificial Intelligence and Statistics*, 2003, pp. 3–6.

[138] D. Tzikas, A. Likas, and N. Galatsanos, "Incremental Relevance Vector Machine with Kernel Learning," in *Hellenic conference on Artificial Intelligence: Theories, Models and Applications*, 2008, pp. 301–312.

[139] D. Silver, Q. Yang, and L. Li, "Lifelong Machine Learning Systems: Beyond Learning Algorithms," in *AAAI Spring Symposium on Lifelong Machine Learning*, 2013, pp. 49–55.

[140] Y. Tang, "Granular Support Vector Machines Based on Granular Computing, Soft Computing and Statistical Learning," Ph.D. dissertation, Georgia State University, 2006.

[141] Y. Tang, Y.-Q. Zhang, N. Chawla, and S. Krasser, "SVM Modeling for Highly Imbalanced Classification," *IEEE Transactions on Systems, Man, and Cybernetics, Part B: Cybernetics*, vol. 39, no. 1, pp. 281–288, 2009.

[142] X. Xiang-min, M. Yun-feng, X. Jia-ni, and Z. Feng-le, "Classification Performance Comparison between RVM and SVM," in *IEEE International Workshop on Anti-counterfeiting, Security, Identification*, 2007, pp. 208–211.

[143] N. Poh, T. Bourlai, and J. Kittler, "A Multimodal Biometric Test Bed For Quality-Dependent, Cost-Sensitive and Client-Specific Score-Level Fusion Algorithms," *Pattern Recognition*, vol. 43, no. 3, pp. 1094–1105, 2010.

[144] Integrated Automated Fingerprint Identification System, Available: http://www.fbi.gov/about-us/cjis/fingerprints_biometrics/iafis/iafis.

[145] X. Tan, B. Bhanu, and Y. Lin, "Fingerprint Identification: Classification vs. Indexing," in *IEEE Conference on Advanced Video and Signal Based Surveillance*, 2003, pp. 151–156.

[146] H. Samet, *The Design and Analysis of Spatial Data Structures*. Boston, MA, USA: Addison-Wesley Longman Publishing Co., Inc., 1990.

[147] J. Bentley, "Multidimensional Binary Search Trees Used For Associative Searching," *Communications of the ACM*, vol. 18, no. 9, pp. 509–517, 1975.

[148] J. H. Friedman, J. L. Bentley, and R. A. Finkel, "An Algorithm for Finding Best Matches in Logarithmic Expected Time," *ACM Transactions on Mathematical Software*, vol. 3, pp. 209–226, 1977.

[149] J. Robinson, "The K-D-B-tree: A Search Structure for Large Multidimensional Dynamic Indexes," in *Proceedings of ACM SIGMOD International conference on Management of data*. ACM, 1981, pp. 10–18.

[150] P. K. Agarwal and J. Erickson, "Geometric Range Searching and Its Relatives," in *Advances in Discrete and Computational Geometry*. American Mathematical Society, 1998, vol. 23, pp. 1–56.

[151] A. Guttman, "R-trees: A Dynamic Index Structure For Spatial Searching," *ACM SIGMOD Record*, vol. 14, no. 2, pp. 47–57, 1984.

[152] D. Lisin, M. Mattar, M. Blaschko, E. Learned-Miller, and M. Benfield, "Combining Local and Global Image Features for Object Class Recognition," in *IEEE Workshop on Learning in Computer Vision and Pattern Recognition*, 2005, p. 47.

[153] Y. Manolopoulos, A. Nanopoulos, A. N. Papadopoulos, and Y. Theodoridis, *R-Trees: Theory and Applications (Advanced Information and Knowledge Processing)*. Secaucus, NJ, USA: Springer-Verlag New York, Inc., 2005.

[154] National Institute of Standards and Technology, Available: http://www.nist.gov/itl/iad/ig/iris.cfm/.

[155] Q. McNemar, "Note on The Sampling Error of The Difference Between Correlated Proportions or Percentages," *Psychometrika*, vol. 12, no. 2, pp. 153–157, 1947.

[156] N. D. Kalka, J. Zuo, V. Dorairaj, N. A. Schmid, and B. Cukic, "Image Quality Assessment for Iris Biometric," in *SPIE Conference on Biometric Technology for Human Identification III*, 2006, pp. 61 020D–1–62 020D–11.

Dissemination

Journals

1. **Hunny Mehrotra**, Mayank Vatsa, Richa Singh, and Banshidhar Majhi. Does Iris Change Over Time? **PLoS ONE**, 8(11): e78333, 2013.

2. **Hunny Mehrotra** and Banshidhar Majhi. Local Feature based Retrieval Approach for Iris Biometrics. *Springer Journal of Frontiers of Computer Science*, 7(5):767–781, 2013.

3. **Hunny Mehrotra**, Pankaj K. Sa, and Banshidhar Majhi. Fast Segmentation and Adaptive SURF Descriptor for Iris Recognition. *Elsevier Journal of Mathematical and Computer Modelling*, 58(1–2):132–146, 2013.

Conferences

1. **Hunny Mehrotra** and Banshidhar Majhi. An Efficient Indexing Scheme for Iris Biometric using K-d-b Trees. In *International Conference on Intelligent Computing*, pages 475–484, Nanning, China, July 2013.

2. **Hunny Mehrotra**, Mayank Vatsa, Richa Singh, and Banshidhar Majhi. Biometric Match Score Fusion using RVM: A Case Study in Multi-unit Iris Recognition. In *IEEE Conference on Computer Vision and Pattern Recognition Workshops*, pages 65–70, Providence, RI, June 2012.

3. **Hunny Mehrotra**, Banshidhar Majhi, and Pankaj K. Sa. Unconstrained Iris Recognition using F-SIFT. In *International Conference on Information, Communications and Signal Processing, IEEE*, pages 1–5, Singapore, December 2011.

Communicated

1. **Hunny Mehrotra**, Richa Singh, Mayank Vatsa, and Banshidhar Majhi. Incremental Granular Relevance Vector Machine: A Case Study in Multimodal Biometrics. *Elsevier Journal of Pattern Recognition*, 2013.

2. **Hunny Mehrotra**, Banshidhar Majhi, Tithy Sahu, and Pankaj K. Sa. Hybrid Coarse-to-fine Retrieval Approach for R-Tree based Iris Identification. *Elsevier Journal of Network and Computer Applications*, 2013.

3. **Hunny Mehrotra** and Banshidhar Majhi. Search Space Reduction in Biometrics: A Survey. *Springer Journal of Real-Time Image Processing*, 2013.

Hunny Mehrotra

Department of Computer Science and Engineering,
National Institute of Technology Rourkela,
Rourkela – 769 008, Odisha, India.
+91 98718 88917

hunny04@gmail.com

Qualification

- PhD (CSE) (*Continuing*)
  National Institute of Technology Rourkela

- M.Tech. (Research) (CSE)
  National Institute of Technology Rourkela, [9.68 CGPA]

- B Level (MCA)
  DOEACC, New Delhi, [B Grade]

Publications

- Journals: 10

- Conferences: 23

- Book Chapters: 02

Permanent Address

48/227 General Ganj,
Kanpur 208 001, Uttar Pradesh.

Date of Birth

4th September 1982

Index